

NORTHWESTERN UNIVERSITY

Molecular mechanisms of MYCⁱ⁹⁷⁵ and MYC target gene dysregulation

A DISSERTATION

SUBMITTED TO THE GRADUATE SCHOOL
IN PARTIAL FULFILLMENT OF THE REQUIREMENTS

for the degree

DOCTOR OF PHILOSOPHY

Driskill Graduate Training Program in Life Sciences

By

Austin Gable Holmes

EVANSTON, ILLINOIS

June 2022

© Copyright by {Austin Holmes, 2022}

All Rights Reserved

Abstract

MYC regulates multiple gene programs, raising questions about the potential selectivity and downstream transcriptional consequences of MYC inhibitors as cancer therapeutics. MYC functions to either globally amplify RNA production or selectively regulates genes by repression or activation. In models of MYC inhibition by small molecules the functionality of MYC is greatly reduced although specific MYC function may be more sensitive than others. Here, we examined the effect of a small molecule MYC inhibitor, MYCi975, on the MYC/MAX cisomes, epigenome, transcriptome and tumorigenesis. These data revealed three major classes of MYCi975-modulated gene targets: Type 1 (downregulated), Type 2 (upregulated) and Type 3 (unaltered). While cell cycle and signal transduction pathways were heavily targeted by MYCi975, RNA biogenesis and core transcriptional pathway genes were spared. MYCi975 altered chromatin binding of MYC, and the MYC network family proteins including MAX and MAX heterodimeric binding partners. Both genome-wide chromatin accessibility and H3K27-acetylation was altered by MYCi975, and motif analysis revealed enrichment of MYC-regulated lineage factors AR/ARv7, FOXA1 and FOXM1. Subsequently, chromatin occupancy analysis following MYCi975 treatment demonstrated loss of lineage factors overlapping differential chromatin accessibility and H3K27ac sites. Consequently, MYCi975 synergistically sensitized resistant prostate cancer cells to enzalutamide and estrogen receptor-positive breast cancer cells to 4-hydroxytamoxifen. Although MYC inhibition induced a loss of chromatin occupancy and expression of many transcription factors, the MYCi975 activated cisome has yet to be elucidated. MYCi975 induced ATF4 protein stability and downstream ATF4 signaling promoting apoptosis. Using MYC knockdown and knockout models we determined that MYCi975 induction of ATF4 is dependent on MYC expression levels

however MYC canonically functions to regulate ATF4 induction. These results demonstrate that MYCi975 selectively inhibits MYC target gene expression and provide a mechanistic rationale for potential combination therapies.

TABLE OF CONTENTS	5
ACKNOWLEDGMENTS	6
LIST OF FIGURES & TABLES	7
CHAPTER 1: INTRODUCTION	8
CHAPTER 2: MYCi975 selectively inhibits the MYC and MAX cistromes	18
CHAPTER 2: DISCUSSION	64
CHAPTER 3: MYCi975 activates ATF4	71
CHAPTER 3: DISCUSSION	80
CHAPTER 4: METHODS	83
REFERENCE LIST	97
APPENDIX	116
VITA	117

Acknowledgments

Professional:

1) I'd like to thank the following mentors and colleagues for their scientific contributions and guidance:

Dr. Debabrata Chakravarti, Dr. Sarki Adbulkadir, Dr. Daniel R. Foltz, Dr. Grant Barish, Dr. J. Brandon Parker, Dr. Vinay Sagar, Mihai Truica, Dr. Huiying Han, Dr. Priyanka Soni

2) I'd like to acknowledge the Graduate School at Northwestern University, the Driskill Graduate Program and the Cell and Molecular Basis of Disease T32 Training Grant.

Personal:

1) I'd like to thank the following individuals who I deeply care for and who have been tremendously supportive, encouraging, kind, gracious and loving, which have made significant contributions to the dissertation work presented here:

Mel Holmes, Bin Zheng, George Holmes, Toni Holmes, Jasmin Holmes, Cynthia Batie, Dr. Rodney E. Batie, the Driskill Graduate Program class of 2017, Pritin Soni, Dr. Poorva Sandlesh, Gini Marziani, Gregory Wrobel, Ian Reed, David Dworshak, Troy Armstrong, Brody Armstrong

LIST OF FIGURES AND TABLES

Figure 1. MYCi975 induces MYC down-regulation and cell growth defects in 22Rv1 cells.

Figure 2. Analysis of differential MYC binding in 22Rv1 cells demonstrates loss of occupancy at canonical MYC target genes.

Figure 3. Genomic distribution and co-factor WDR5 occupancy at MYCi975 sensitive and insensitive sites.

Figure 4. Differential gene expression induced by MYCi975 in 22Rv1 cells.

Figure 5. MYCi975 selectively affects MYC binding to promoters and target gene expression.

Figure 6. Type 4 MYCi975 insensitive sites and comparison of MYCi975 types 1-3.

Figure 7. MYC-bound promoter-distal sites exhibit significant CTCF and FOX factor motif enrichment.

Figure 8. MYC and CTCF occupancy at promoter distal and proximal peaks in response to MYCi975.

Figure 9. ATAC-seq analysis overlapping MYC and at differential ATAC-seq peaks.

Figure 10. MYCi975 induced differential MAX binding and its overlap with MYC

Figure 11. Differential MAX, MGA and MNT chromatin binding alterations in MYCi975-treated cells.

Figure 12. MYCi975 alters H3K27ac activity and chromatin occupancy in cancer cells at enriched sites for FOX factors and nuclear hormone receptors.

Figure 13. 22Rv1 H3K27ac ChIP-seq, quality metrics and increase at MYCi975 type 2 peaks.

Figure 14. MYCi975 reduces FOXA1 and AR protein levels and chromatin occupancy in cancer cells.

Figure 15. MYCi975 enhances the efficacy of anti-hormone therapy.

Figure 16. ATF4 motif enrichment at both sites of open chromatin accessibility and increased H3K27ac ChIP-seq in response to MYCi975.

Figure 17. MYCi975 induces ATF4 signaling.

Table 1. Related to Figure 4.

Table 2. Related to Figures 4 and 5.

Chapter 1: introduction

The MYC transcription factor and rationale for therapeutic targeting

MYC is one of the most widely investigated genes throughout human history. The discovery of MYC is coupled to its functional role in transforming normal cells into malignant disease (1–5). First identification of the nucleotide sequence was found in avian erythroblastosis retroviruses and further characterized to originate from the host genome (1, 5). MYC localization in cells was determined to be nuclear with some insights into functions of gene expression (2, 3). The function of MYC nuclear localization was demonstrated to have a high affinity for binding double-stranded DNA (6). It was then determined that MYC binds double stranded DNA in a sequence specific manner (7). This landmark article predicted the now well characterized sequence specific E-box motif (CACGTG) for MYC. A primary domain of MYC is the basic-helix-loop-helix (bHLH) zipper which classically mediates homo- and/or hetero-dimerization of other bHLH motif containing proteins. Given this domain presence within the MYC protein, it is likely that MYC functions through homo- or hetero-dimerization or both and thus finding MYC binding partners was critical. MYC associated proteins were later found with the use of chemical cross-linkers which led to the discovery of MAX, for which the MYC/MAX heterodimeric nucleoprotein complex was further characterized for its role in neoplastic growth (8–10).

Major technological advances since then have uncovered normal and malignant functions of MYC. In normal biology, mitogenic growth signals temporally up-regulate MYC activity in a cell-cycle dependent manner (11). In part, mitogenic signals alter the protein stability of MYC and thus functional activity. Mitogenic signals activate downstream protein kinases subsequently phos-

phorylating the MYC protein at a cluster of serine and threonine residues which regulate the stability and nuclear localization of MYC proteins (12, 13). In particular, the up-regulated activity of MYC is associated with regulation of cell growth pathways (14). Multiple gene pathways are related to cell growth and further understanding of the distinct cell pathways regulated by MYC is imperative to understanding its role in tumor biology.

As studies have continued, MYC primarily functions as a putative transcription factor and regulates many gene pathways including ribosome biogenesis, mRNA translation, miRNA regulation, cell cycle progression, DNA-replication and -repair, immune response, metabolism and apoptosis (15–17). When cells divide it is necessary to relatively double its size and genome and MYC has been implicated in both processes. MYC target genes include ribosomal proteins, RNA biogenesis machinery and additional factors they are necessary for ribosome biogenesis and assembly (17). Thereby stimulation of MYC may induce cell growth through increased expression of protein synthesis associated genes. In models of MYC induced cell growth using chimeric MYC-ER (estrogen receptor) protein expression, when MYC is activated protein synthesis occurs first and precedes DNA synthesis (14).

MYC has been shown to associate with DNA synthesis complexes such as the preinitiation complex and play a major role at origins of replication on DNA during DNA replication (18). In addition, MYC transcriptional control of cell cycle factors such as E2Fs and cyclins promote cell cycle entry and subsequent DNA synthesis (19). MYC thus binds chromatin at sites of both cell cycle gene regulatory elements and DNA origins of replication in a cell cycle dependent manner.

In the context of cancer, MYC regulates the immune response by transcriptional regulation of programmed death ligand-1 (PD-L1) which is linked to immune evasion, a hallmark of cancer (20). Importantly, upon inactivation of MYC in tumor cells, an immune response is reinvigorated leading to significant increase in tumor regression (20, 21). In this way, tumor cells with high MYC expression have high PD-L1 which disrupts the canonical immune response, hence immune evasion, and MYC inhibition can reverse these effects. MYC is regulated by the dominant nutrient sensor mammalian target of rapamycin complex 1 (mTORC1) at the level of translational regulation (22). mTORC1 inactivation can thus increase MYC nuclear localization and transcription of key metabolic genes. MYC has the potential to regulate miRNA processing through the regulation of Drosha, a canonical component of the miRNA processing machinery (23). In addition, MYC targets miRNAs and regulates their gene expression. In one example, MYC has been implicated to directly control the expression of oncogenic miRNAs in Burkitt Lymphoma (24). Taken altogether, MYC has a vast repertoire of gene targets that are not apparently related. MYC's control of many gene pathways has led to further studies to elucidate whether MYC functions to alter transcription globally or selectively.

Investigations of MYC function on transcriptional output demonstrate both global and selective gene regulation (25–28). In models of lymphomagenesis MYC occupies the promoter of nearly all transcribed genes and functions to selectively regulate genes by both down- and up-regulation (25). To this end, an alternative model demonstrates MYC functions as a global amplifier of transcription and thus increasing total RNA production (27). Another hallmark of the global amplifier model is the concept of MYC enhancer invasion where increased levels of MYC are correlated with increase enhancer occupancy (27). Although two competing paradigms of MYC

function exists; a third model includes the observation that MYC can act as a transcriptional repressor and activator, and gene pathways controlled by MYC can feedback to increase global RNA production (28). In the context of cancer, MYC amplification causes a global increase in MYC mRNA. It is necessary to model MYC-driven tumors in the context of increased expression and understand the downstream chromatin binding events and transcriptional outcomes. Experimental and mathematical modeling studies have suggested that higher levels of oncogenic MYC promote chromatin binding to activate and repress transcription of specific genes (29). The specificity of MYC chromatin binding and gene expression changes in models of MYC overexpression suggest that variations in promoter affinities and cofactor recruitment are underlying determinants that regulate distinct biological processes (30). These models suggest that a predisposed or potentially activated set of factors may underlie the binding sites and downstream transcriptomic or cellular changes. These models include MYC amplification, however models of MYC inhibition are indeed informative as well. Given that a comparison of low-to-high MYC levels accounts for enhancer invasion and a discrete set of transcriptional changes, it is therefore plausible that a high-to-low MYC study, such as using a MYC inhibitor, will inform of high MYC sites and low-MYC sites. If MYC inhibition is partial, or results in downregulation of MYC protein the remaining MYC functionality could inform drug efficacy. In addition, MYC co-factors such as WDR5, may predispose the affinity for MYC binding to certain loci on chromatin (30). Taken together, the alteration of MYC occupancy and thus potential for transcriptional regulation depend on multiple protein factors and models of MYC regulation.

Dysregulated MYC expression is strongly associated with tumorigenesis and is considered a hallmark of cancer, effecting numerous cancer types (31–33). Gene amplification is one of the

most common mechanisms of MYC deregulation in cancer. Considering that MYC activity is up-regulated transiently by mitogenic signals, in the amplification setting MYC may remain constitutively active even in the absence of growth signals. Some of the first findings of MYC amplification were in human cell models of leukemia (34). Copy number amplifications of the genome that include MYC are typically associated with upregulated MYC mRNA expression levels. MYC amplification has been reported in numerous cancer types and is characterized by somatic copy number alterations (SCNA) (35). Utilizing the cancer genome atlas, MYC amplification is present in nearly all cancer types and among the highest amplified are ovary, breast and prostate (36).

For primary prostate cancer the overexpression of MYC by amplification predicts cancer recurrence (37). n-MYC, a homolog of c-MYC, is associated with neuroendocrine phenotype prostate cancer and controls specific genes programs (38). For the majority of prostate cancers, androgen receptor (AR) signaling is the primary driver of disease progression. In prostate cancer tissue both the expression of the AR is positively correlated with MYC expression (39). The androgen receptor functions as a ligand dependent nuclear hormone receptor and in prostate cancer AR signaling increases. Molecular targeting of AR and molecular approaches to reduce systemic androgens (i.e., androgen deprivation therapy) blunt the AR signaling capacity and have served as a standard of care for prostate cancer. However, mechanisms of resistance arise in which androgen signaling can persist even in the presence of AR targeted therapy and are associated with more aggressive prostate cancer attributes like castration resistance (40). A common mechanism of resistant for prostate cancer is the expression of isoforms of AR that are ligand independent which are prognostic markers for disease progression and resistance (41). These AR isoforms maintain

the DNA binding capacity of AR full lengths but lack the ligand binding activation domain. Therefore, the ligand binding site for androgens and anti-androgens is lost and provides a mechanism for sustained AR signaling even with androgen deprivation therapy. The binding profile on chromatin for these isoforms is similar to AR-full length although there tends to be a more repressive effect by the recruitment of repressive complexes to chromatin at key tumor suppressor genes (42). Taken together, in the context of MYC amplification, AR and AR isoform levels tend to correlate and contribute to a more aggressive disease. Therefore, the study of MYC in prostate cancer is directly related to that of AR, and in models where AR signaling is bypassed, MYC amplification is enriched.

MYC dysregulation in cancer has always prompted extended search of small molecules for therapeutic targeting. Throughout the process, however small molecule inhibitors have been difficult to generate for an otherwise intrinsically disordered protein. Many studies have focused on binding to MYC and disrupting the MYC/MAX heterodimerization domain. A dominant-negative mutant MYC peptide (Omomyc) was developed that binds directly to MYC and abrogates MYC function by disrupting MYC/MAX heterodimerization (43, 44). Omomyc peptides specifically bind to both c-MYC, n-MYC and MAX and it prevents the chromatin binding of MYC at canonical E-box containing motifs and reduces target gene expression (43). MYC function includes induction of apoptosis. In the E μ -myc transgenic mouse model, experiments suggests that progression of MYC-driven tumors may require inactivation of p53 to suppress the apoptotic signaling enhanced by MYC overexpression (15, 45). These data suggest that MYC regulation of apoptosis must be attenuated by down regulation of key factors such as p53. Importantly for the study of

Omomyc, MYC inhibition occurs at cancer specific genes and the remaining MYC function enhances apoptosis (44). The genomic distribution of MYC at target gene promoters and enhancers can provide additional clues to the transcriptionally oncogenic properties of MYC. In models of MYC/MAX heterodimer inhibition with Omomyc peptide, promoter occupancy of MYC target genes was found to be significantly altered (46). These data suggest a therapeutic opportunity for the inhibition of MYC in cell and tumor models of MYC driven cancers. Achieving a deliverable expression of Omomyc peptides or future iterations in the clinical setting seems implausible, and thus small molecule inhibitors have been generated to probe MYC function as well as test the potential efficacy of therapeutically targeting MYC.

Inhibition of MYC has been difficult due to multiple factors. There is no defined ligand binding domain and therefore identifying a pharmacophore for MYC has been a major challenge (47). Conceptually, given that MYC regulates multiple cell processes how could the effects of an inhibitor spare the normal cell function of MYC while specifically targeting cancer cells. Small molecule MYC inhibitors aim to alter oncogenic MYC activity and disrupt the MYC/MAX heterodimerization. Several small molecule inhibitors (e.g. 10075-G5, 10058-F4) disrupt MYC/MAX dimerization and have been shown to reduce MYC activity (48, 49). Some of the inhibitors have known putative MYC binding sites that have been determined and pharmacophores identified (50). Other approaches have included the use of covalent inhibitors to disrupt MYC function (51). Use of various inhibitors as molecular probes has led to a significant increase in knowledge regarding MYC function and a continued focus on the potential of MYC inhibitors as cancer therapeutics (49). Small molecule inhibitors of the transcription of MYC have also been demonstrated to inhibit MYC-driven cancers (52). JQ1 is a bromodomain and extraterminal (BET) inhibitor specifically

targeting BRD2, BRD3 and BRD4 and disrupts their function (52). BRDs function by binding acetylated chromatin which has subsequent effects on downstream transcriptional activation, in particular MYC transcription. Thus, in MYC-driven cancers inhibition of chromatin recruitment of BET domain binding to regulatory elements of MYC will inhibit MYC transcription and downstream MYC processes. In addition, small molecules have been generated that promote MAX-MAX homodimerization and function to inhibit MYC (53). MAX-MAX homodimers and MYC/MAX heterodimers have affinity for the same E-box sequence genome wide, although each nucleoprotein complex has been implicated in contrasting transcriptional roles. KI-MS2-008, a small molecule MAX homodimerizing compound, promotes MAX binding at sites where MYC occupancy is lost on chromatin and induces further gene repression (53). The major challenge is the development of MYC inhibitors with clinical applicability. Although MYC inhibition has been utilized as a non-genetic tool to understand MYC inhibition and MYC biology, the extended research has yet to find clinical applicability. In fact, many of the small molecules developed over the years have failed to be approved, due to a multitude of reasons including toxicity, low potency and selectivity (49). Continued research and development of MYC inhibitors has a heightened awareness of their clinical challenges and aims to address these hurdles.

Given that MYC generally functions as a transcription factor, it is critical to understand the molecular mechanisms by which MYC inhibitors limit chromatin binding of MYC and the formation of MAX heterodimers, and the subsequent effects on target gene expression. Given MYC has a wide range of gene networks, understanding the total cisomic and transcriptomic changes that transpire as a result of MYC inhibition may give insight into potential selectivity and rational combination therapies. In addition, unbiased approaches that aim to recover MYC alterations as

well as additional factors and processes that are inhibited will elucidate the complete mechanism of small molecule inhibitors. Drug efficacy may be further elucidated by the discovery of primary and secondary effects. It is important to understand that pharmacology is within an exaggerated mechanism paradigm, by which a majority of cancer therapeutics tested demonstrate drug efficacy is driven by off-target effects (54–57). Using CRISPR/Cas9 mediated knockout there was no effect on the proliferation of cells when the intended drug target was completely deleted (57). Off-target effects can help understand drug efficacy and further their advancement by way of alleviating or enhancing the process the off-target effect induces. For example, cells resistant to OTS964, a putative PBK inhibitor, demonstrated inactivating mutations for CDK11 which led to the discovery OTS964 binding to CDK11 and further advancement in treating cancer by CDK11 inhibition (57). Off-target effects of safe drugs may lead to further advancement of cancer treatment models, and they may explain the treatment efficacy which can be leveraged. In an age of high-volume genomic sequencing and personalized medicine, expression markers need to match drug targets and there is a need to find cause not just correlation. For novel small molecule MYC inhibitors, the full spectrum of effects and potential targets needs to be identified. Models of cancer therapeutics and targets have demonstrated that on average for hundreds of small molecules there are numerous targets per molecule. It is therefore naive and extremely exaggerated to discuss small molecules as binding one target. Rather the likelihood is multiple targets, and it is up to researchers to find out which targets drive efficacy.

In the context of small molecule inhibitors, there will always be a partial defect to the targets of interests, whereby the drugs limit the function of their intended target without complete loss of function. Whether MYC inhibitors selectively modulate MYC binding and/or target gene

expression is not clear but has important implications for tolerability as a cancer therapeutic. Furthermore, the histone epigenetic landscape may provide further mechanistic insight into the effects of MYC inhibition. Histone H3 lysine 27 acetylation (H3K27ac) is an epigenetic mark of active promoters and enhancers, and MYC has been shown to recruit histone acetyltransferases and induce genome-wide chromatin acetylation at histone H3K27 (58, 59). Binding of MYC at enhancers in models of MYC amplification demonstrate enhancer invasion and a variant MYC DNA binding profile (27). Unbiased approaches that are integrated with multiple datasets provides a more complete picture into the effects of small molecules as therapeutic and the mechanism of action. Understanding the epigenetic landscape overlapping MYC binding sites indicates associated active chromatin marks, and in the context of MYC inhibition sites with co-loss of MYC and H3K27ac will likely decrease transcriptional activity. MYC inhibition induced alterations of H3K27ac outside of the MYC cistrome may represent secondary effects of MYC target genes.

We recently developed and characterized a small molecule MYC inhibitor, MYCi975, that binds directly to MYC, disrupts MYC/MAX dimerization, and promotes proteasomal mediated MYC degradation resulting in decreased tumor growth *in vivo* (60, 61). MYCi975 was rigorously tested for mechanisms of action and has been shown to induce MYC protein proteasomal mediated degradation (60). In addition, *in vivo* tolerability of MYCi975, which has been a common pitfall of developed MYC inhibitors, allowed for the fundamental understanding that MYCi975 induces an immune response in syngeneic mouse prostate tumors. The immune response induced by MYCi975 can be leveraged and combination treatment with anti-PD1 potentiates immune therapy in mouse prostate tumors, of which checkpoint therapy in prostate cancer has been largely unsuccessful (60, 62). To further understand the efficacy of MYCi975 and the potential MYC regulated

pathways spared in the MYC inhibitor setting, we elucidated the epigenomic and transcriptomic changes induced by MYCi975 in prostate cancer cells. In this work, we examined the sensitivity of MYC/MAX binding sites and the global epigenomic landscape to MYCi975, established the extent to which MYCi975 limits MYC genomic function, and provide evidence supporting the rationale for combination cancer therapies. We also provide analysis of secondary transcription factor activation that contributes to apoptotic signaling in cancer cells treated with MYCi975 and provide additional pathways that in part explain MYCi975 efficacy.

Chapter 2: MYCi975 selectively inhibits the MYX and MAX cistromes to modulate target gene expression

All panels from figures 1-15 are references from the original (63). Figures 1-14 were generated in original format by Austin G. Holmes. Figure 15A was data generated by Mihai I. Truica and Figures 15B-E were data generated from Vinay Sagar.

The MYC cistrome is altered at canonical targets and genome-wide in response to MYCi975 to regulate specific gene expression programs

To profile changes in MYC occupancy and target gene expression in response to MYCi975 treatment, we first evaluated the kinetics of MYC protein down-regulation in response to 10 μ M MYCi975 for 1, 4, 8, 24, and 48 hours in the high MYC expressing 22Rv1 prostate cancer cell line. In a time-dependent manner, MYCi975 induced MYC protein down-regulation, achieving approximately > 90% decrease of MYC protein levels by 48 hours (Figure 1A). Protein levels of MYC heterodimeric binding partner MAX and related protein MNT were also reduced (~20-30% at 48h), while MXD1 protein levels remained relatively stable; (Figure 1A, B). 10 μ M MYCi975 reduced 22Rv1 cell proliferation by half, represents the IC₅₀ of 22Rv1 cells, suppressing cell

growth and colony formation after 4 days and reducing cell viability (Figure 1C-F). MYCi975 treatment induced poly(ADP-ribose) polymerase (PARP) cleavage, a hallmark of apoptosis, in 22Rv1 cells (Figure 1G) suggesting apoptosis as a possible mechanism for MYCi975-induced cell death. Based on these results we chose to perform genome-wide analysis on cells treated with MYCi975 for up-to 48 hours.

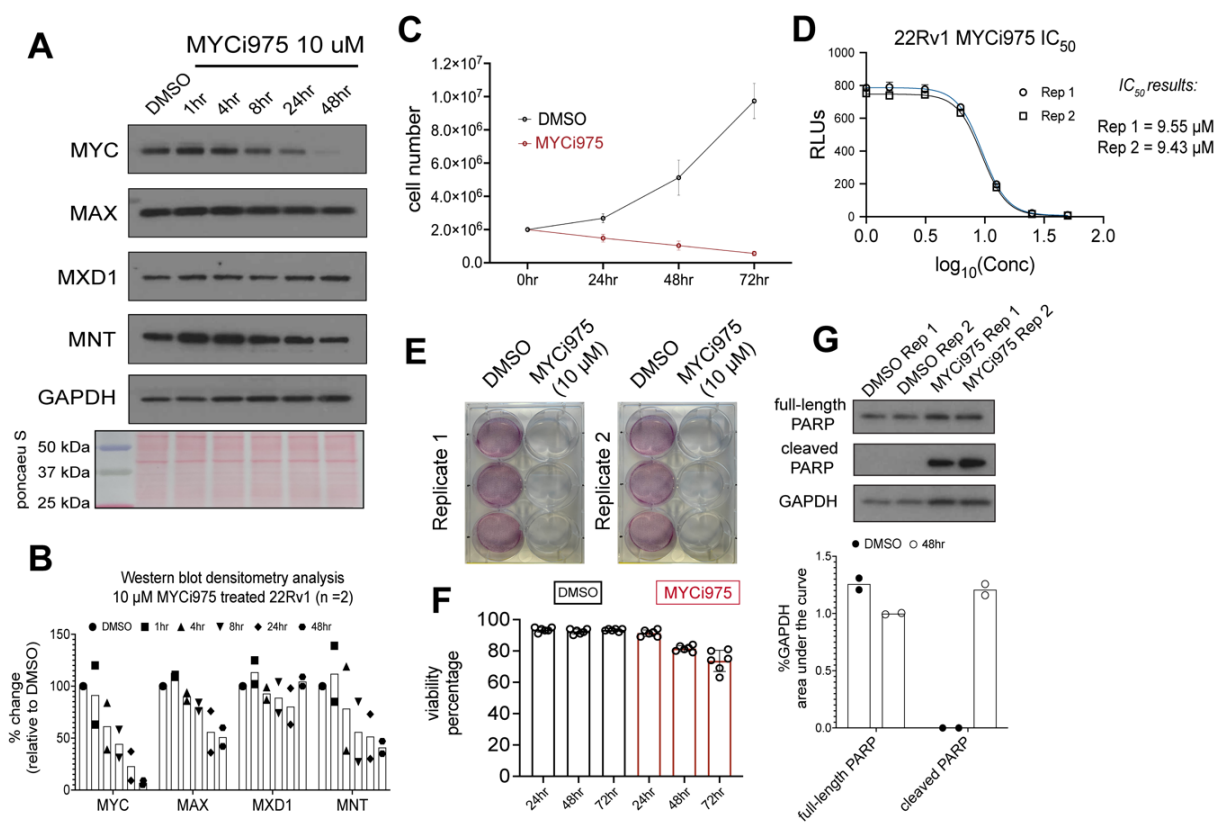


Figure 1. MYCi975 induces MYC down-regulation and cell growth defects in 22Rv1 cells.

(A) 22Rv1 cells were treated with 10 μ M MYCi975 for the indicated times followed by immunoblot analyses for the indicated proteins. **(B)** Densitometry analysis of MYC family proteins (n=2) processed by ImageJ (64) with the area under the curve method representing the signal as a percentage of loading control protein GAPDH for two biological replicates. Loading control GAPDH was set to 100% and each timepoints was compared relative to GAPDH (individual values shown, bars represents sample mean). **(C)** Total cell number of 22Rv1 cells as determined by trypan blue exclusion assay for both vehicle control and 10 μ M MYCi975-treated 22Rv1 cells (n = 4, errors bars represent \pm SEM). **(D)** IC₅₀ curve analysis of 22Rv1 cells treated for 3 days. IC₅₀ values were calculated using log₁₀(μ M MYCi975) vs. response sigmoidal curves and nonlinear regression. **(E)** 22Rv1 cells were plated in 6-well plates at low density (25,000 cells/well), treated with MYCi975 (10 μ M) for 4 days, and visualized by staining with 0.1% crystal violet. **(F)** Cell viability as determined by trypan blue exclusion assay of both vehicle control and 10 μ M MYCi975-treated 22Rv1 cells (n = 4, individual values shown, bar represents sample mean, error bars = standard deviation). **(G)** 22Rv1 cells were treated with 10 μ M MYCi975 for 48 hrs and 20 μ g of whole cell protein extract was used to determine poly(ADP-ribose) polymerase (PARP) and cleaved-PARP protein levels (individual values shown, bar represents sample mean).

Next, we performed MYC chromatin immunoprecipitation (ChIP)-seq in 22Rv1 cells treated with MYCi975 for 1, 4, 8, 24, and 48 hours. Principal component analysis (PCA) demonstrated clustering of the early timepoints (1-, 4- and 8-hour groups), whereas continued treatment led to a maximum separation of the 24- and 48-hour groups (Figure 2A). This suggested that the effects of MYCi975 on MYC chromatin occupancy are coincident with MYC protein degradation. Consistent with this possibility, we found that after 1 hour of MYCi975 treatment, both the total peak number and ChIP efficiency remained relatively stable; at all other timepoints, these values were significantly reduced (Figure 2B-C). Differential binding analysis comparing each MYCi975 timepoint to the DMSO-treated control group revealed time-dependent effects of MYCi975 treatment on MYC chromatin occupancy. Significant changes in MYC ChIP-seq signal were evident as early as 8 hours after MYCi975 treatment (327 differentially bound peaks, FDR < 0.01). Maximal differential MYC binding was found in the 48-hour MYCi975-treated cells (28,056 peaks, FDR < 0.01) where more than 62% of the total MYC cistrome was altered (Figure 2D). We defined the peaks with statistically significant changes (FDR < 0.01) in MYC occupancy as “MYCi975-sensitive” sites. Genome distribution analysis showed that early MYCi975-sensitive sites are significantly enriched for promoter-distal (>2kb from nearest transcription start site [TSS]) bound MYC and have low c-Myc motif significance compared to later timepoints (Figure 2E). To analyze the global changes in the MYC-bound promoter network in response to MYCi975, we integrated promoter annotation and gene set enrichment analysis (GSEA) (65). MYC consensus peaks were

annotated in reference to the nearest TSS to define promoter-proximal (± 2 kb from the TSS) and promoter-distal (more than ± 2 kb from the TSS) MYC binding sites. MYC-bound promoter-proximal sites were ranked based on fold change and FDR from differential peak analysis. Differential MYC-bound promoters revealed significant loss of canonical MYC target gene programs (“HALLMARK_MYC_TARGETS_V2”, Figure 2F). Cell cycle gene pathways are among the canonical MYC target gene lists and figure 2 G-H demonstrates downregulation of MYC occupancy and RNA at both cell cycle genes *MCM2* and *MCM10*.

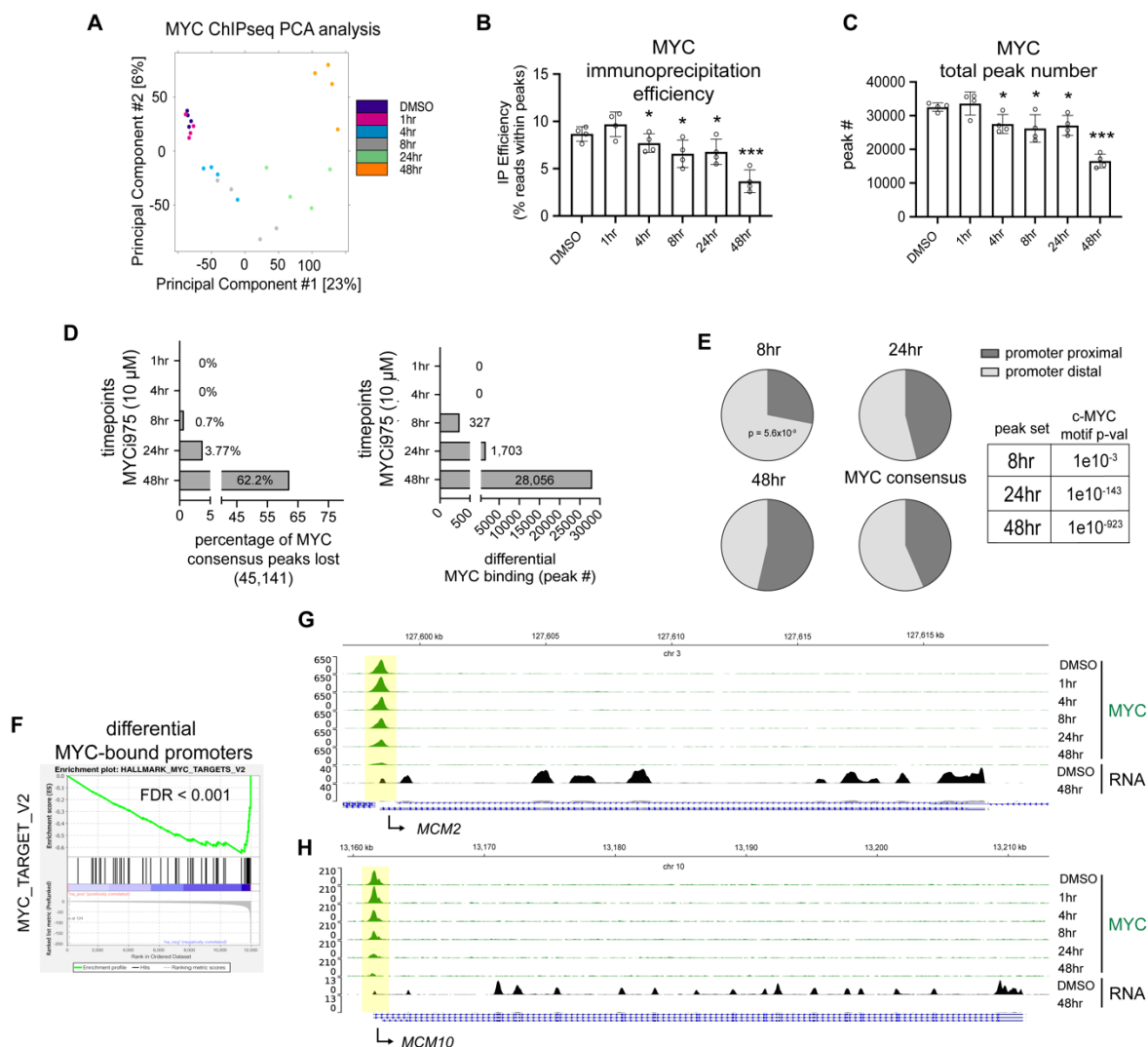


Figure 2. Analysis of differential MYC binding in 22Rv1 cells demonstrates loss of occupancy at canonical MYC target genes. (A) PCA analysis of differential peaks of all MYC ChIP-seq biological replicates for each timepoint ($n = 4$ for each timepoint). **(B)** Immunoprecipitation (IP) efficiency (% of reads within peaks) of all MYC ChIP-seq biological replicates. **(C)** Total peak number in all biological replicates of MYC ChIP-seq samples. (individual values shown, bar represents sample mean, error bars represent mean \pm SEM, * $p < 0.05$; *** $p < 0.0001$) **(D)** Percentage of differential MYC binding peaks lost in response to MYCi975 compared to MYC

consensus peaks ($n = 4$, left panel). Total number of differentially bound MYC peaks following differential binding analysis ($n = 4$, right panel) for each timepoint. **(E)** Pie chart distribution of 8-, 24- and 48-hr differential MYC-bound peaks significantly altered ($FDR < 0.01$) by MYCi975 and MYC consensus peaks from control conditions. The cumulative distribution function (CDF) of the hypergeometric distribution was used to test for significant differences in differential peak set distribution (promoter-proximal [± 2 kb from TSS], promoter-distal [$> \pm 2$ kb from TSS]) using each timepoint vs. MYC consensus peaks. Each peak set was used as input for motif enrichment and the statistical p-value reported (right panel). **(F)** Differential gene expression analysis was pre-ranked (same as for ChIP-seq data) and used as input for GSEA. Results demonstrated significant enrichment for canonical MYC target genes. **(G, H)** Gene loci analysis of *MCM2* and *MCM10* reveals MYC chromatin occupancy loss (green) with associated RNA level loss (black) in response to MYCi975 in 22Rv1 cells.

To investigate both MYCi975-sensitive sites and those with an $FDR > 0.01$ (“MYCi975-insensitive”) we analyzed both MYC and well characterized MYC co-factor WDR5 (66). We plotted the normalized tag density of both MYC and WDR5 chromatin binding at MYCi975-sensitive and MYCi975-insensitive peaks and found that both MYC and WDR5 tag density is significantly lower at MYCi975-insensitive sites (Figure 3A). Genome wide distribution analysis of both peak sets revealed that MYC bound MYCi975-insensitive sites were predominantly promoter distal (Figure 3B). Surprisingly, both peak sets contained significant motif enrichment for the canonical c-Myc motif (Figure 3C). MYCi975-insensitive peaks annotated to promoters were used as input for gene ontology analysis demonstrating significant enrichment for nervous system development

and cell differentiation suggesting downstream MYC regulated gene pathways may remain unaltered (Figure 3D). Further analysis is focused on the statistically significant MYCi975-sensitive sites.

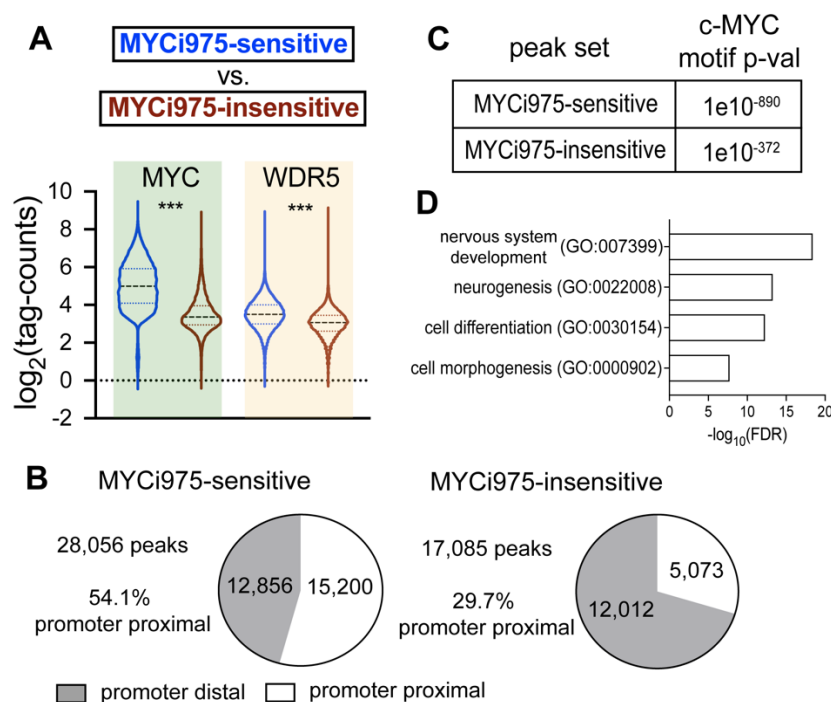


Figure 3. Genomic distribution and co-factor WDR5 occupancy at MYCi975 sensitive and insensitive sites. (A) Log₂(tag-counts) of MYC (shaded green) and WDR5 (shaded brown) ChIP-seq signal at both MYCi975-sensitive (blue) and peaks where differential MYC binding analysis in MYCi975 treated 22Rv1 cells was insignificant (MYCi975-insensitive, red). A two-tailed unpaired parametric t-test was run on MYCi975-sensitive vs. MYCi975-insensitive log₂(tag-counts). (***)p < 0.0001 **(B)** Both MYCi975-sensitive and MYCi975-insensitive peaks were split into promoter-proximal ($\pm 2\text{kb}$ from TSS) or promoter distal ($> \pm 2\text{kb}$ from TSS). **(C)** Canonical c-Myc motif enrichment analysis of both MYCi975-sensitive and MYCi975-insensitive sites. **(D)**

Gene ontology analysis (<http://geneontology.org>) of promoter proximal annotated MYC peaks where differential binding was insignificant (MYCi975-insensitive, 5,073 peaks from right panel (B)).

Our previous study of transcriptomic profiles after exposure to MYCi975 demonstrated disruption of canonical MYC gene programs (60). To determine the time-dependent effects of MYCi975 on gene expression, we treated 22Rv1 cells with MYCi975 for 24 and 48 hours to induce extensive MYC chromatin occupancy loss, and then performed RNA-seq. To control for RNA abundance levels, we included a spike-in control and isolated the same number of cells for each MYCi975 treatment timepoint. We filtered gene expression based on the lower limit of detection determined by the spike-in control and plotted the lower limits of detection (Figure 4A). We found no significant difference in total RNA yield in 22Rv1 cells treated with MYCi975 for 24 or 48 hours compared to controls (Figure 4B). As a quality control, we used a Euclidean sample distance matrix to assess sample similarity (\log_2 normalized counts, DESeq2 (67)), which confirmed that the MYCi975-treated samples were similar to each other and distinct from controls (Figure 4C).

We next performed differential gene expression analysis comparing DMSO control vs. 24-hour MYCi975 or DMSO control vs. 48-hour MYCi975 treatment. The 24- and 48-hour MYCi975-treated cells had 6,973 and 9,080 differentially expressed (DE) genes, respectively (FDR < 0.01) (Table 1). Differential gene expression data was pre-ranked ($-\log_{10}\text{FDR} \times \log_2\text{Fold-Change}$) and used as input for GSEA (65, 68). The top differential gene program, “HALL-MARK_MYC_TARGETS_V2”, was suppressed in both 24- and 48-hour MYCi975-treated cells; we found that the same gene set contained promoter-proximal MYCi975-sensitive sites (Figure 4D, Table 1). Taken together, these findings suggest that MYCi975 treatment results in the loss of

MYC chromatin occupancy and associated gene expression at hallmark MYC target genes, including the key cell cycle-associated genes *MCM2* (Figure 2G) and *MCM10* (Figure 2H). Interestingly, from analysis of the 327 MYC lost peaks at 8h, 93 are promoter proximal. Gene ontology on the 93 genes reveals the following gene sets are weakly significant (FDR < 0.01): DNA metabolic process (GO:0006259), heterocycle metabolic process (GO:0046483) and DNA replication (GO:0006260) and *MCM10* is identified as one of these early MYCi975 response genes.

To further analyze the MYCi975-regulated transcriptome and identify common dysregulated genes in multiple cancer cell models, we integrated our RNA-seq results comparing DMSO vs. 10 μ M MYCi975 for 24 hours in 22Rv1 cells with previously reported RNA-seq datasets (PC3: 8 μ M for 24 hours, P493-6: 6 μ M for 24 hours) (60). Overlapping differentially expressed genes (FDR < 0.01) for each dataset were visualized using a Venn diagram (Figure 4E). A total of 1,183 genes were dysregulated by MYCi975 in all three datasets. Gene ontology analysis of this common gene list revealed significant enrichment for regulation of nucleic acid metabolism, DNA replication, and cell cycle pathways (Figure 4E, right panel). These data suggest that MYCi975 has a significant effect on a core set of DNA synthesis and cell cycle progression genes.

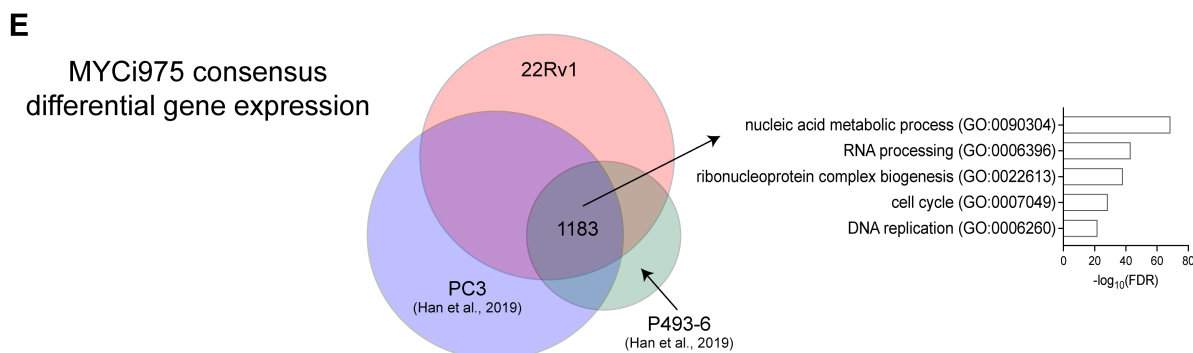
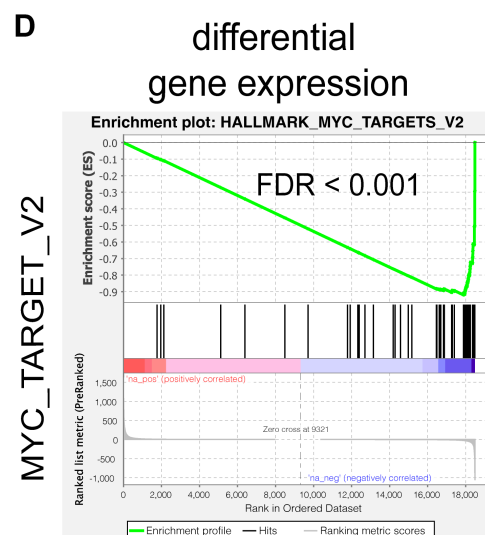
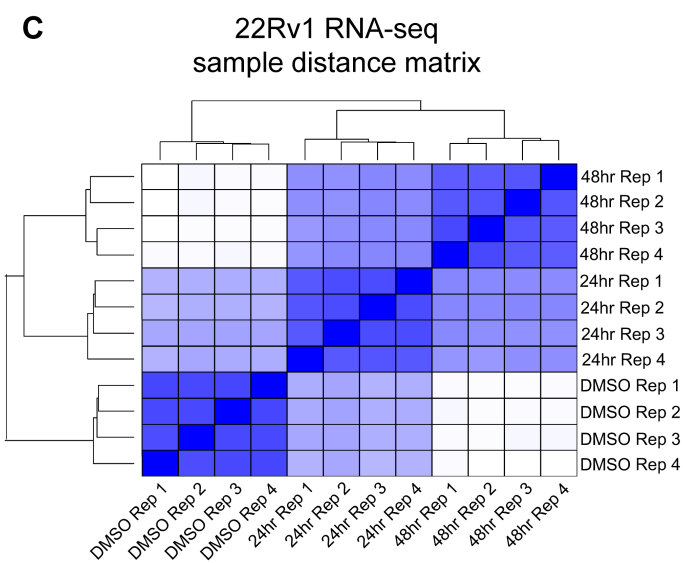
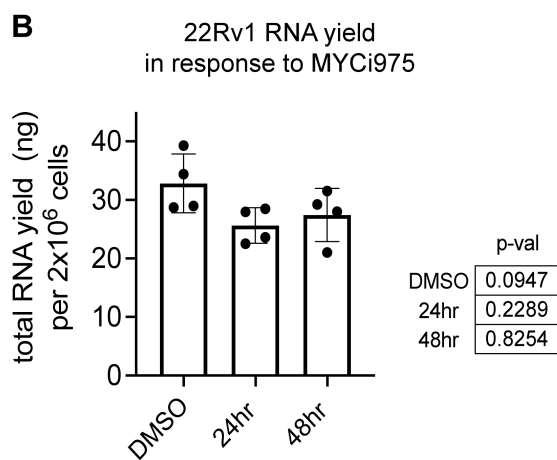
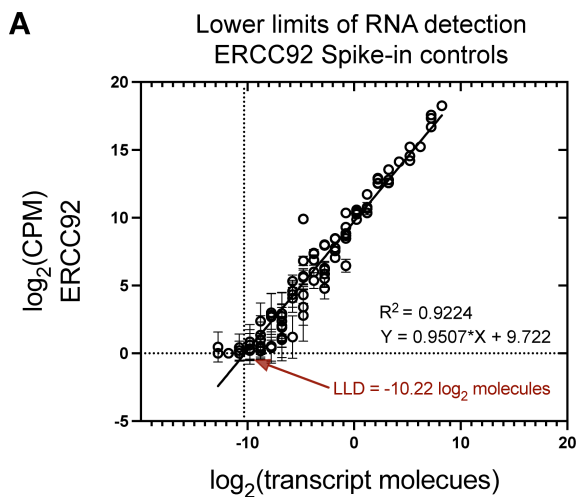


Figure 4. Differential gene expression induced by MYCi975 in 22Rv1 cells. (A) Correlation plot for \log_2 (ERCC92 transcript molecules) detected within RNA-seq samples and the \log_2 (known transcripts molecules) to assess the lower limits of gene expression detection. (B) Total RNA yield from 2×10^6 22Rv1 cells treated with either DMSO or 10 μ M MYCi975 for 24 or 48 hrs. One-way ANOVA analysis to test for significance of variance results are listed (right panel). (individual values shown, bar represents sample mean, errors bars = standard deviation). (C) Sample distance matrix calculations of \log_2 normalized gene counts by DESeq2 with biological duplicates and all timepoints for RNA-seq in MYCi975-treated cells. (D) Differential gene expression analysis was pre-ranked (same as for ChIP-seq data) and used as input for GSEA. Results demonstrated significant enrichment for canonical MYC target genes. (E) Publicly available RNA-seq results from MYCi975-treated PC3 and P493-6 cells ((60), GSE135877) was used to overlap consensus dysregulated genes. All differentially expressed genes were analyzed for overlap. In total, 1,183 genes were differentially expressed in all cell lines. Gene ontology enrichment analysis was run on the 1,183 consensus genes and the top enriched gene sets are reported (lower panel, <http://geneontology.org>).

MYCi975 selectively affects MYC binding to promoters and target gene expression

To analyze the global binding patterns of MYC and the downstream transcriptional impact in response to MYCi975, we integrated differential binding analysis at MYC-bound promoters with differential gene expression analysis. We categorized MYC-bound sites into ‘types’ based on whether MYCi975 led to loss of MYC binding and changes/no changes in the RNA levels of target genes (Figure 5A, Table 2). Among the MYC-bound promoters within MYCi975-sensitive sites, we found that associated target gene expression was either decreased (Type 1), increased (Type 2), or unchanged (Type 3) (Figure 5A, B). Figure 2C shows representative examples of MYCi975 target gene Types 1-3. Using gene ontology analysis, we found that Type 1 genes were significantly enriched for cell cycle and DNA replication gene programs generally important for conferring proliferative advantages to cancer cells (Figure 5D, top panel, Table 2). Type 2 genes were strongly enriched for kinase and signal transduction pathways (Figure 5D). Notably, Type 2 genes among others included *ROR α* , a transcription factor known to play a tumor suppressive role in breast cancer by stabilizing p53 and activating p53 gene transcription (69, 70). Type 3 genes, which demonstrated changes in MYC promoter occupancy with no change in RNA levels, were significantly enriched for basic RNA metabolic processes and core transcriptional pathways important for normal cell function (Figure 5D, lower panel). Overall, these data indicate that the effects of MYCi975 on MYC-binding to target gene promoters and subsequent changes in RNA levels are not uniform, with MYC target genes representing cell cycle and DNA replication genes more sensitive to the effects of MYCi975 than MYC target genes involved in basic RNA metabolic and gene transcription processes.

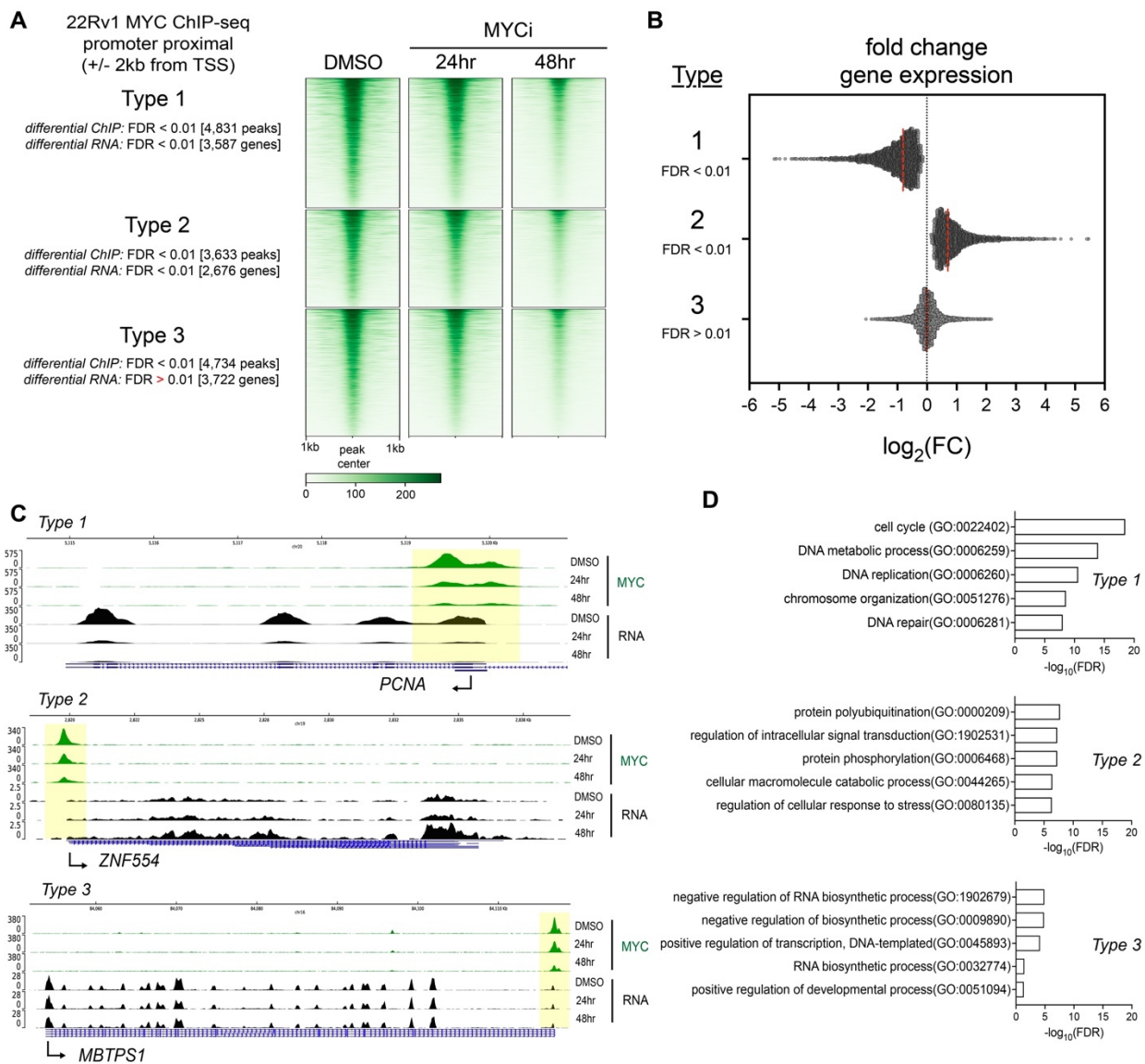


Figure 5. MYCi975 selectively affects MYC binding to promoters and target gene expression.

(A) Heatmap representation of ChIP-seq signal at annotated promoters of MYCi975-sensitive sites (Types 1, 2 and 3). **(B)** $\text{Log}_2(\text{foldchange})$ of genes for each Type as calculated from differential gene expression analysis of DMSO vs. 48-hr MYCi975-treated 22Rv1 cells. These genes have an occurrence of MYC bound at or near the promoter. The red dotted line indicates the mean $\text{log}_2(\text{foldchange})$ for each Type. **(C)** Genome browser tracks of representative genes for each MYCi975 gene Type, demonstrating outcomes of MYC ChIP-seq data (green) and RNA-seq data (black). **(D)** Type 1-3 genes were used as input for gene ontology enrichment (<http://geneontology.org>). The top 5 results for each gene Type are displayed.

We investigated the MYCi975-insensitive promoter proximal peaks and integrated differential expression levels. There was a final type (Type 4, consisting of MYCi975-insensitive peaks) of target genes that had far fewer tag density when compared to the other three types and for which MYC binding and target gene expression remained unchanged after MYCi975 treatment (Figure 6A-C). MYC binding and gene expression changes in Type 4 were not statistically significant (both differential binding and RNA levels with an FDR > 0.01) when compared to the other three types and therefore were not further investigated.

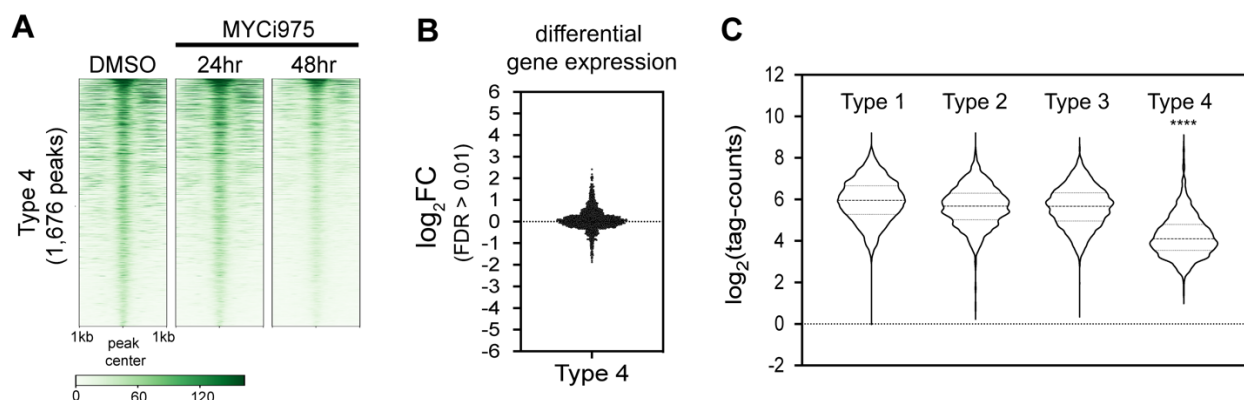
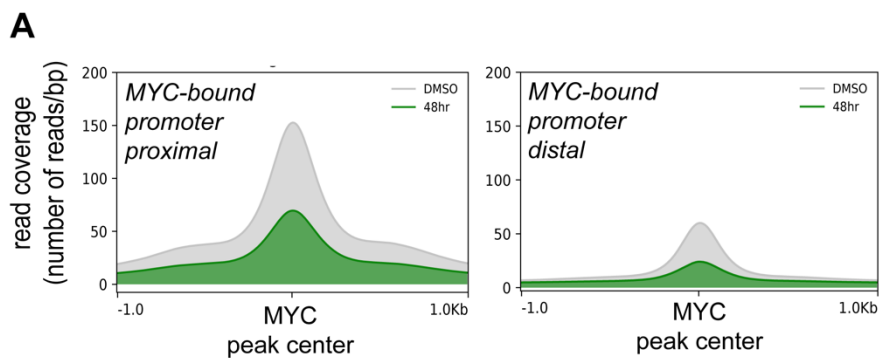


Figure 6. Type 4 MYCi975 insensitive sites and comparison with MYCi975 types 1-3. (A) MYCi975 Type 4 target gene heatmap representation demonstrating MYC promoter occupancy in cells treated with DMSO control or MYCi975 for 24 and 48 hrs. **(B)** $\text{Log}_2(\text{fold change})$ of MYC target genes in MYCi975 Type 4 sites demonstrating all genes with no significant change in RNA levels in DMSO vs. 48-hr MYCi975 treatment. **(C)** $\text{Log}_2(\text{tag-counts})$ for MYCi975 target gene Types 1-4. Using one-way ANOVA and Tukey's multiple comparison test with a single pooled variance, MYCi975 Type 4 target genes demonstrate a decrease in tag density compared to MYCi975 Type 1-3 target genes (**** $p < 0.0001$).

The MYCi975-sensitive MYC cistrome differs at promoter-proximal and promoter-distal regions

To further analyze MYC chromatin occupancy at genomic regions beyond promoters, we split MYC-bound sites into promoter-proximal and promoter-distal peaks (71). MYC-bound sites in 22Rv1 cells consisted of 20,915 promoter-proximal and 27,108 promoter-distal peaks. To determine the extent to which MYCi975 sensitivity encompasses both genomic regions, we plotted read coverage in both vehicle control and MYCi975-treated cells at MYC-bound promoter-proximal and promoter-distal sites (Figure 7A). MYC occupancy was reduced at both regions following MYCi975 treatment. Motif analysis of MYC promoter-proximal peaks demonstrated significant enrichment for canonical E-box sequences (Figure 7B), whereas MYC promoter-distal peaks demonstrated significant enrichment for CTCF and FOX motifs, along with canonical MYC motif enrichment (Figure 7C), suggesting a possible transcription factor cooperativity at promoter-distal sites in regulating target genes.



B promoter proximal motif analysis

Rank	Factor	Motif	p-val	%TWM %BWM
1	C-MYC		1e10 ⁻⁴³³	19.0 9.02
2	N-MYC		1e10 ⁻⁴³⁰	17.6 8.05
3	MAX		1e10 ⁻⁴¹³	14.2 5.93
4	MNT		1e10 ⁻³⁸⁴	15.6 7.08
5	CLOCK		1e10 ⁻³⁵⁵	13.3 5.77
19	CTCF		1e10 ⁻¹⁵³	4.14 1.47
55	FOXA1		1e10 ⁻³⁹	4.00 2.46

C promoter distal motif analysis

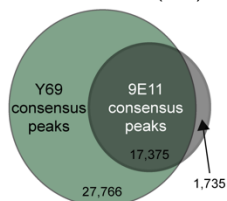
Rank	Factor	Motif	p-val	%TWM %BWM
1	CTCF		1e10 ⁻²⁴²⁰	12.0 0.91
2	FOXA1		1e10 ⁻¹⁹⁰⁶	30.4 9.92
3	FOXA2		1e10 ⁻¹⁸⁹⁴	25.2 6.99
4	FOXM1		1e10 ⁻¹⁸²⁰	30.3 12.0
5	FOXA3		1e10 ⁻¹⁶³⁰	15.2 2.88
17	C-MYC		1e10 ⁻⁹⁴⁵	16.6 5.44

Figure 7. MYC-bound promoter-distal sites exhibit significant CTCF and FOX factor motif enrichment. (A) MYC consensus peaks were separated into promoter-proximal (± 2 kb from TSS) or promoter distal ($> \pm 2$ kb from TSS). The mean MYC ChIP-seq read coverage is plotted at both promoter proximal and distal MYC-bound sites in vehicle control and 48-hr MYCi975-treated 22Rv1 cells. (B) Motif enrichment analysis of MYC-bound promoter-proximal peaks, listing the top 5 enriched motifs, in addition to CTCF (#19) and FOXA1 (#55) for contrast (%TWM = percentage of targets with motif, %BWM = percentage of background with motif). (C) Motif enrichment analysis of MYC-bound promoter-distal peaks, listing the top 5 and including c-MYC (#17).

To validate these findings and enhance rigor, we used an alternative MYC antibody (clone 9E11, see Methods). More than 90% of 9E11 MYC-bound peaks overlapped with those identified with the clone Y69 antibody used above (19,110 peaks recovered with 9E11 and 45,141 with Y69: Figure 8A). Although the total peak number for the clone 9E11 antibody was lower, motif analysis of both promoter-proximal and promoter-distal sites recapitulated the CTCF and FOX factor enrichment at promoter-distal regions demonstrated with Y69 (Figure 8 B, C). To directly test the extent to which MYC-bound promoter distal sites are enriched for CTCF, we performed CTCF ChIP-seq following 48-hour MYCi975 treatment, given that MYC occupancy is significantly reduced at tens of thousands of sites at the 48-hour MYCi975 treatment timepoint. In total, CTCF chromatin occupancy was altered at only 4,719 peaks, comprising 6.91% of the CTCF cistrome (4,719/68,274). To determine whether MYC binding affects CTCF occupancy, we plotted both MYC and CTCF signals centered at MYC -bound MYCi975-sensitive sites (Figure 8 D, E). Differential binding analysis demonstrated that CTCF occupancy at MYC-bound MYCi975-sensitive sites remains relatively stable and unaltered after 48 hours of MYCi975 treatment, suggesting CTCF binding is not dependent on co-occupancy of MYC (Figure 8E). Of the differential lost CTCF sites, only 85 (0.3%) overlapped with MYCi975-sensitive sites (Figure 8F). To further examine the general occurrence of motif enrichment at promoter-distal MYC peaks in independent data sets, we analyzed motif enrichment for MYC, FOXA1, FOXM1, and CTCF in publicly available MYC ChIP-seq datasets from multiple cancer cell lines representing diverse tissues of origin. Of the 10 cell lines analyzed, 22Rv1 cells from our study and five cell lines (MCF7 - breast, MCF10A - breast, NB4 - leukemia, P493-6 - lymphoma and HeLa - cervical) (72–74) displayed significant motif enrichment for CTCF at MYC-bound promoter-distal peaks, whereas 22Rv1,

MCF7, MCF10A and MycCap cancer cell lines also showed motif enrichment of FOX factors (Figure 8G). Together, these results suggest that binding of MYC, CTCF, and FOX family transcription factors to promoter-distal sites may be necessary for MYC target gene expression in nuclear hormone receptor-positive prostate and breast cancer cells. Supporting our observations, FOX factors have been shown to function as pioneering factors for chromatin accessibility by nuclear receptors such as the androgen receptor (AR) and estrogen receptor (ER) in prostate and breast cancer cells, respectively (75, 76). CRISPR-based deletion and HiC-based chromatin looping assays will be necessary to address the possibility of factor cooperativity in future studies.

A 9E11 vs. abcam (Y69)



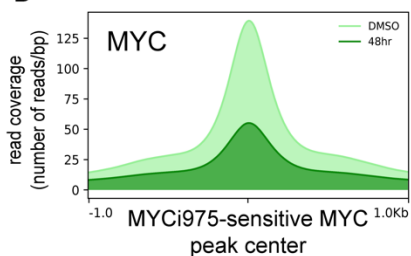
B 9E11 promoter proximal

Rank	Factor	Motif	p-val	%TWM %BWM
1	C-MYC		1e10 ⁻³²⁷	23.7 9.92
3	CLOCK		1e10 ⁻²⁸⁹	20.7 8.36
51	CTCF		1e10 ⁻³²	3.31 1.57
95	FOXA2		1e10 ⁻¹³	2.35 1.71

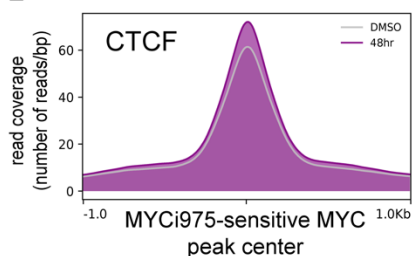
C 9E11 promoter distal

Rank	Factor	Motif	p-val	%TWM %BWM
3	C-MYC		1e10 ⁻⁷²⁵	28.8 8.52
8	CLOCK		1e10 ⁻⁶⁰⁹	23.1 6.42
11	CTCF		1e10 ⁻³⁹⁵	3.31 1.57
14	FOXA1		1e10 ⁻¹³	2.35 1.71

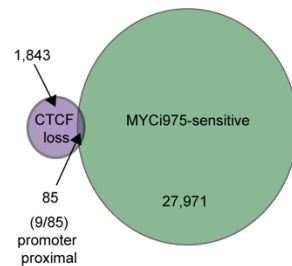
D



E



F



G

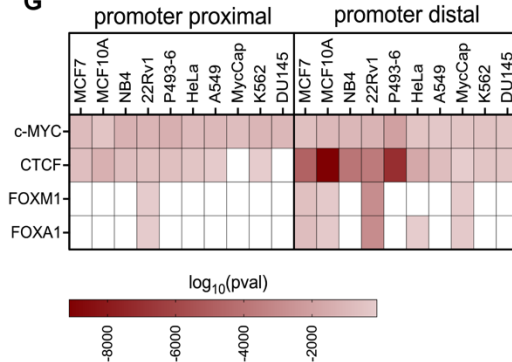


Figure 8. MYC and CTCF occupancy at promoter distal and proximal peaks in response to MYCi975. (A) Venn diagram of overlapping peaks in 22Rv1 cells using both Y69 and 9E11 (ab56) antibody clones (see Methods for details). Peak numbers are displayed. (B,C) Motif analysis of MYC peaks for the 9E11 antibody at promoter-proximal and promoter-distal sites (%TWM = percentage of targets with motif, %BWM = percentage of background with motif). (D) Mean MYC ChIP-seq read coverage plotted over sites with significant loss of MYC (DMSO vs. 48-hr MYCi975 treatment; 28,056 peaks). (E) Mean CTCF ChIP-seq read coverage plotted over MYC binding sites with significant loss of MYC (DMSO vs. 48-hr MYCi975 treatment; 28,056 peaks). (F) Venn diagram showing overlap of MYCi975-sensitive sites and differential CTCF lost sites in 22Rv1 cells treated with MYCi975 for 48 hrs. (G) Publicly available MYC ChIP-seq peaks from ENCODE and Cistrome Data Browser (<https://www.encodeproject.org>), <http://cistrome.org/db/>) were retrieved, converted to hg38 genome if applicable and split into promoter-proximal and promoter-distal sites. The heatmap plots the motif enrichment results as $\log_{10}(\text{p-value})$ for each motif (c-MYC, CTCF, FOXM1 and FOXA1) (HOMER v4.11.1).

Chromatin accessibility is a key event in gene regulation. To independently assess the chromatin accessibility changes induced by MYCi975 and determine whether differential MYC binding alters chromatin accessibility, we performed ATAC-seq in 48-hour MYCi975-treated 22Rv1 cells. At both promoter-proximal and promoter-distal MYC-bound sites, the majority of ATAC-seq signal remained relatively unchanged (Figure 9A). In total <9% of the MYCi975-sensitive sites (2,381/28,056) and <0.3% of MYCi975 Type 1-3 target genes (37/13,200) overlap with differential ATAC peaks (36,238 differentially lost, Figure 9B). Given that a large portion of differential ATAC-seq peaks did not overlap with differential MYC binding, we used motif enrichment analysis to investigate the differential ATAC-seq peaks. We found both Forkhead/FOX factor and CTCF motif enrichment (Figure 9C). To determine whether a similar feature is observed in ER-positive MCF7 breast cancer cells, in which Forkhead factors are critical for ER chromatin occupancy and transcriptional response, we performed ATAC-seq in MCF7 cells and determined whether large-scale chromatin accessibility also changed in response to MYCi975. We found that both CTCF and FOX factors were among the most enriched motifs at differential ATAC sites in MCF7 cells (Figure 9D; 22,038 differentially lost peaks). These results suggest that MYCi975 has minimal effects on chromatin accessibility at MYC-only binding sites but alters chromatin accessibility at sites enriched with CTCF and FOX TF binding sites.

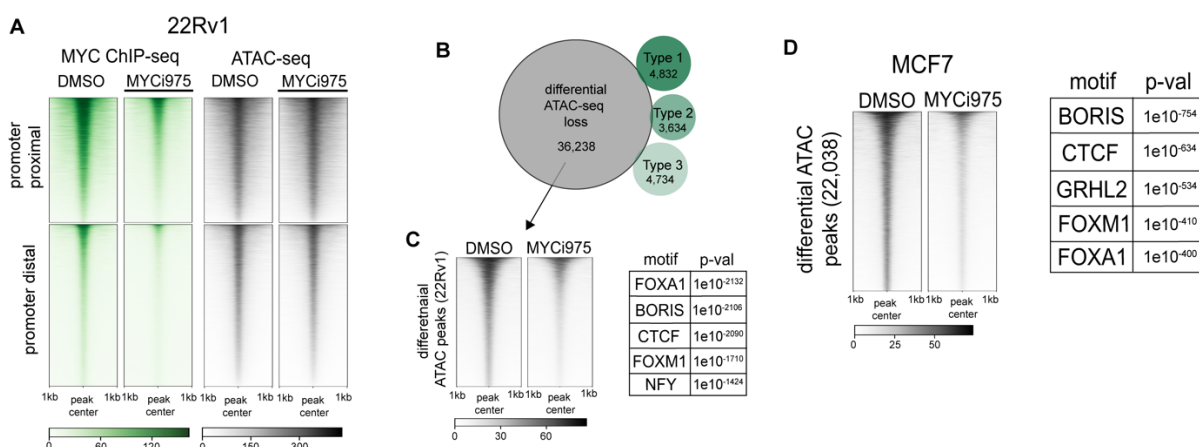


Figure 9. ATAC-seq analysis overlapping MYC and at differential ATAC-seq peaks. (A) Heatmap representation of all-MYC bound sites separated into promoter -proximal and promoter-distal sites, showing MYC ChIP-seq coverage and 22Rv1 ATAC-seq coverage in DMSO vs. 48-hr MYCi975-treated 22Rv1 cells. **(B)** Venn diagram demonstrating overlap of the differential MYCi975 types 1-3 with differential ATAC-seq peaks in DMSO vs. 48-hr MYCi975-treated 22Rv1 cells. **(C)** Motif enrichment analysis of the differentially lost ATAC-seq peaks (left panel) in MYCi975-treated 22Rv1 cells. Motif enrichment analysis was run on differential ATAC-seq peaks outside of the MYC cistrome, showing enrichment for both CTCF and FOX factors (right panel). **(D)** Heatmap representation of differential ATAC-seq peaks in MYCi975-treated MCF7 cells ($n=2$, left panel) and motif enrichment analysis results from the differential ATAC-seq peaks (right panel).

MAX cistrome changes in response to MYCi975

MAX is the key heterodimeric partner of MYC, and can also form homodimers and heterodimerize with MNT, MGA and MXD1 (77). Since ATAC signal did not change significantly at MYC-only binding sites, it was critical to determine chromatin occupancy of MAX and its heterodimeric partners. In 24-hour and 48-hour MYCi975-treated cells, we showed that while MYC level decreased significantly, MAX, and MNT protein levels decreased slightly and MXD1 remained relatively stable at varying levels when compared to DMSO-treated control cells (Figure 1A/B). To determine MAX chromatin occupancy in response to MYCi975, we performed MAX ChIP-seq, using the same timepoints as in the MYC ChIP-seq studies. The total peak number and ChIP efficiency significantly decreased only after 48 hours of MYCi975 treatment (Figure 10A, B). Principal component analysis of differential MAX binding analysis revealed clustering at 24 hours and 48 hours after MYCi975 treatment (Figure 10C). Considering that MYC heterodimerizes with MAX, we examined whether MYC loss on chromatin is associated with MAX loss. We also determined the extent to which MAX heterodimeric binding partners MNT, MGA, and MXD1 are altered by ChIP-seq (see below). MAX occupancy overlapped with greater than 80% of the MYC consensus cistrome (Figure 10D), suggesting that MYC-MAX complex is a predominant component of the MYC cistrome. The MAX cistrome was disrupted after 24 and 48 hours of MYCi975 treatment vs. DMSO, with 31.3% (15,153 peaks) of the total MAX cistrome altered after 48 hours of MYCi975 treatment (Figure 10E). These results also indicate that ~70% of the MAX cistrome remained unaltered upon MYCi975 treatment. We next investigated the overlap of MYCi975-sensitive MYC and differential MAX peaks. In MYCi975-treated cells, the total number of differentially bound MYC peaks (28,056) was greater than the number of differentially

bound MAX (15,153) peaks, suggesting stable MAX chromatin binding irregardless of significant MYC loss. Peak overlap analysis using a Venn diagram demonstrated that differential MAX occupancy is largely predicted by differential MYC occupancy (Figure 10F). As expected, at a subset of MYCi975-sensitive MYC sites, MAX occupancy was lost along with MYC occupancy.

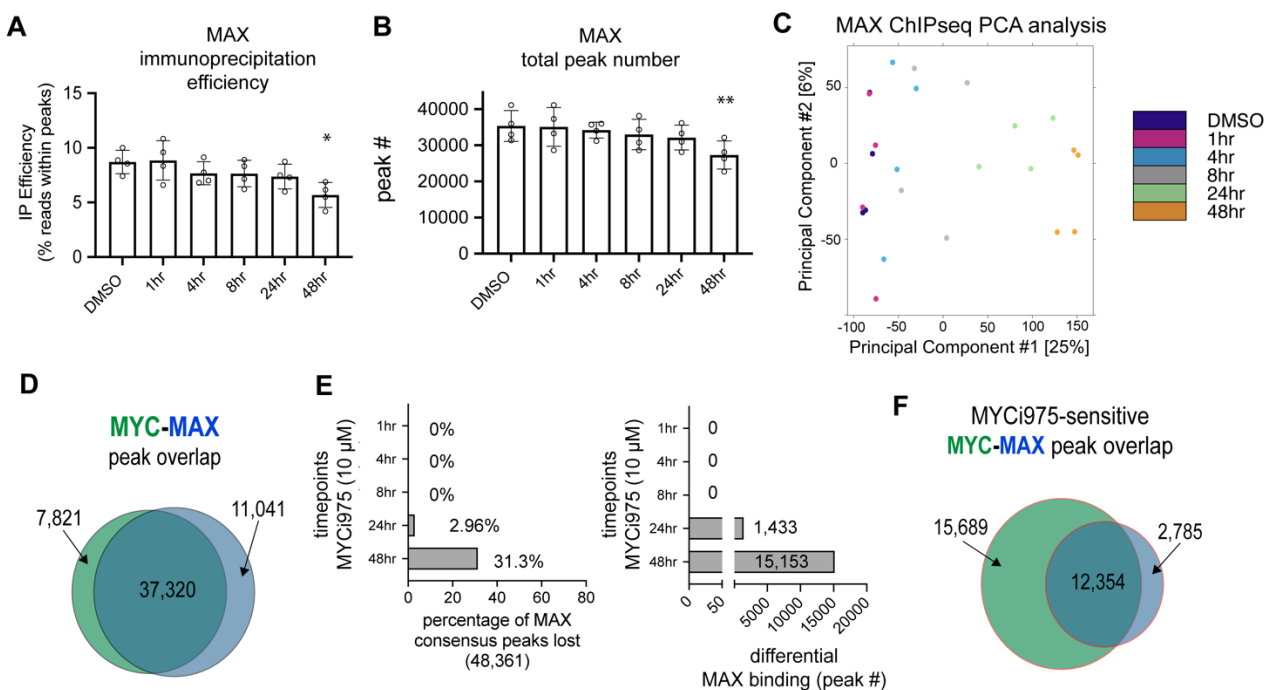


Figure 10. MYCi975 induced differential MAX binding and its overlap with MYC. (A) Immunoprecipitation (IP) efficiency (% of reads within peaks) of all MAX ChIP-seq biological replicates. (B) Total peak number in all replicates of MAX ChIP-seq samples (* $p < 0.05$; ** $p < 0.001$, bar represents sample mean, error bars represent mean \pm SEM). (C) PCA analysis of differential peaks in all MAX ChIP-seq biological quadruplicates for each timepoint. (D) Peak overlap analysis of MYC and MAX consensus peaks ($n = 4$). (E) Percentage of differential MAX binding peaks lost in response to MYCi975 compared to MAX consensus peaks ($n = 4$). (F) Total number of differentially bound MAX peaks following differential binding analysis ($n = 4$).

MYC-independent MAX lost sites (6,812 sites) upon MYCi975 treatment may represent MAX homodimer or MAX-MGA/MNT/MXD1 heterodimer binding due to the partial degradation of these proteins in MYCi975-treated cells (Figure 1A, B). To further determine binding overlap between all five transcription factors (MYC, MAX, MNT, MGA, and MXD1), we performed ChIP-seq and used the data sets in an upset plot to analyze replicate peak calls from each transcription factor (78). As expected, the top overlapping result was MYC/MAX; MAX-only sites were extensive, followed by the MYC and MAX heterodimeric binding partners (Figure 11A). Given that chromatin accessibility at MYC binding sites remained largely unaffected, it is possible that DNA remains accessible to binding of MAX and its heterodimeric binding partners (as determined by ATAC) upon MYC loss induced by MYCi975 treatment. We identified 6,812 MYC/MAX binding sites by overlapping MYCi975-sensitive MYC peaks and unaltered (FDR > 0.01) MAX binding sites (DMSO vs. 48-hr MYCi975). Figure 11B shows MAX retained sites where MAX occupancy (FDR > 0.01) was relatively insensitive to MYCi975 treatment within the MYCi975-sensitive MYC cistrome. At these sites, it is possible that MAX occupancy is stabilized by MAX/MAX homodimers or bound by MAX/MAX-family member heterodimers. To analyze the occupancy of MYC, MAX, MGA, MNT and MXD1 at the 6,812 MAX retained peaks we plotted the \log_2 (normalized tag-counts) in DMSO and 48-hr MYCi975 treated 22Rv1 cells (Figure 11C). By selecting for MAX retained sites (differential binding FDR > 0.01), occupancy analysis of both MGA and MNT decreased whereas MXD1 increased (Figure 11C). These data suggest that MAX retention in spite of MYC loss is coupled to alterations in canonical MAX heterodimeric partners. In particular, MXD1 increase in tag density suggests a change in the MAX heterodimeric complex formation at MAX retained sites. We find that while MAX and MGA remained relatively stable

overall, MNT occupancy decreased, whereas MXD1 occupancy increased. Of the MAX retained binding sites, RNA expression data from promoter proximal peaks was plotted and demonstrated both down- and up-regulated RNA levels (Figure 11D). Gene Ontology analysis of promoter proximal MAX retained peaks demonstrated enrichment for developmental, cell differentiation and neurogenesis pathways (Figure 11E). These data suggests that the loss of MYC accompanied by MAX retention is not uniformly associated with either RNA up- or down-regulation. This is not surprising, since at these MAX retained sites the MYC/MAX complex is no longer predominant and potentially MAX/MAX homodimers and MAX heterodimers will act antagonistically. In a gene-specific analysis of *AURKB*, which is highly sensitive to MYCi975 with regards to MYC promoter-proximal occupancy, MAX remained bound after MYCi975 treatment (Figure 11F). In particular, at the *AURKB* promoter proximal site loci, MGA occupancy is lost whereas MNT remains bound and MXD1 increases (Figure 11F). Altogether, MAX binding and canonical MAX heterodimeric partner binding at MYC binding sites were significantly affected by MYCi975 treatment, though a subset of sites showed relatively stable MAX binding.

Figure 11. Differential MAX, MGA, MXD1 and MNT chromatin binding alterations in MYCi975-treated cells. (A) Upset plot of peak overlap analysis of MYC, MAX, MNT, MGA, and MXD1 in 22Rv1 prostate cancer cells (78). (B) Heatmap representation of MYC, MAX, MGA, MNT and MXD1 at MYCi975-sensitive sites demonstrating no significant change in MAX occupancy (6,812 peaks in total). (C) Log₂(normalized tag counts) for MYC, MAX, MGA, MNT and MXD1 at MAX retained peaks in 22Rv1 cells. The middle-dashed line represents the sample median, and the upper and lower dotted lines represent upper and lower quartiles, respectively. (D) Differential gene expression analysis of MAX-retained peaks annotated to promoters (+/- 2kb from the TSS). (E) Gene ontology analysis of promoter-bound MAX retained peaks. (F) Gene browser tracks of *AURKB* showing loss of MYC (green), retention of MAX (blue), an increase in MXD1 (red) and loss of *AURKB* mRNA (black) in 48-hr MYCi975-treated cells. MGA (gray) and MNT (yellow) are also displayed.

Alterations in FOXA1, AR, and global chromatin H3K27-acetylation in response to MYCi975

Transcription factors such as MYC regulate gene transcription by recruiting histone acetyltransferases to promote histone H3 lysine 27 acetylation (H3K27ac), a mark of active promoters and enhancers (59, 79). To determine the effect of MYCi975 treatment on global H3K27ac, we performed H3K27ac ChIP-seq in MYCi975-treated cells at the same timepoints used for the MYC and MAX ChIP-seq studies above. To integrate changes in MYC/MAX occupancy with changes in H3K27ac, we overlapped MYCi975-sensitive sites in 48-hour treated cells with the differential H3K27ac signal. At 2,218 MYCi975-sensitive sites, we observed significant co-loss of H3K27ac and MYC and MAX occupancy in response to MYCi975 (Figure 12A). These data suggest that loss of chromatin bound MYC/MAX induced by MYCi975 leads to specific dysregulation of H3K27ac. Next, we annotated the MYCi975-sensitive differential H3K27ac peaks with MYC/MAX co-loss to promoters, overlapped with DE genes in 48-hour MYCi975-treated cells (304 out of 2,218). H3K27ac loss at promoters induced by MYCi975 was associated with down-regulation of gene expression, including of key cell-cycle genes (e.g., *MCM2*, *MCM3*; Figure 12B).

We next investigated motif enrichment of the differential H3K27ac peaks, to identify MYC targets modulated by MYCi975 treatment. We analyzed the 8,386 promoter-proximal and promoter-distal sites where H3K27ac was lost (Figure 12C). We reasoned that these sites might represent binding sites of MYC and MYC-regulated transcription factor(s) whose down-regulation after MYCi975 treatment leads to a loss of the H3K27ac active chromatin mark. We performed motif enrichment analysis and found that the most significantly enriched motifs were the FOX family of proteins and nuclear receptors such as AR and glucocorticoid receptor (GR), among

others (Figure 12D). Given that the differential ATAC signal in MYCi975-treated cells also revealed CTCF and FOX factor enrichment, we overlapped both the differential H3K27ac and differential ATAC-seq peaks in MYCi975-treated 22Rv1 cells (Figure 12E) and found that almost half of differential H3K27ac peaks overlapped with differential ATAC peaks. Notably, CTCF motif enrichment was only within differential ATAC peaks and not within differential H3K27ac peaks (Figure 12D), whereas FOX factor enrichment was found in both differential ATAC and H3K27ac peaks (Figure 9C (right panel), Figure 12D), suggesting multiple genome-wide chromatin alterations at FOX factor motifs.

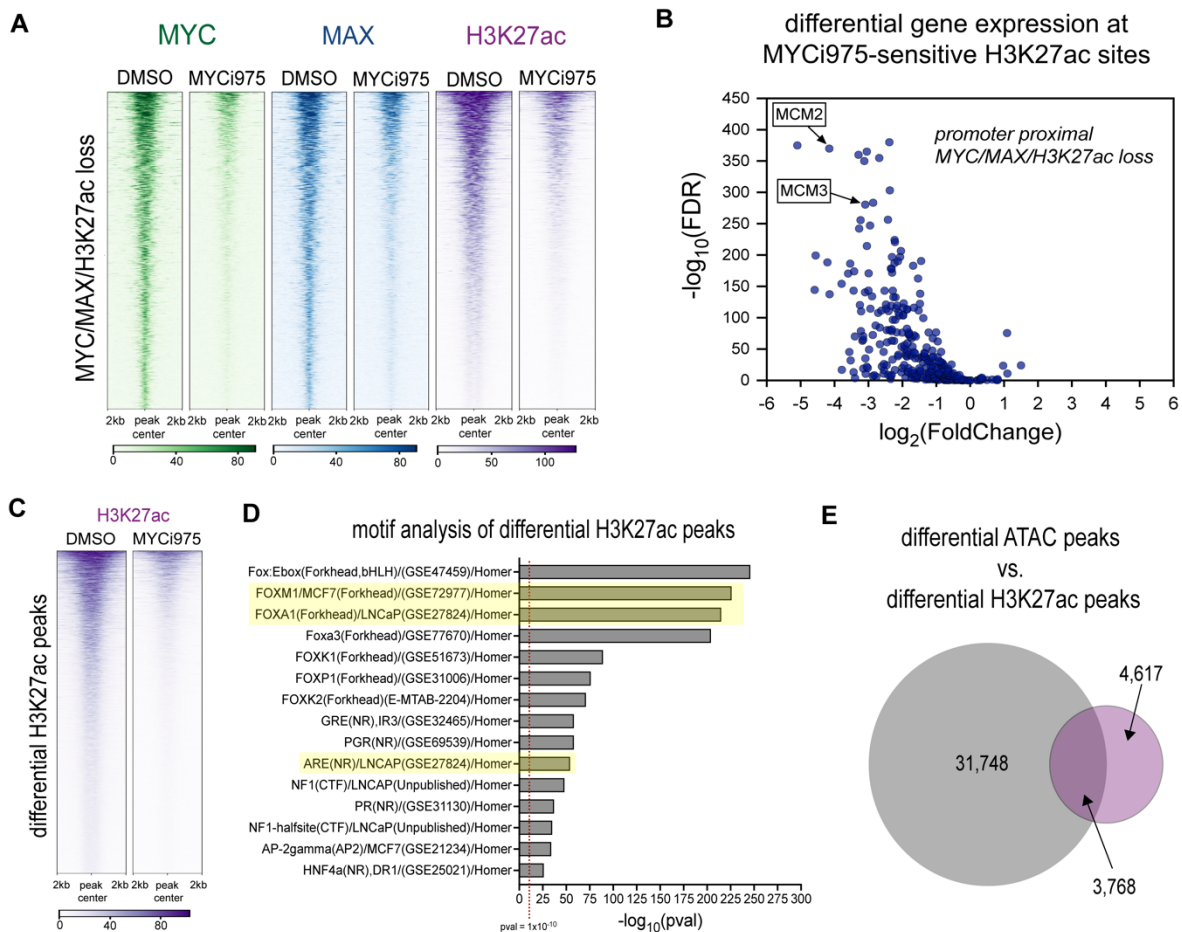


Figure 12. MYCi975 alters H3K27ac activity and chromatin occupancy in cancer cells at enriched sites for FOX factors and nuclear hormone receptors. (A) Heatmap representation of MYC (green), MAX (blue), and H3K27ac (purple) ChIP-seq signals at overlapping sites, with loss of signal in MYCi975-treated cells (2,218 peaks). (B) Differential binding analysis of H3K27ac ChIP-seq was performed and overlapped with MYCi975-sensitive sites. Sites annotated to promoters were cross-referenced with differential gene expression data consisting of 304 genes. The plot demonstrates that loss of MYC/MAX occupancy and H3K27ac signal results in down-regulated gene expression. (C) Heatmap representation of H3K27ac loss of signal in MYCi975-treated cells (8,385 peaks). ChIP-seq signal in the MYCi975 column represents 48-hr MYCi975 treatment. (D) Motif enrichment analysis was performed to assess the differential H3K27ac signal, showing enrichment for FOX factors and nuclear receptors (AR, GR, and progesterone receptor [PGR]). Each p-value reported was converted to $-\log_{10}(\text{p-value})$. (E) Venn diagram representing differential H3K27ac and differential ATAC-seq peak overlap in MYCi975-treated 22Rv1 cells (H3K27ac n = 2, ATAC-seq n = 3).

PCA analysis demonstrated that maximal H3K27ac signal separation occurred in cells treated with MYCi975 for 24 and 48 hours (Figure 13A). Overall, the total H3K27ac peak number (~37,000 peaks) remained relatively stable however IP efficiency significantly increased suggesting that some H3K27ac peaks increase in occupancy (Figure 13B, C). We reasoned that Type 2 peaks, where RNA levels are up regulated upon MYCi975 treatment represent candidate sites for increases in H3K27ac. Heatmap representation of H3K27ac signal at MYCi975 type 2 sites demonstrates an increase in H2K27ac which is consistent with the IP efficiency increase observed upon MYCi975 treatment (Figure 13D).

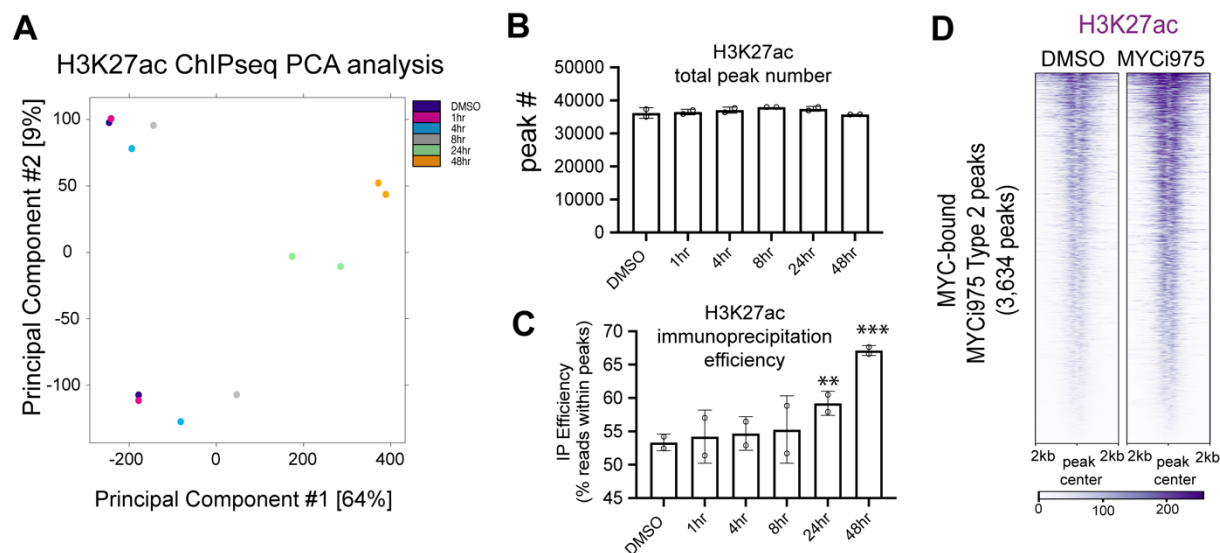


Figure 13. 22Rv1 H3K27ac ChIP-seq, quality metrics and increase at MYCi975 type 2 peaks.

(A) PCA analysis of differential peaks in all H3K27ac ChIP-seq biological duplicates for each timepoint. (B) Total peak number in all replicates of H3K27ac ChIP-seq samples. (C) Immunoprecipitation (IP) efficiency (% of reads within peaks) of all H3K27ac ChIP-seq biological replicates (* $p < 0.05$; ** $p < 0.001$, bar represents sample mean, error bars represent mean \pm SEM). (D) Heatmap representation of H3K27ac occupancy at MYC-bound promoters in the MYCi975 Type 2 peak set demonstrating an increase.

Our RNA-seq results indicated down-regulation of key prostate AR-related lineage transcription factors *FOXA1*, *FOXMI*, and *AR* (Table 1), which may contribute to MYCi975 efficacy in the prostate cancer cell models used here. We verified AR, FOXM1, and FOXA1 protein loss in the solubilized nuclear fraction of 22Rv1 cells (Figure 14A). We also found that FOXM1, FOXA1, AR, and the AR splice variant ARv7 were all greatly reduced after MYCi975 treatment (Figure 14A). To determine whether the relative loss of these key transcription factors is due to transcriptional regulation by MYC binding, we analyzed MYC occupancies at the promoters of *FOXA1*, *FOXMI*, and *AR* genes in both DMSO vs. 48-hour MYCi975-treated 22Rv1 cells. For each target gene, MYC occupied both promoter proximal and -distal sites and was significantly lost in MYCi975-treated cells (Figure 14B). These results show that MYC occupies regulatory regions of *FOXA1*, *FOXMI*, and *AR* genes, and MYCi975 leads to a decrease in MYC occupancy and a subsequent decrease in their respective mRNA and protein levels.

Based on the extensive loss of FOX factor and AR motifs in differential H3K27ac peaks, we performed AR and FOXA1 ChIP-seq in control and 48-hour MYCi975-treated 22Rv1 cells. Peak overlap analysis demonstrated that more than half the differential AR peaks overlap with differential FOXA1 peaks (Figure 14C). In total, 5,049 AR peaks were lost (~25% of the AR cistrome) while 6,640 FOXA1 peaks were lost (~10% of the FOXA1 cistrome) in response to MYCi975 treatment. Plotting the read coverage in heatmap representation of differential AR peaks for both AR and FOXA1 signal demonstrated co-loss of both FOXA1 and AR (Figure 14D). Both the differential AR and FOXA1 peaks were annotated and for both factors, peaks were predominantly promoter distal with less than 5% of peaks annotated to promoter proximal regions. Given that both 22Rv1 and MCF7 cells demonstrated differential chromatin accessibility enriched for

FOX factor motifs, we also performed FOXA1 ChIP-seq in 48-hour MYCi975-treated MCF7 cells. Differential binding analysis revealed 2,557 differential FOXA1 peaks (~4% of the FOXA1 cistrome; Figure 14E). To determine if the differential FOXA1 peaks overlapped with co-occurring ER α peaks, publicly available ER α ChIP-seq data was obtained from cistromeDB (<http://cistrome.org/db/#/>, cistromeDB: 68875, (80)). Nearly 60% of the differential FOXA1 peaks overlapped with ER α peaks, and the differential FOXA1 peaks were enriched for both FOXA1 and ER α motifs (Figure 14F, G). Taken together, in both prostate and breast cancer models, we found that FOXA1 binding is altered at nuclear hormone receptor co-occupied sites in response to MYCi975 treatment.

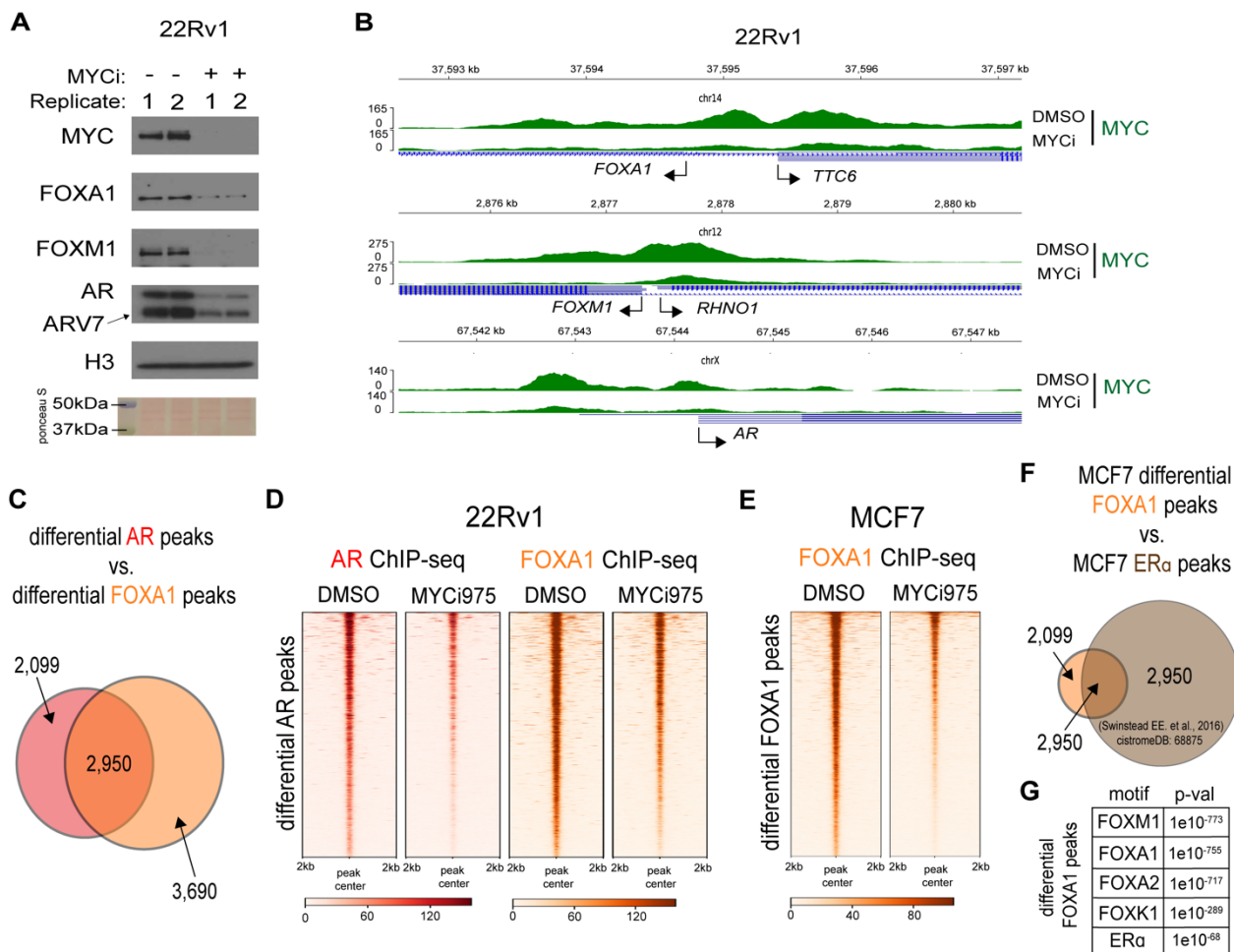


Figure 14. MYCi975 reduces FOXA1 and AR protein levels and chromatin occupancy in cancer cells. (A) Immunoblot showing loss of FOXM1, FOXA1, AR, and AR variant protein levels in sonicated nuclear fractions of MYCi975-treated 22Rv1 cells. Replicates (1, 2) represent biological replicates of cells treated with 10 μ M MYCi975 for 48 hrs. (B) Genome browser tracks of MYC (green) ChIP-seq data at the FOXA1, FOXM1, and AR gene loci in MYCi975-treated 22Rv1 cells. Transcription start site of each gene is indicated by an arrowhead. (C) Venn diagram representing differential AR and FOXA1 peak overlap in MYCi975-treated 22Rv1 cells. (D) Heatmap representation of AR and FOXA1 ChIP-seq signal at differential AR peaks in MYCi975-treated 22Rv1 cells (n = 3). (E) FOXA1 ChIP-seq signal in MCF7 cells at differential FOXA1 peaks found in MYCi975-treated MCF7 cells (n = 2). (F) MCF7 differential FOXA1 peak overlap with publicly available MCF7 ER α ChIP-seq peaks (<http://cistrome.org/db/#/>, PMID: 27062924). (G) Motif enrichment analysis results of the differential FOXA1 peaks.

MYCi975 enhances the efficacy of anti-hormone therapy

The results demonstrate that MYC occupies regulatory regions of FOXA1, FOXM1, and AR genes, and MYCi975 leads to a decrease in MYC occupancy and a subsequent decrease in their respective mRNA and protein levels. Based on these results, we reasoned that AR occupancy and gene expression changes induced by MYCi975 may enhance the efficacy of the clinically used AR targeting compound enzalutamide (ENZ) to suppress cell viability. Using ATP luminescence as a surrogate for cell viability (CellTiter-Glo 2.0, Promega cat#: G9242), we determined the Bliss index score in 22Rv1, LNCaP and C4-2B prostate cancer cell lines after treatment with ENZ and MYCi975, alone or in combination (81) (Figure 15A). These results show that MYCi975 acted synergistically with ENZ to decrease prostate cancer cell viability in all three cell lines. Given MCF7 cells also exhibit sensitivity to MYCi975 and demonstrate differential FOXA1 occupancy at ER-bound sites (thereby altering ER activity), we also tested for synergy of MYCi975 with clinically used anti-estrogen 4-hydroxytamoxifen (4-OHT). As with the prostate cancer cell lines, MYCi975 and 4-OHT synergized to decrease MCF7 breast cancer cell viability as determined by the Bliss index (Figure 15A, lower panel). Altogether, both anti-androgen and anti-estrogen treatment enhanced MYCi975 efficacy in prostate and breast cancer cellular models, respectively. These results also suggest that dysregulation of *MYC*, *AR*, and *FOXA1* gene expression by MYCi975 contributes to decreased cell proliferation and viability and increased cell death (see Figure 1).

To extend these observations *in vivo*, we first assessed MYCi975 efficacy in 22RV1 xenograft-bearing nude mice, treated with 100 mg/kg MYCi975 BID. This treatment led to a significant inhibition of tumor growth without any adverse effect on mouse body weight (Figure 15B,

C). We then examined the effect of a lower dose of MYCi975 (100 mg/kg QD) alone or in combination with ENZ (25 mg/kg QD) in the same 22RV1 xenograft mouse model. MYCi975 enhanced ENZ efficacy in this model without affecting mouse body weight (15 D, E). These results support our in vitro cell-based studies and provide a plausible mechanism for future development of combinatorial therapeutics for prostate cancer.

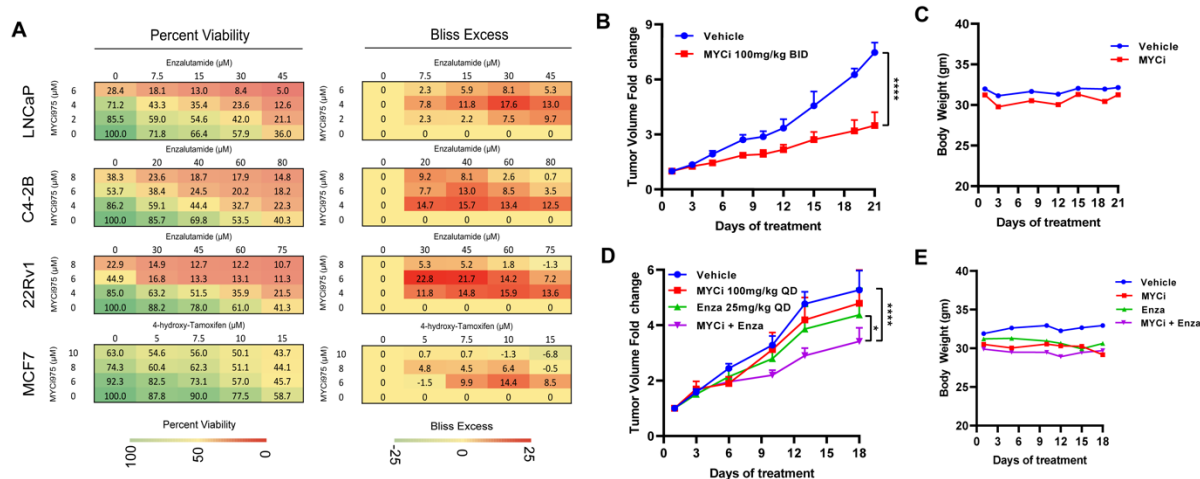


Figure 15. MYCi975 enhances the efficacy of anti-hormone therapy. (A) Representative 4 x 5 dose-response matrices showing percentage viability (left) and Bliss index (right) analysis of predicted vs. observed cell viability of prostate cancer cells (LNCaP, C4-2B, 22RV1) treated with MYCi975 and enzalutamide (ENZ) or the breast cancer line MCF-7 treated with MYCi975 and 4-OHT (n=3). Bliss scores > 0 indicate synergy, close to zero indicate additivity, and < 0 denote antagonism. (B) Fold change tumor volumes of 22RV1 xenografts in nude mice treated with MYCi975 (100 mg/kg BID p.o.) or Vehicle, 5 days a week for 3 weeks. n = 4 - 7 grafts/group (from 3-4 mice). (C) Mouse average body weight (gm) from Figure 15B. (D) Fold change tumor volumes of 22RV1 xenografts in nude mice treated with MYCi975 (100 mg/kg QD p.o.), ENZ (25 mg/kg QD i.p.), combination MYCi975/ENZ, or vehicle for 18 days. n = 7 - 8 grafts/group (from 4-5 mice). Error bars represent mean ± SEM and analyzed by two-way ANOVA in Graph Pad Prism for (B and C). (*p < 0.05; ****p < 0.0001). (E) Mouse average body weight (gm) from Figure 15C.

Chapter 2: DISCUSSION

Successful and specific targeting of MYC has the potential to significantly advance cancer therapeutics. In this study, we leveraged a small molecule MYC inhibitor, MYCi975, to probe the effects of MYC inhibition on chromatin binding of MYC, MAX, heterodimeric MAX binding partners, the chromatin landscape, and associated gene regulation and cell fate in cancer cells. Through comprehensive profiling of altered chromatin occupancy of MYC, MAX, MNT, MGA, MXD1, AR, FOXA1; epigenomic H3K27ac marks and chromatin accessibility; and transcriptional response, we characterized selective modulation of chromatin and MYC target genes by MYCi975, yielding important insights into its mechanism of action. In particular, our results indicate a differential effect on mRNA levels of MYC target genes despite uniform chromatin occupancy loss. Type 1 gene targets showed loss of MYC binding and decreased gene expression after MYCi975 treatment. Type 2 targets showed loss of MYC binding and increased gene expression. These data together support a model in which MYC regulates transcription through both repression and activation, a model well validated. Although not all MYC target genes demonstrated differential expression in response to MYCi975. Type 3 genes showed no change in gene expression after MYCi975, despite loss of MYC binding. Differential effects of MYCi975 on some canonical MYC functions and not others supports the concept of the “coalition model” (82) which aims to reconcile the wide variety of MYC interactors (83) and resultant MYC complexes. In this model, MYC protein complexes, while exhibiting independent functions, cooperate to achieve a collective transcriptional output that reflects the overall MYC function in cells. The fact that some genes, particularly those involved in RNA biogenesis in normal cell function and viability, were not significantly affected by MYCi975 in terms of MYC binding and target gene RNA levels provides

support for MYCi975 selectivity and tolerability as a potential cancer therapeutic. These genes may be candidate pathways that provide tolerability of MYCi975, and also potential target pathways when inhibited, potentiates the efficacy of MYCi975.

It is notable, by contrast, that MYCi975-sensitive Type 1 target genes were enriched for pathways that are hijacked by cancer cells such as cell cycle progression, DNA replication, and DNA repair. The significant loss of MYC binding and reduced gene expression after MYCi975 treatment is consistent with previous work identifying these genes as low-affinity MYC targets (30). The MYCi975 mechanism of action in tumor cells is thus likely to be dependent on the suppression of these pathways. Our findings argue for rational approaches to enhancing MYCi975 function, e.g., by combining them with agents whose efficacy is dependent on suppressing the cell cycle or DNA replication. In this way, the effects of MYCi975 could be enhanced and efficacious dosages for each given drug may be reduced. Alternatively, Type 2 genes were highly affected by MYC inhibition with regard to loss of MYC binding but were upregulated. These genes were enriched for signal transduction and protein ubiquitination/phosphorylation pathways. MYCi975-upregulated genes, such as pyruvate dehydrogenase kinase 4 (PDK4), has been associated with cancer aggressiveness and positive metabolic regulation of glycolysis (84–86). In addition, the MYCi975 upregulated gene FTH1 has been identified as a tumor suppressor in both breast (87) and ovarian (88) cancer. Type 3 target genes include members of MYC-regulated pathways that are spared by MYCi975, e.g., RNA metabolism, which could be targeted with other agents in future therapeutic or preclinical studies. Outside of active promoters, particularly in high MYC-expressing cancer cells, MYC binds low-affinity variant E-box enhancers (27). Our results demonstrated alterations in predominantly promoter-distal H3K27ac-marked sites where MYC/MAX

heterodimer binding is significantly lost in MYCi975-treated cells, suggesting a role for MYC/MAX heterodimer binding and H3K27ac at putative enhancers. However, gene expression changes that occur as a consequence of MYCi975-induced loss of putative enhancer-bound MYC/MAX heterodimers and H3K27ac marks have yet to be determined. Understanding the mechanism by which MYC loss from putative enhancers alters gene expression is imperative to understanding the MYCi975 sensitive cistrome. Alterations in long-range contacts between promoter-distal and promoter-proximal MYC binding, driven by MYC/MAX bound to enhancers, may be induced by MYCi975. Further investigation into the differential enhancer-promoter contacts induced by MYCi975 using promoter capture Hi-C (89, 90) may reveal the role of enhancer-bound MYC/MAX heterodimers in MYCi975-sensitive gene regulation. At these sites, in models of high-MYC expression enhancers are invaded and are associated with disease progression and MYCi975 has the potential to limit high-MYC driven processes by altering putative enhancer bound MYC.

Another key finding of this study was the discovery of CTCF and FOX transcription factor enrichment at promoter-distal MYCi975-sensitive sites in a cell-type specific manner. These findings suggest that lineage-specific transcription factors cooperate with MYC in regulating gene programs and may be sensitive to MYCi975. Both MYC, FOXA1 and AR have been demonstrated to co-occupy sites on chromatin, both promoter distal and proximal, and MYC in particular occupies the promoter regions of both genes. MYCi975 limits chromatin occupancy of MYC at *FOXA1* and *AR* promoter loci resulting in loss of mRNA expression levels of these key hormone responsive cancer associated genes. As our study primarily focused on prostate cancer cells, we showed that AR and the AR pioneer-factor FOXA1 may collaborate with MYC to promote tumorigenesis

which has previously been reported (91). MYCi975 treatment reduced expression of *AR*, AR splice variant *ARv7* (which is important in driving anti-androgen resistance (92)), and *FOXA1*. Furthermore, MYCi975 predominantly reduced chromatin occupancy of both AR and FOXA1 at putative enhancers both within and outside of the MYC cistrome. MYCi975 directly influences expression of these lineage-specific factors, which in turn regulates their target genes, thereby exerting a robust cumulative effect on overall gene expression reprogramming leading to cell proliferation defects and cell death. The results demonstrated that lineage factors chromatin binding was significantly affected as a result of MYCi975 outside of the total MYC cistrome. These data demonstrate that the downstream dysregulation of MYC target genes induced by MYCi975 has not only an effect on chromatin occupancy but active chromatin attributes such as H3K27ac and chromatin accessibility. Chromatin accessibility changes such that chromatin is significantly closing may affect transcription factor binding regardless of differently expressed genes induced by MYCi975. In the MYCi975 setting, for lineage transcription factors, both factor occupancy loss and chromatin accessibility loss are associated. Consistent with that premise, we found that the loss of AR upon MYCi975 treatment synergistically sensitized multiple prostate cancer cell lines, including castration- and treatment-resistant cells, to the second-generation anti-androgen enzalutamide (ENZ). Additionally, ENZ anti-tumor efficacy in 22Rv1 xenografts, which are intrinsically resistant to ENZ due to *ARv7* expression, was enhanced by MYCi975 combination treatment. In prostate cancer tumors, c-MYC levels positively correlate with AR isoforms including ARv7, and suppression of c-MYC sensitizes ENZ-resistant cells to ENZ (39). Studies have suggested that FOXA1 plays a role in not only prostate cancer but also breast cancer as a mediator of hormone response (93, 94). Although MYCi975 did not reduce FOXA1 or ER α protein levels in breast

cancer cells, FOXA1 occupancy was reduced at co-occurring ER α binding sites and MYCi975 synergistically sensitized ER α -positive MCF7 cells to anti-estrogen 4-OHT. These data are consistent with the notion that loss of chromatin occupancy of pioneering factor FOXA1 and subsequent loss of chromatin accessibility alters signaling of co-occupied ER α regardless of loss of protein levels. These data suggests that MYCi975 reprograms the chromatin accessibility genome-wide by alterations in MYC target gene expression, thereby hindering the activity of TFs that may not be regulated by MYC or MYCi975. The mechanism underlying this cell-specific effect of differential expression induced by MYCi975 is not currently clear, however MYCi975 may be selective towards distinct pathways in a cell type specific manner consistent with the long-standing understanding of MYC biology regulating multiple gene pathways.

MYC and MAX are part of an extended network of transcription factors (95). While the obligate MYC heterodimerization partner MAX is highly sensitive to chromatin loss of MYC caused by MYCi975 treatment, we also observed sites where MYC loss was not associated with MAX loss. This was expected since MAX binding to chromatin, unlike MYC, may occur through multiple dimerization partners as well as homodimerization (77). Our upset plot of the binding profiles of MYC, MAX, and its heterodimeric partners throughout the genome clearly established MAX homodimer binding as a key event along with MYC-MAX binding. Although our analysis does not include factor occupancy data for every known MAX binding partner, MAX occupancy was shown to have a large number of peaks outside of the MYC/MAX complex cistrome analyzed here in 22Rv1 cells. Additionally, observed peaks of MYC, MAX, and MAX heterodimeric partners in genomic loci by bulk ChIP-seq may represent cellular heterogeneity of MYC factor binding rather than all factors binding to the same locus. Such an observation underscores the limits of

bulk ChIP-seq and suggests single-cell sequencing approaches may better identify differences in transcription factor occupancy in individual cells. Although single-cell analysis allows for differentiation of cellular heterogeneity, there are limitations of our understanding of what complex binds temporally and with what binding partner. For example, sites where MYC is lost but MAX remains bound, both the presence of MNT, MGA and MXD1 suggest that each heterodimeric complex combination has the potential to bind these genomic loci tandemly and not concurrently. In this way, heterodimeric complexes compete for binding to the same genomic loci and the balance of each factor's protein stability may dictate the binding and subsequent fate of target genes. MYCi975 disrupts that balance of potential MYC/MAX heterodimers, leaving MAX and alternative MAX binding partners in dominant percentages and subsequently changing the downstream expression of what was once a target gene of MYC/MAX heterodimers. Analysis of MAX heterodimers with MNT and MGA suggest occupancy loss at MYCi975 MAX retained target genes; however, MXD1 shows a slight increase, and retention of MAX at these sites suggests a role for active repression by MAX homo- and heterodimers (95, 96). Notably, MAX binding to DNA independent of MYC has been associated with differentiation and cell arrest gene programs, competition with canonical MYC/MAX E-box motifs, and interaction with different transcriptional co-regulators (77). Our results are consistent with the notion that MYCi975 establishes a new MAX regulatory cistrome and gene program that promotes cell cycle arrest, cell differentiation and development. In the context of disease, MAX could function as a tumor suppressor independent of MYC, e.g., in small cell lung cancer (97). Stabilization of the MAX homodimer disrupts MYC function (98). Therefore, use of MAX homodimer stabilizing compounds along with

MYCi975 may establish a dysregulated gene expression network that decreases cell proliferation and promotes cell death.

In summary, this chapter highlights the impact of a small molecule inhibitor of MYC on the genome and epigenome of cancer cells leading to differential regulation of gene programs. As MYC regulates a myriad of gene programs in normal and cancer cells in a pleiotropic manner, our findings highlight the importance of carrying out detailed unbiased molecular analyses to obtain a more complete picture of the mechanism of action of MYC targeting agents as future cancer therapeutics.

Chapter 3: Abstract

MYCi975 induces up-regulation of thousands of genes which leaves potential for activated pathways with downstream consequences that play a role in drug efficacy. One transcription factor up regulated by MYCi975 is ATF4, which has both roles in cell survival and cell death. MYC has previously been demonstrated to positively regulate ATF4, however within MYCi975 treatment ATF4 is activated. Here, we elucidate differentially transcribed genes induced by ATF4 and determined whether ATF4 induction is dependent on MYC expression levels. We demonstrated in models of MYC genetic ablation that ATF4 induction levels depend on MYC expression and differential gene expression suggests ATF4 induces both ER stress and cell death gene pathways.

Chapter 3: Introduction

Activating transcription factor 4 (ATF4) is a master regulator of cellular stress response (99). Cells have developed a rapid response to manage cellular stresses. Multiple external and internal stresses induce ATF4 activation and subsequent downstream signaling such as amino-acid deprivation, endoplasmic reticulum imbalances, viral infection, hypoxia and heme deprivation (100). This type of cellular activation that converges on a common pathway through multiple stimuli is termed the Integrated Stress Response (ISR) and eukaryotic initiation factor 2 alpha (eIF2 α) phosphorylation is upstream of selective translational control of ATF4 (101). Within the ISR, ATF4 signaling is in balance with both pro-survival and pro-death mechanisms. In general, when ATF4 activation is persistent and without negative feedback the pro-survival effects may induce cell death (100). For example, when ATF4 activation induces autophagy, although autophagy may relieve cellular stresses that inform that activation of ATF4, autophagy can also induce cell death independent of apoptosis (102). ATF4, as a transcription factor, binds chromatin in a sequence

specific manner (TGACGTCA) to regulate target gene expression of gene pathways related to alleviating the cellular stress (103). At sites on chromatin, ATF4 binds with additional co-factors and generally binds with heterodimeric partners CCAAT enhancer-binding proteins (CEBPs) to elicit the transcriptional response (104).

In the context of cancer, ATF4 pro-survival signaling affects have been implicated as a requirement for cell growth. ATF4 has been demonstrated to alleviate the MYC-driven cellular stresses and function in a pro-survival manner in tumors (105). In particular, ablation of ATF4 signaling significantly delays tumor progression in lymphomagenesis models suggesting a role for ATF4 in enhanced tumor progression (105). MYC transcriptional programs induce cell growth pathways and globally amplifies the transcription of all transcribed genes (27). In this way, cells increase rates of translation and total protein which in turn can have negative effects of the endoplasmic reticulum and the unfolded protein response. Therefore, ATF4 and MYC correlated expression levels provide an avenue for which tumors have growth advantages. ATF4 is transcriptionally controlled by MYC and thus in models of MYC overexpression the levels of ATF4 increase (105). For MYCi975, in addition to selective MYC dysregulation, ATF4 is induced. It is therefore imperative to determine whether activation of ATF4 functions in a MYC-dependent manner and whether ATF4 may provide in part cell-death signaling. However previous reports demonstrate that MYC regulates ATF4 gene expression and thus the ATF4 activation induced by MYCi975 may be tempered. Lastly, ATF4 regulated gene pathways may point to the dual role of ATF4 and suggests pro-survival or pro-death effects in response to MYCi975.

Chapter 3: MYCi975 activate ATF4

MYCi975 induces activation of ATF4

Loss of ATAC-seq signal led to the findings that MYCi975 dysregulates *FOXA1* and *AR* expression levels and chromatin occupancy, however analysis inclusive of all significantly altered peaks has yet to be determined. In this way both activated and repressed transcription factor motifs may give insight into the activity of MYCi975 and in particular TFs that may be de-repressed in MYCi975 treated cells. To determine the differential activity of transcription factors we utilized DASTk (106). Peaks are cross referenced with 340 known transcription factors and putative TF activity was determined by the ratio of ATAC-seq peaks within a 1,500 bp region centered on known TF motifs. For both 22Rv1 and MCF7 ATAC-seq datasets differential transcription factor activity demonstrated activation of ATF4 as determined by the canonical ATF4 motif (Figure 16A top and middle panel). To elucidate the effect of ATF4 induction in additional cell models, we treated MycCap prostate cancer cells with MYCi975 for 6hr and detected ATF4 activation (Figure 16A, bottom panel). Isolation of the ATF4 motif within each dataset demonstrated activation or gain of ATAC-seq signal at or near the motif center (Figure 16B). From the differential peak datasets, 22Rv1 cells demonstrate an increase in 24,261 peaks and for MCF7 cells there was an increase in 13,106 peaks (Figure 16C). Additionally, 22Rv1 cells demonstrate an increase in H3K27ac signal (Figure 16D). For increases in H3K27ac ChIP-seq and ATAC-seq signal, motif analysis reveals an enrichment for the ATF4 motif. Altogether these results suggest both opening of chromatin and deposition of H3K27ac, a mark of active enhancers and promoters, are enriched for the ATF4 canonical motif in response to MYCi975.

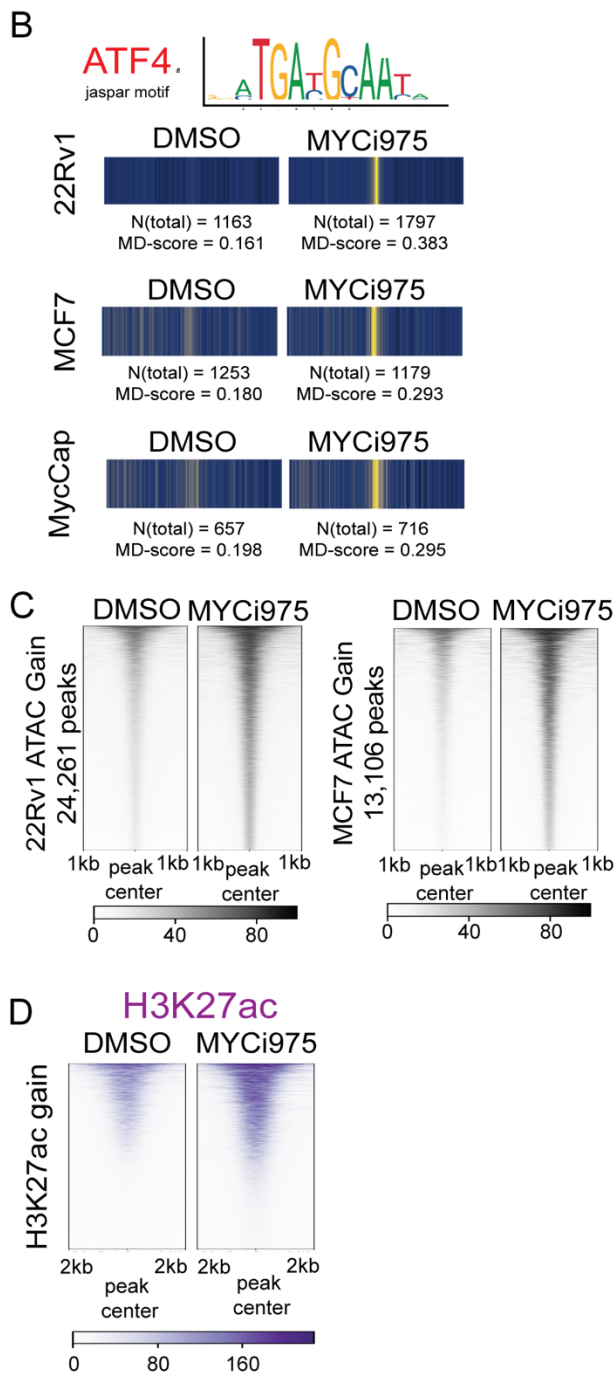
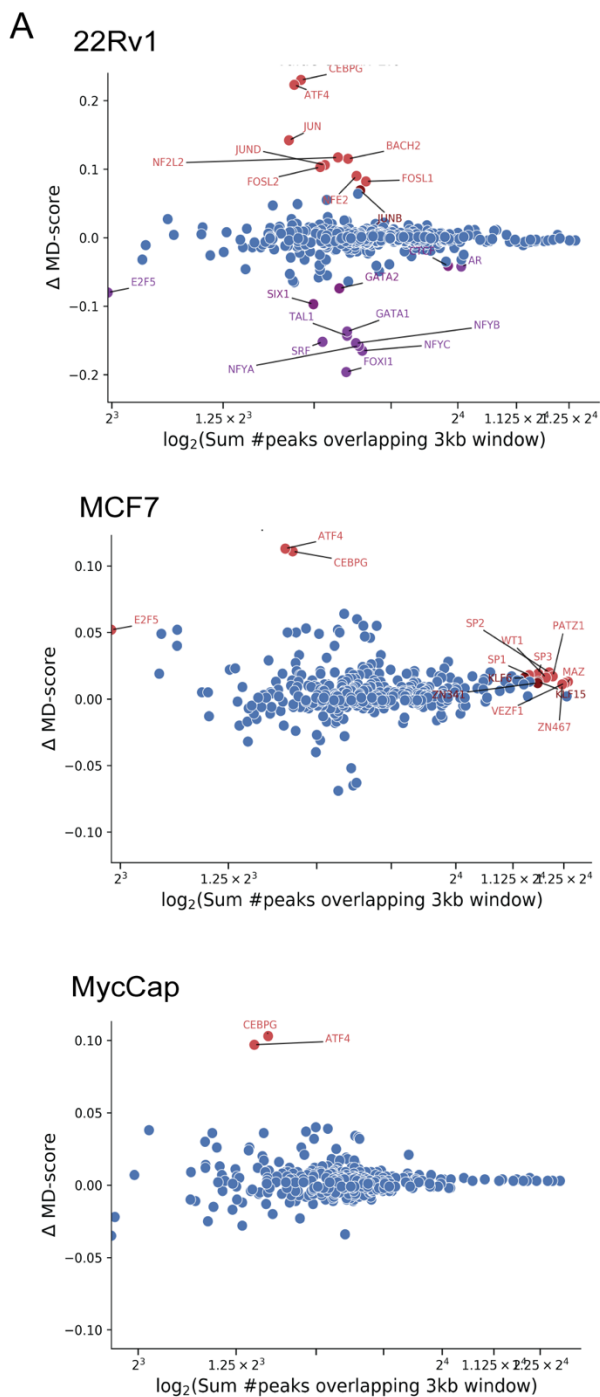


Figure 16. ATF4 motif enrichment at both sites of open chromatin accessibility and increased H3K27ac ChIP-seq in response to MYCi975. (A) MA plots representing the change in motif displacement (MD) (Δ MD-score) when comparing DMSO vs MYCi975 treatment for 22Rv1, MCF7 and MycCap cells. The differential MD-score was calculated with DASTk (106). (B) Bar-coded motif displacement sliding window for the human ATF4 motif. Yellow stripes indicate peaks within a 1,500 bp sliding window of all known ATF4 motifs in the human hg38 genome. (Reference for the ATF4 motif image: <https://jaspar.genereg.net/matrix/MA0833.1/>) (C) Heatmap representation ATAC-seq peaks that increase in response to MYCi975 in both 22Rv1 and MCF7 cells. (D) Heatmap representation of significant increase in H3K27ac signal in 22Rv1 cell in response to MYCi975.

We next determined if ATF4 stabilization by protein levels is induced by MYCi975. We determined how early ATF4 induction occurs in MYCi975 treated 22Rv1 cells and demonstrated induction of ATF4 protein levels as early as 4-hours (Figure 17A). For MycCap cells, ATF4 motif activity was shown in the 6-hour MYCi975 treated cells, and that is associated with an increase in ATF4 protein levels (Figure 16A, Figure 17B). We then determined the ATF4 binding sites by ChIP-seq in 22Rv1 cells and found 23,919 ATF4 binding sites with a significant increase, of which 89% are promoter distal (Figure 17C). We next determined whether ATF4 induction is MYC dependent using both a doxycycline inducible MYC knockdown and MYC-knockout models. In the tet-inducible P-4936 lymphoma cells, the addition of doxycycline to the media induces rapid MYC knockdown. P-4936 cells were pre-treated with either vehicle control or doxycycline for 24-hour, then given either 0.02% DMSO, 10 μ M MYCi975 or 100 nM Thapsigargin (Tg) for an additional 24-hours. Thapsigargin functions through inhibition of the sarcoendoplasmic reticulum Ca^{2+} ATPase (SERCA) and is used as a positive control for ATF4 induction. The knockdown of MYC reduced the ATF4 induction by MYCi975, suggesting that ATF4 induction is MYC-dependent (Figure 17D). Analysis of Thapsigargin demonstrated that MYC knockdown greatly reduced the ability of Thapsigargin to induce ATF4 as well (Figure 17D). These data suggest that MYCi975 induction of ATF4 is MYC dependent and furthermore canonical activators of ATF4 are severely impaired in MYC-knockdown P-4936 cells. Rat fibroblasts (TGR.1) cells were used to generate MYC-knockout cells (HO15.19) previously used in studies of MYCi975 (60). TGR.1 and HO15.19 cells were treated with either 0.02% DMSO, 10 μ M MYCi975, 100 nM Thapsigargin or 10 μ g/ml of Tunicamycin (Tunic) for 24-hours. In TGR.1 cells 10 μ M MYCi975 is insufficient to

observe appreciable MYC protein down-regulation however it is sufficient to achieve ATF4 induction (Figure 17E). Both positive controls, Thapsigargin and Tunicamycin, activate ATF4 in TGR.1 cells. To determine if ATF4 induction is dependent on the expression of MYC we next tested the same treatment in MYC-knockout cells. In MYC-knockout cells MYCi975 is sufficient to activate ATF4. Importantly, there is an appreciable reduction in ATF4 activation for both positive control treatments suggesting that the activity of ATF4 is altered in MYC knockout cells compared to MYC wild type (Figure 17E). Most likely MYC regulates *ATF4* gene expression and thus MYC attenuation is coupled to decreased *ATF4* basal gene expression levels. To further investigate the similarities and differences between TGR.1 and MYC-knockout cells, we performed RNA-seq in biological duplicate and analyzed by gene ontology the differentially expressed genes (Figure 17F). Stress response and cell death were regulated in both cell models. Given both models activate ATF4, these data suggests that regardless of the expression of MYC the differential transcriptome demonstrated cell death and stress response pathways are activated. Direct overlap of differentially expressed genes from both cell models suggests that some MYCi975 differential gene expression levels are independent of MYC (Figure 17G). Taken together, these data suggest the contribution of ATF4 induction by MYCi975 leads to cell death and stress response pathways and may play a role in the overall efficacy of MYCi975.

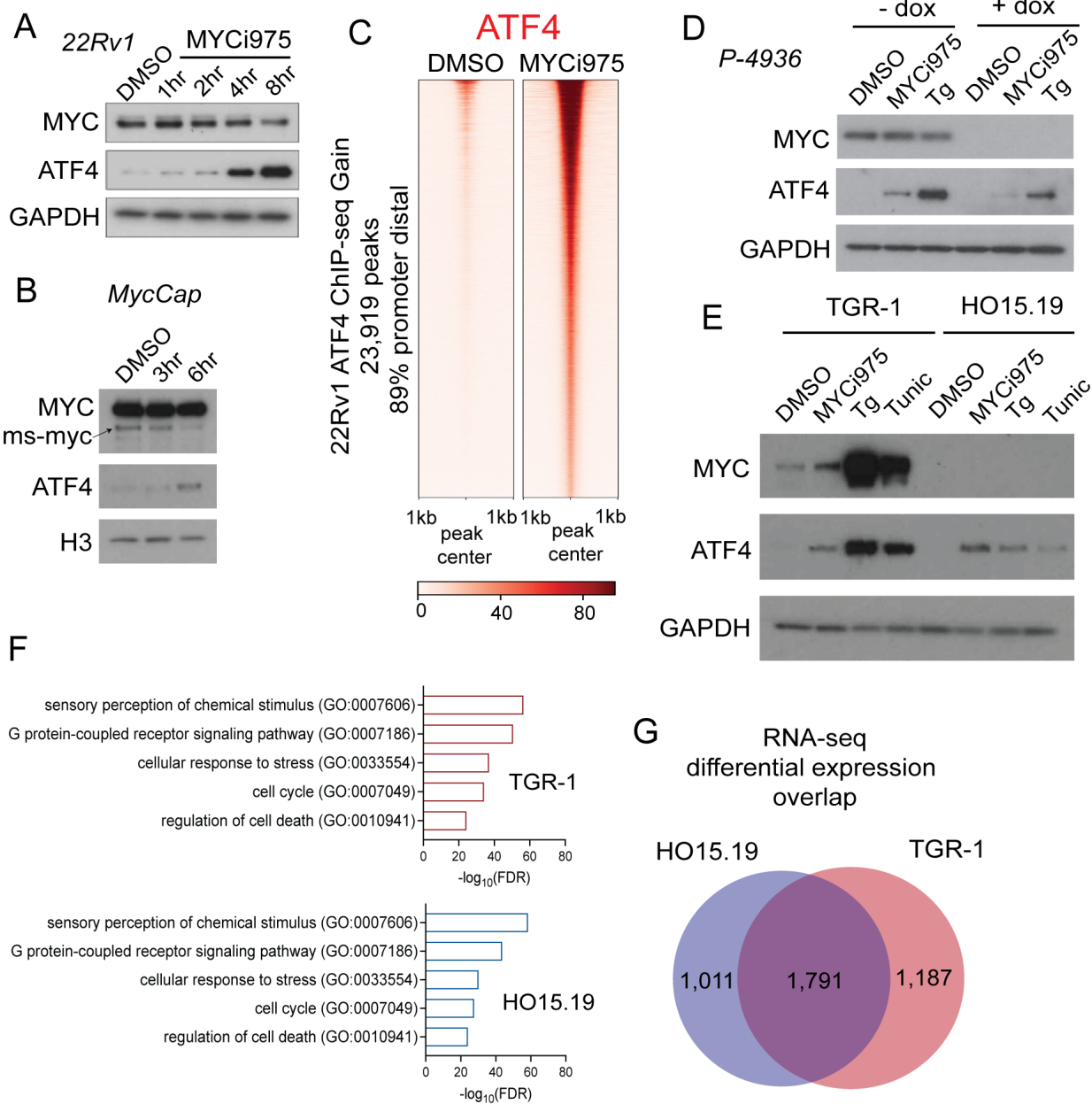


Figure 17. MYCi975 induces ATF4 signaling. (A) Early induction of ATF4 protein levels in 22Rv1 cells in response to MYCi975. (B) Nuclear extracts from ATAC-seq demonstrated increased ATF4 protein levels in response to MYCi975. (C) Increase in ATF4 chromatin binding in 22Rv1 cells in response to MYCi975. (D) P493-6 lymphoma cells were treated with either vehicle control of doxycycline to induce rapid MYC knockdown. In both cell groups, cells were treated with either DMSO (0.02%), 10 μ M MYCi975 or 100 nM Thapsigargin (Tg) to detect ATF4 protein induction levels. (E) Parental TGR.1 rat fibroblasts and MYC-knockout rat fibroblasts HO15.19 cells were treated with either DMSO (0.02%), 10 μ M MYCi975, 100 nM Thapsigargin (Tg) or 10 μ g/ml of Tunicamycin (Tunic) to detect ATF4 protein induction levels. (F) Differentially expressed genes were used as input for gene ontology analysis (<http://geneontology.org>) and the top 5 results are displayed for either TGR.1 (red) or HO15.19 (blue) cells. (G) Venn diagram gene overlap of the differentially expressed genes either TGR.1 of MYC-knockout HO15.19 cells treated with MYCi975 for 48hr (n = 2).

Chapter 3: Discussion

ATF4 induction by MYCi975 is found in multiple cell lines and by utilizing MYC-knock-out cells we demonstrate that ATF4 induction leads to the activation of cell death and stress response pathways. These pathways could in part be responsible for the efficacy of MYCi975 whereby now the mechanism includes both inhibition of MYC, likely through canonical cell cycle and DNA-repair pathway inhibition, and activation of ATF4 driven pathways such as cell death and cellular stress response. Importantly the levels of MYC alter the ATF4 protein induction levels with both MYCi975 and with canonical activators of ATF4. It is likely that MYC regulates ATF4 expression by direct targeting or potentially downstream effects of MYC target gene dysregulation induced by MYCi975. MYC has been shown to target ATF4 and control its expression in normal biology and MYC regulated ATF4 expression is required for cancer cell growth (105). In addition, MYC and ATF4 have been associated to collaborate in cell death, protein synthesis and tumorigenesis cellular properties (105, 107–110). Given that MYCi975 significantly disrupts MYC function, it is likely that the ATF4 induction induced by MYCi975 is tempered or at least limited. This may be a key feature to the MYCi975 induced ATF4 effects and the role ATF4 induction plays in MYCi975 tumor efficacy. Future studies should emphasize the limiting MYC function in cells treated with MYCi975 and the subsequent capacity of ATF4 signaling and define whether the MYCi975 pharmacophore induces ATF4 through MYC dependent or independent effects. Additionally, studies aimed to understand the tumor immune efficacy may be related to ATF4 signaling, and models of MYCi975 treatment in both ATF4 wild type and ATF4 knockout tumor cells will be sufficient to elucidate this effect. Taken together, when using MYCi975 the activation of

ATF4 is potentially limited and further studies to increase activation may potentiate MYCi975 efficacy and the cell death pathways induced by ATF4.

Small molecule inhibitors have off-target effects. It is an “exaggerated” phenomenon that a small molecule remains inert to everything it comes into physical contact with except its intended molecular target. In fact, it is exaggerated to conclude there is one on-target effect and one off-target effect when there is now evidence of multiple predicted targets on average for hundreds of small molecules (56). Small molecule off target effects have been discovered through novel computational and genetic screening (54, 55, 111), and evaluation of the full panel of targets for each drug will be required for personalized medicine. In this study, the results suggest MYCi975 induced ATF4 may function through off-target effects although ATF4 induction is regulated by MYC protein levels in cells. Overall, drug promiscuity and the discovery of drug targets will allow scientists to classify drugs, their putative targets and match correctly with biomarkers in disease. One major ramification of the results is that patient genomic databases can be effectively data-mined for relevant biological targets. In a simplified model, if you classify a drug as a target of A, although the drug efficacy acts in part or fully through B, clinical data that is imported to evaluate drug responses are defined by certain genetic variables of A. To build a more precise model, evaluation of the genetic variables of both A + B could be cross referenced with drug targets. However, in practice a small molecule inhibitor consists of multiple known targets (i.e., A, B, C, ..., n). Additionally, drug targets have effects on cellular pathways, and it is not always clear what types of alterations in cellular pathways occur due to a particular drug binding another biomolecule. Many identified or predicted drug targets rely on functional biological studies to demonstrate an overall effect on a particular drug target’s biological function in cells. Phenotypic cell death *in*

in vitro is a weak assessment of on-target efficacy and thus widespread genomic screens, and gene pathway analysis may provide target pathways relevant to drug efficacy.

In summary, these results determined that MYCi975 activates ATF4 in multiple cell models. Utilizing genome-wide chromatin accessibility datasets led to the initial hypothesis of downstream ATF4 signaling, which overlaps with ATF4 chromatin binding occupancy and increased H3K27ac. ATF4 induces pathways that are enriched for canonical ER stress response signaling and in particular cell death pathways. Taken together, ATF4 signaling by MYCi975 may contribute to drug efficacy and further a more comprehensive mechanism of action for MYCi975.

Chapter 4: Methods

Cell lines:

22Rv1 (CRL-2505), DU145 (HTB-81), MCF7 (HTB-22), MycCap (CRL-3255), and LNCaP (CRL-1740) cells were purchased from ATCC. The C4-2B cell line was a generous gift from Dr. Hongwu Chen of University of California, Davis. All cell lines in this study were maintained in RPMI (ThermoFisher, Cat#: 11875093) supplemented with 10% Gibco FBS (REF:26140-079) in a humidified incubator at 37°C with 5% CO₂. All cell lines in this study were maintained at maximum until passage 20, then discarded.

Antibodies and reagents:

Antibodies used in this study were CTCF (Active Motif, Cat#:61932), c-MYC (abcam, [ab56-9E11](#)), c-MYC (abcam, [ab32072-Y69](#)), ATF4 (Cell Signaling Technologies, 11815S), WDR5 (Proteintech Cat#: 15544-1-AP), FOXA1 (Bethyl Laboratories, A305-249A), H3K27ac (Active Motif, Cat#:39685), AR (Abcam, ab108341), MAX (Proteintech, Cat#: 10426-1-AP), full-length PARP (Cell Signaling Technologies, 46D11, cat#:9532T), cleaved-PARP (Cell Signaling Technologies, D64E10, cat#:5625T), MNT (Bethyl Laboratories, A303-627A), MXD1 (Proteintech, Cat#: 17888-1-AP), MGA (Bethyl Laboratories, A302-865A), FOXM1 (Diagenode, Cat#: C15410232), Histone H3 (abcam, ab10799), GAPDH (Sigma-Aldrich, G9545). MYCi975 was synthesized as described (60). Thapsigargin was obtained from Sigma Aldrich (cat#: T9033). Tunicamycin was obtained from obtained from Millipore Sigma (cat#: T7765).

Whole cell extraction and immunoblotting:

Cells were washed with ice-cold 1X phosphate buffered saline (PBS) 3 times and isolated by cell scraping into ice-cold 1X PBS. Cell pellets were frozen in liquid nitrogen briefly, allowed to thaw for 2 min, then resuspended in 5 cell-pellet volumes of whole cell extract lysis buffer (20 mM Tris-HCl pH 7.6, 150 mM NaCl, 1 mM EGTA, 1mM EDTA, 1% IGEPAL CA-630, 0.5% Sodium Deoxycholate, 0.1% SDS). The cell resuspension was kept on ice for 20 min with brief vortexing every 5 min. Cell debris was cleared by centrifugation at $> 20,000g$ for 25 min at 4°C and samples were assessed for protein concentration with BCA (Thermo Scientific, Cat#: 23209). For each sample, 20 μ g of protein was separated by SDS-PAGE, transferred onto a nitrocellulose blotting membrane (Amersham Protran, cat#:10600001) and probed with antibodies in PBS, 0.1% Tween-20, 5% nonfat dry milk (dilutions: (Y69) MYC-1:10,000, MAX-1:2000, MNT-1:2000, MXD1-1:2000, GAPDH-1:20,000). For immunoblotting solubilized nuclear fractions, 15 μ g of ChIP input was separated and probed with antibodies exactly as described above (dilutions: (Y69) MYC-1:10,000, FOXM1-1:500, FOXA1-1:1000, AR-1:2000, Histone H3-1:10,000). To quantify western blot exposure densitometric analysis was conducted with the image J (64) gel analyzer tool and quantified using the area under the curve. Gel loading control protein was set to 100% in order to quantify the percent changes in protein as compared to loading control.

Crystal violet staining:

Cells were plated into 6-well plates at 25,000 cells per well and the media was supplemented in triplicate with either DMSO (0.2%) or 10 μ M MYCi975 unless noted otherwise. Cells were treated for 4 days with a media change 48 hours after plating. The media was aspirated, and ice-cold PBS

was carefully added to the side of the wells. The PBS was aspirated, and cell washing was performed once more. After the last wash, 1 mL of crystal violet solution (0.1% crystal violet in 20% ethanol) was added, and the plate was gently rocked for 5 min. Crystal violet was discarded and wells were washed with deionized water 3-5 times until clear and then plates were inverted to dry.

Cell viability and IC₅₀ determination:

22Rv1, LNCaP, and C4-2B cells were plated into 96-well plates at 2,500 cells/well supplemented in triplicate with either DMSO, MYCi975, Enzalutamide (ENZ) (Selleckchem, Cat#: S1250), or both drug treatments (n = 2). 22Rv1 cells were treated with 25 μ M ENZ while LNCaP and C4-2B cells were treated with 10 μ M ENZ. Both the LNCaP and C4-2B cell lines express full-length androgen receptor, whereas 22Rv1 cells express both full-length and ligand-independent androgen receptor variant 7 (ARv7) which drives a mechanism of anti-androgen resistance (92). Given these differences, cells were treated with different concentrations of ENZ to reflect sensitivity. The plates were incubated at 37°C for 4 days. Media from wells was removed, 50 μ l of CellTiterGlo 2.0 reagent (Promega, Cat#: G9241) was added, and the plate was protected from light while shaking for 20 min. A 1:1 addition of culture media was added and allowed to equilibrate for 5 min while shaking, then the solution was read for luminescence signal. For IC₅₀ curves, 22Rv1 cells were seeded at 2,000 cells/well in 96-well plates and analyzed in quadruplicate. Cells were plated and allowed to attach for 24 hours, then treated with the indicated concentration of MYCi975 for 72 hrs. IC₅₀ curves were extrapolated from the ATP content signal from 22Rv1 cells using nonlinear regression.

Bliss index analysis:

LNCaP, 22RV1, C4-2B, and MCF-7 cell lines were cultured in RPMI-1640 (Gibco) supplemented with 10% heat-inactivated fetal bovine serum (FBS, Gibco) and 1% Penicillin-Streptomycin (10,000U/ml, Life Technologies) and grown in a 37°C incubator with 5% CO₂. While the prostate cancer lines were plated for drug combination experiments in the same media, the MCF-7 cell line was plated in phenol red-free RPMI-1640 (Gibco) supplemented with 10% charcoal-stripped FBS 24 hours prior to drug treatment. ENZ or 4-OHT was combined with MYCi975 in 4 x 5 dose-response matrices in 96-well plates. The prostate cancer lines (LNCaP, 22RV1, C4-2B) were seeded at 1000 cells/well, while the breast cancer line MCF-7 was seeded at 2000 cells/well. Relative cell viability was determined using the CellTiter-Glo 2.0 Cell Viability Assay (Promega, G9242) after 72 hours of drug treatment as shown, and luminescence signals were acquired using plate reader (Perkin Elmer Victor 3V). For the Bliss Matrix synergy experiments, the tested concentrations of the two drugs were chosen such that the effect on cellular viability after 72 hours of treatment is similar for both drugs over the tested concentrations. The goal was to choose a range of concentrations with effects spanning 30-100% viability. Concentrations that affect the cell at more than 30% viability were reasoned to be unlikely to show synergy, since most of the effect is due to one drug in this scenario. For the prostate cancer cell lines, the range used for MYCi975 was very similar, which is a result of MYCi975 showing similar IC₅₀ values in these lines. However, these lines behave very differently towards Enzalutamide alone, with LNCaP being enzalutamide sensitive (IC₅₀ value ~35 μM), while C42B and 22RV1 are Enzalutamide resistant lines (IC₅₀ ~60-70 μM for both). The Enzalutamide concentrations used in this study reflect this behavior, as can be seen in the percent viability matrices. Drug combination data was assessed using

the SynergyFinder package employing the Bliss Independence Model (81), which converts percent viability values to fraction affected (F_a). The predicted fractional growth inhibition of the drug combination is calculated using the equation $F_A + F_B - (F_A \times F_B)$, where F_A and F_B are the fractional growth inhibitions of the drugs A and B at a given dose. Bliss excess is the difference between the expected growth inhibition and the observed inhibition. A bliss excess score of > 0 = synergy, close to zero = additivity, and < 0 denote antagonism (112).

ChIP-seq:

Cells were plated into 15 cm² plates at a density of 5 million cells per plate and MYCi975 was supplemented such that cells would be isolated at the same time. Accordingly, the total number of plates equaled the total number of samples on day 0 of plating (DMSO, 1-, 4-, 8-, 24-, 48-hrs). 24 hours after cell plating, MYCi975 was added to one plate for the 48-hr timepoint. Another 24 hours later (48 hours after cell plating), all plates were given fresh media. At this time, the plate that was previously treated (48-hr timepoint) was supplemented with MYCi975 immediately, along with a new plate as the 24-hr timepoint. On the third day, the 1-, 4- and 8-hr plates were given MYCi975 such that the end of all timepoints occurred at the same time. ChIP was carried out as previously described (113) with slight modifications. Once all plates were treated at their respective timepoints, 1% formaldehyde cross-linking was performed by an addition of 2 ml of 16% paraformaldehyde (Electron Microscopy Sciences, cat#: 15710) to each plate, which contains 30 ml of culture media, for 10 min. Glycine was added to a final concentration of 119 mM (1.6 mL of 2.5M Glycine) for 5 min to quench cross-linking. Cells were washed with ice-cold 1X PBS 3 times and then scraped into PBS and pelleted by centrifugation at 1000g for 10 min at 4°C. The cell pellet was flash frozen with liquid nitrogen, allowed to thaw on ice, and resuspended in 1 ml of Lysis

Buffer 1 (LB1) (50 mM HEPES-KOH pH 7.6, 140 mM NaCl, 1 mM EDTA, 0.5 mM EGTA, 10% Glycerol, 0.5% IGEPAL-CA630, 0.25% Triton X-100). Then 2 ml of LB1 was added to the cell resuspension and mixed end-over-end for 10 min at 4°C, then pelleted by centrifugation at 2000g for 5 min at 4°C. The pellet was resuspended in 1 ml of Lysis Buffer 2 (LB2) (10 mM Tris-HCl pH 8.0, 200 mM NaCl, 1 mM EDTA, 0.5 mM EGTA) then 2 ml of LB2 was added to cell resuspension and mixed end-over-end for 10 min at 4°C. The nuclei pellet was resuspended in 0.9 ml of Lysis Buffer 3 (10 mM Tris-HCl pH 8.0, 200 mM NaCl, 1 mM EDTA, 0.5 mM EGTA, 0.1% Sodium Deoxycholate, 0.5 % Sarkosyl) and sonicated with a Misonix micro-tipped sonicator at ~5W for 12 cycles for 15 seconds of sonication then 45 seconds cooling (tubes are immersed in an ice-water bath). 10% Triton X-100 was added for a final concentration of 1%. The sonicated nuclear fraction was pelleted for cell debris by centrifugation (>20,000g) for 25 min at 4°C. Protein concentration was determined by BCA (Thermo Scientific, Cat#: 23209) and 300 µg of chromatin was used for ChIP (c-MYC (Y69) – 1 µg, c-MYC (ab56) – 2 µg, WDR5 – 2 µg, MAX – 2 µg, MNT – 2 µg, MXD1 – 2 µg, MGA – 2 µg, H3K27ac – 2 µg, CTCF – 2 µg, FOXA1 – 2 µg, AR – 1 µg In addition, input DNA was obtained from 10% of ChIP (30 µg) and used as control.

Immunoprecipitation (IP) was performed at 4°C with end-over-end mixing for 12-16 hrs. Protein G Dynabeads (Life Technologies, Cat#: 10004D_3641869636) were used to pull-down antibody (20 µl) bound to DNA fragments. IPs were washed 4 times with ice-cold ChIP-RIPA (50 mM HEPES-KOH pH 7.6, 500 mM LiCl, 1 mM EDTA, 1.0% IGEPAL-CA630, 0.7% sodium deoxycholate, 0.2 µm filter sterilized before use). For the 5th wash, 1 ml of TE-NaCl (10 mM Tris-HCl pH 8.0, 1mM EDTA, 50 mM NaCl, 0.2 µm filter-sterilized before use) was added to IPs and fully resuspended by end-over-end mixing. Beads were aggregated using a magnet rack and TE-NaCl

was completely aspirated. DNA was eluted with addition 50 μ l of elution buffer (0.1M NaHCO₃ and 1% SDS), held at 65°C with vigorous circular mixing for 15 min, and the eluate was collected. Beads were incubated with another 50 μ l for a total of 2 elution steps followed by pooling. Cross-links were reversed by bringing the sample to 65°C in 190mM NaCl (5 μ l of 4M NaCl into 100 μ l of eluate) for 12 hours with vigorous circular mixing. Proteinase K (Invitrogen, Cat#: 25530-015) and RNase (Worthington Biochemical Corp., Cat#: LS002132) digestion was carried out followed by DNA isolation with Qiagen miniElute PCR kit (Cat#: 28004). As input for library preparation, <1 ng – 5 ng of immunoprecipitated DNA was used. Library preparation was carried out with KAPA Hyper Prep Kit (Cat#: KK8502). Adaptor ligation was carried out for 60 min followed by 0.7-0.9X double-sided size selection with Ampure XP beads (Cat#: A63880) and a final 1X cleanup post library amplification (12 cycles total). Library concentration was determined with Qubit and library profile analyzed by an Agilent 2100 Bioanalyzer. Libraries were sequenced in multiplex and library pool concentrations were calculated with KAPA Biosystems library quantification kit (Cat#: KK4835). Single end reads (76bp) were sequenced using an Illumina NextSeq500.

RNA-seq:

Cells were plated into 6-well plates and 24 hours later treated with either 10 μ M MYCi975 or DMSO (0.2%). Cells were trypsinized and counted in duplicate using a Countess II (Thermo Scientific cat#: AMQAF1000) and 0.4% trypan blue (Thermo Scientific cat#: T10282) and 2×10^6 cells from each treatment group were washed in ice-cold PBS and centrifuged at 500g for 5 min at 4°C. RNA was isolated from cell pellets from biological quadruplicates (cells from different

passages) with Qiagen RNeasy kit (Cat#: 74134). For each sample, ~500 ng (equal aliquots of RNA to control for abundance) of RNA was used as input for RNA sequencing library preparation. Into each sample, a 1:100 dilution of ERCC92 Spike-In Mix 1 (Thermo Scientific, cat#: 4456740) was added and incorporated into the analysis pipeline. In order to capture a broader scope of RNA species, ribosome depletion library kits were used (KAPA Biosystems, Cat#: KK8560). RNA libraries were multiplexed, and final concentration was calculated with the same method as ChIP-seq. Next-generation sequencing was performed with paired-end reads (2x42bp) on an Illumina NextSeq500.

ATAC-seq:

Cells were plated in 10 cm² plates and treated with 10 μ M MYCi975 or DMSO (0.2%) for 48 hrs. ATAC-seq libraries were generated as previously described with slight modifications (114, 115). Treated and control cells were trypsinized and 1 million cells were washed in ice-cold PBS. Cells were pelleted at 500g for 5 min at 4°C and resuspended in 1 ml of lysis reaction mix (0.1% Tween-20, 0.1% IGEPAL (Sigma, cat#: I8896), 0.01 % Digitonin (Promega, cat#: G9441) in ATAC resuspension buffer (10 mM Tris-HCl pH 8.0, 10 mM NaCl, 3 mM MgCl₂). The lysis reaction was carried out on ice for 3 min, then 4 ml of wash buffer (0.1% Tween-20 in ATAC- resuspension buffer) was added and mixed end-over-end. Nuclei were pelleted at 500g for 10 min at 4°C. The pellet was resuspended in 125 μ l of ice-cold PBS and the nuclei were counted and inspected for quality. In total, 12,500 nuclei were aliquoted into the transposase tagmentation mix (2.5 μ l TDE1 enzyme and 25 μ l of TD Buffer (Illumina, FC-121-1030), 16.5 μ l of nuclei in ice-cold PBS, 0.5

μl of 1% Digitonin, 0.5 μl of 10% Tween-20 and 5 μl molecular biology-grade water). Tagmentation was carried out at 37°C for 30 min in a Thermomixer (Eppendorf) at 300 rpm. DNA was isolated using the Zymo DNA clean and concentrator (cat#: D4013) and amplified for 9 cycles with New England Biosystems High Fidelity 2X PCR Master Mix (NEB, cat#: M0541S) as described (114). PCR amplified ATAC-seq libraries were purified using the Zymo kit (cat#: D4013) and Ampure XP beads (Cat#: A63880) were used for 0.6X-1.8X size selection. Library distribution was analyzed with an Agilent 2100 Bioanalyzer. Paired-end sequencing was performed (2x42bp) using an Illumina NextSeq 500.

Data analysis:

For single-end ChIP-seq reads, raw fastq files were aligned with bowtie (v1.2.2, settings: *-t --best -m 1*) using pre-built genome indexes (NCBI) for both hg38 and mm10, downloaded from <http://bowtie-bio.sourceforge.net/manual.shtml>. For paired-end ATAC-seq, reads were aligned with bowtie2 (v2.2.6, settings: *--very-sensitive -X 800*). For paired-end RNA-seq, reads were aligned to the hg38 reference genome (NCBI, GRCh38.p12) using STAR (116) (v2.7.5, settings: *--alignIntronMin 20 --alignIntronMax 500000*). All fastq files were analyzed for quality control using FastQC (version 0.11.9). ERCC92 controls were aligned to the “ERCC92.fa” genome and processed through the RNA-seq pipeline (117). ChIP- and ATAC-seq sequence alignment files were converted to binary format using samtools (version 1.9). ChIP-seq files were used as input for creating HOMER (118) (v4.11.1) tag directories and subsequent peak calling (settings: *-tbp 1, style = factor/histone*). For ATAC-seq, MACS2 (v2.2.6) (119) was used for peak calling using the

DNase-seq enriched cut site method (`--nomodel --shift -75 --extsize 150 --nolambda -p 0.01`). Using DiffBind (v3.12, settings: `minMembers = (# of biological replicates), score=DBA_SCORE_TMM_MINUS_FULL`) for differential binding analysis, each timepoint (1-, 4-, 8-, 24- and 48-hr) was compared to DMSO and peaks called by HOMER were used to define a consensus peak list (120). Using DESeq2 (67) differences in RNA levels were determined by comparing DMSO vs. 24hr and DMSO vs. 48hr (default settings). Supplemental Table 2 provides differential binding and differential RNA level results for all MYCi975 target gene types comparing DMSO vs. 48-hr MYCi975-treated 22Rv1 cells. To determine the genomic region distribution, we used the HOMER `annotatePeaks.pl` (hg38) function with the appropriate reference genomes and selected for promoter-proximal (± 2 kb from TSS) or promoter-distal ($> \pm 2$ kb from TSS). Motif enrichment databases and statistics were calculated using the HOMER `findMotifsGenome.pl` function.

Visualization for ChIP-seq data including bigwigs, heatmaps, and read coverage histograms were generated with `deeptools bamCoverage` (settings: `--binSize 1 --normalizeUsing RPGC --effectiveGenomeSize mouse/human --extendReads 120 --ignoreDuplicates`), `plotHeatmap` and `plotProfile` function (121). Replicates were merged with `bigWigMerge` (`kentUtils`, v302) and `bedGraphs` were converted back to normalized bigwigs with `bedGraphToBigWig` function using the `chrom.sizes` file downloaded from UCSC (<https://hgdownload.cse.ucsc.edu/goldenpath/hg38/bigZips/>). Gene count matrices were generated using `featureCounts` (122) with the following NCBI reference genome annotation GTF: “hg38.ncbiRefSeq.gtf” (<http://hgdownload.soe.ucsc.edu/goldenPath/hg38/bigZips/genes/>) (subread v1.6.1). Bigwig files for RNA-seq visualization were created using a similar method as ChIP-seq with merging both the forward and reverse strands using

the recommended methods from deeptools (additional commands: samtools sort; bamCoverage – effectiveGenomeSize 2913022398 -e -normalizeUsing CPM v3.3.0) (121). For genome browser tracks we used pyGenomeTracks (123, 124) with merged bigwig files from biological replicates to display occupancy at certain gene loci. Scale settings were normalized for each experimental ChIP-seq or RNA-seq group (i.e., DMSO, 24-hr, 48-hr). For any overlapping peaks analyzed (i.e., MYCi975-sensitive vs. MYCi975 H3K27ac loss), we used the function mergePeaks (-d 200 when comparing MYC and MAX, -d 200 when comparing ATAC peaks with TF peaks, -d 1000 when comparing with H3K27ac peaks, HOMER v4.11.1). Tag densities for ChIP-seq signals at each MYCi975 gene target type were calculated with annotatePeaks.pl (settings: hg38, -size 400, -norm 0) using tag directories for each DMSO-treated biological replicate. To compare tag densities of multiple peak sets, each peak tag density (normalized by total tag counts in directory) was \log_2 transformed. MYCi975 gene target types were selected from MYC-bound annotated promoters. For each peak, differential binding analysis and differential RNA levels were overlapped for the annotated promoters. The differential binding data was sorted based on false discovery rate (FDR) and peaks with $FDR < 0.01$ were used to select MYCi975 gene target Types 1-3. Type 1 and 2 genes represent all differentially lost MYC-bound promoters with either up- or downregulated RNA levels, respectively. MYCi975 Type 3 genes represent all differentially MYC-bound promoters with differential RNA level data such that $FDR > 0.01$. Type 4 consists of “MYCi-insensitive” promoter proximal MYC-bound peaks that represent genes with low tag density, no differential MYC binding and no differential gene expression ($FDR > 0.01$). Differential MAX binding was overlapped with MYC binding sites and sorted based on FDR. Of the differential MYC bind-

ing sites (MYCi975-sensitive), overlapping MAX analysis determined 6,812 peaks where no significant changes in MAX was determined (differential MAX binding FDR > 0.01) and is described as the MAX retained sites. ATAC-seq alignment files were filtered for mitochondrial reads using `sed` and adaptors were removed with `NGmerge (v0.2_dev)` (125). Differential ATAC analysis was carried out using `DiffBind` with the same score setting as above. MACS2 ATAC-seq peaks were used from each individual replicate for `diffBind`. Peaks from each ATAC-seq dataset (DMSO vs. 48-hr MYCi975) were used as input for differential transcription factor activity analysis (`DAStk`) using default settings (106). Visualization tracks were generated from read pileup files (`.bdg`, MACS2) from peak calling and all replicates were merged with the same protocol as above. For GSEA (65) analysis of RNA-seq each gene was assigned a rank metric $[-\log_{10}(\text{FDR}) \times \log_2(\text{fold-change})]$ and this pre-ranked list was used as input for GSEA hallmarks v7.4 database. For ChIP-seq data the rank metric was calculated for promoter proximal MYC bound genes and differential MYC binding data using the same hallmarks database as above. For multiple peaks that annotate to a single promoter the average rank metric of each ‘multi-peak promoter’ was used as input in the final pre-ranked list for GSEA.

ENCODE/cistromeDB analysis:

Using the ENCODE ChIP-seq matrix (<https://www.encodeproject.org>) to locate deposited MYC ChIP-seq datasets, bed files were downloaded. The following is a list of cell lines with MYC ChIP-seq peak datasets that were downloaded from ENCODE using the “Transcription Factor” and “cell line” tabs selected: NB4 (ENCFF002CZO), K562 (ENCFF002CWI), HeLa (ENCFF950LQM),

A549 (ENCFF542GMN), and MCF7 (ENCFF370EQJ). In addition, two MYC ChIP-seq peak datasets were downloaded from the Cistrome Data Browser (<http://cistrome.org/db/#/>); P493-6 (encode: GSM1036404), MCF10A (encode: GSM935491). All other cell lines (22Rv1, DU145 and MycCap) were analyzed according to the ChIP-seq protocol above. Peaks were then called with HOMER (v.4.11.1, findPeaks -style factor). All reference genomes were converted to hg38 using CrossMap (v0.3.6) with the “over.chain” files downloaded from source (<http://crossmap.sourceforge.net>) (126). Once all peaks were converted to the hg38 reference genome, peak files were annotated with HOMER annotatePeaks.pl and then split into either promoter-proximal (HOMER promoter annotated) or -distal (all other HOMER annotations) regions. HOMER motif analysis was run on all peak sets with default settings. Motif enrichment results are displayed as $\log_{10}(\text{p-value})$ for CTCF, FOXA1, FOXM1, and c-MYC motifs from HOMER.

In vivo experiments:

All animal experiments and procedures were performed in compliance with ethical regulations and the approval of the Northwestern University Institutional Animal Care and Use Committee (IACUC). CD1-Foxn1nu (086) mice were obtained from the Charles River. All mice were housed in a pathogen-free animal barrier facility. All *in vivo* experiments were initiated with mice at 6 to 8 weeks of age. 22Rv1 prostate cancer cells (2×10^6) suspended in 100 μl BD Matrigel were subcutaneously injected into flanks of mice. Tumor volume (mm^3) was calculated by the following formula ($\text{length} \times \text{width}^2$)/2. When the tumor size reached 150 to 200 mm^3 , mice were then randomized into groups with similar average tumor size in each group. MYCi975 was prepared and administered as described (60). ENZ was purchased from MedChem Express (HY-70002) and

prepared in 5% DMSO in corn oil, and given by P.O. Tumors were harvested after 18 or 21 days of treatment. Mouse body weight was monitored every 2-3 days.

References

1. D. Sheiness, J. M. Bishop, DNA and RNA from Uninfected Vertebrate Cells Contain Nucleotide Sequences Related to the Putative Transforming Gene of Avian Myelocytomatosis Virus. *J. Virol.* **31**, 514–521 (1979).
2. H. D. Abrams, L. R. Rohrschneider, R. N. Eisenman, Nuclear location of the putative transforming protein of avian myelocytomatosis virus. *Cell.* **29**, 427–439 (1982).
3. K. Alitalo, G. Ramsay, J. M. Bishop, S. O. Pfeifer, W. W. Colby, A. D. Levinson, Identification of nuclear proteins encoded by viral and cellular myc oncogenes. *Nature.* **306**, 274–277 (1983).
4. R. Wiess, The myc oncogene in man and birds. *Nature.* **299**, 9–10 (1982).
5. D. Sheiness, L. Fanshier, J. M. Bishop, Identification of nucleotide sequences which may encode the oncogenic capacity of avian retrovirus MC29. *J. Virol.* **28**, 600–610 (1978).
6. R. A. Watt, A. R. Shatzman, M. Rosenberg, Expression and characterization of the human c-myc DNA-binding protein. *Mol. Cell. Biol.* **5**, 448–456 (1985).
7. T. K. Blackwell, K. Leo, B. E. M, R. N. Eisenman, H. Weintruab, Sequence-Specific DNA Binding by the c-Myc Protein. *Science (80-.).* **250**, 1149–1151 (1990).
8. E. M. Blackwood, L. Kretzner, R. N. Eisenman, Myc and Max function as a nucleoprotein complex. *Curr. Opin. Genet. Dev.* **2**, 227–235 (1992).
9. D. A. Gillespie, R. N. Eisenman, Detection of a Myc-associated protein by chemical cross-linking. *Mol. Cell. Biol.* **9**, 865–868 (1989).
10. E. M. Blackwood, B. Luscher, L. Kretzner, R. N. Eisenman, The Myc:Max protein complex and cell growth regulation. *Cold Spring Harb. Symp. Quant. Biol.* **56**, 109–117

- (1991).
11. K. Kelly, B. H. Cochran, C. D. Stiles, P. Leder, Cell-specific regulation of the c-myc gene by lymphocyte mitogens and platelet-derived growth factor. *Cell*. **35**, 603–610 (1983).
 12. B. Lutterbach, S. R. Hann, Hierarchical phosphorylation at N-terminal transformation-sensitive sites in c-Myc protein is regulated by mitogens and in mitosis. *Mol. Cell. Biol.* **14**, 5510–5522 (1994).
 13. A. Seth, F. A. Gonzalez, S. Gupta, D. L. Raden, R. J. Davis, Signal transduction within the nucleus by mitogen-activated protein kinase. *J. Biol. Chem.* **267**, 24796–24804 (1992).
 14. E. V. Schmidt, The role of c-myc in cellular growth control. *Oncogene*. **18**, 2988–2996 (1999).
 15. S. B. McMahon, MYC and the control of apoptosis. *Cold Spring Harb. Perspect. Med.* **4**, 1–10 (2014).
 16. M. Eilers, R. N. Eisenman, Myc's broad reach. *Genes Dev.* **22**, 2755–2766 (2008).
 17. A. Y. and D. W. F. Jan van Riggelen, MYC as a regulator of ribosome biogenesis and protein synthesis. *Nat. Rev. Cancer*. **10**, 301–309 (2010).
 18. D. Dominguez-Sola, J. Gautier, MYC and the Control of DNA Replication. *Cold Spring Harb. Perspect. Med.* **4** (2014), doi:10.1101/cshperspect.a014407.
 19. G. Bretones, M. D. Delgado, J. León, Myc and cell cycle control. *Biochim. Biophys. Acta - Gene Regul. Mech.* **1849**, 506–516 (2015).
 20. S. C. Casey, V. Baylot, D. W. Felsher, The MYC oncogene is a global regulator of the immune response. *Blood*. **131**, 2007–2015 (2018).
 21. K. Rakhra, P. Bachireddy, T. Zabuawala, R. Zeiser, L. Xu, A. Kopelman, A. C. Fan, Q.

- Yang, L. Braunstein, E. Crosby, S. Ryeom, D. W. Felsher, CD4+ T Cells contribute to the remodeling of the microenvironment required for sustained tumor regression upon oncogene inactivation. *Cancer Cell*. **18**, 485–498 (2010).
22. F. R. Dejure, M. Eilers, MYC and tumor metabolism: chicken and egg. *EMBO J*. **36**, 3409–3420 (2017).
23. X. Wang, X. Zhao, P. Gao, M. Wu, C-Myc modulates microRNA processing via the transcriptional regulation of Droscha. *Sci. Rep.* **3**, 1–7 (2013).
24. A. Onnis, G. de Falco, G. Antonicelli, M. Onorati, C. Bellan, O. Sherman, S. Sayed, L. Leoncini, Alteration of microRNAs regulated by c-Myc in Burkitt Lymphoma. *PLoS One*. **5** (2010), doi:10.1371/journal.pone.0012960.
25. A. Sabò, T. R. Kress, M. Pelizzola, S. De Pretis, M. M. Gorski, A. Tesi, M. J. Morelli, P. Bora, M. Doni, A. Verrecchia, C. Tonelli, G. Fagà, V. Bianchi, A. Ronchi, D. Low, H. Müller, E. Guccione, S. Campaner, B. Amati, Selective transcriptional regulation by Myc in cellular growth control and lymphomagenesis. *Nature*. **511**, 488–492 (2014).
26. M. Muhar, A. Ebert, T. Neumann, C. Umkehrer, J. Jude, C. Wieshofer, P. Rescheneder, J. J. Lipp, V. A. Herzog, B. Reichholf, D. A. Cisneros, T. Hoffmann, M. F. Schlapansky, P. Bhat, A. Von Haeseler, T. Köcher, A. C. Obenauf, J. Popow, S. L. Ameres, J. Zuber, SLAM-seq defines direct gene-regulatory functions of the BRD4-MYC axis. **805**, 800–805 (2018).
27. C. Y. Lin, J. Lovén, P. B. Rahl, R. M. Paranal, C. B. Burge, J. E. Bradner, T. I. Lee, R. A. Young, Transcriptional amplification in tumor cells with elevated c-Myc. *Cell*. **151**, 56–67 (2012).

28. T. R. Kress, A. Sabò, B. Amati, MYC: Connecting selective transcriptional control to global RNA production. *Nat. Rev. Cancer*. **15**, 593–607 (2015).
29. S. Walz, F. Lorenzin, J. Morton, K. E. Wiese, B. Von Eyss, S. Herold, L. Rycak, H. Dumay-Odelot, S. Karim, M. Bartkuhn, F. Roels, T. Wüstefeld, M. Fischer, M. Teichmann, L. Zender, C. L. Wei, O. Sansom, E. Wolf, M. Eilers, Activation and repression by oncogenic MYC shape tumour-specific gene expression profiles. *Nature*. **511**, 483–487 (2014).
30. F. Lorenzin, U. Benary, A. Baluapuri, S. Walz, L. A. Jung, B. von Eyss, C. Kisker, J. Wolf, M. Eilers, E. Wolf, Different promoter affinities account for specificity in MYC-dependent gene regulation. *Elife*. **5**, 1–35 (2016).
31. and D. F. Gabay, Meital, Yulin Li, MYC Activation Is a Hallmark of Cancer Initiation and Maintenance Meital. **36**, 186–194 (2009).
32. C. V. Dang, MYC on the path to cancer. *Cell*. **149**, 22–35 (2012).
33. D. Hanahan, R. A. Weinberg, Hallmarks of cancer: The next generation. *Cell*. **144**, 646–674 (2011).
34. S. Collins, M. Goudine, Amplification of endogenous myc-related DNA sequences in a human myeloid leukaemia cell line. *Nature*. **298**, 3–4 (2015).
35. R. Beroukhi, C. H. Mermel, D. Porter, G. Wei, S. Raychaudhuri, J. Donovan, J. Barretina, J. S. Boehm, J. Dobson, M. Urashima, K. T. McHenry, R. M. Pinchback, A. H. Ligon, Y. J. Cho, L. Haery, H. Greulich, M. Reich, W. Winckler, M. S. Lawrence, B. A. Weir, K. E. Tanaka, D. Y. Chiang, A. J. Bass, A. Loo, C. Hoffman, J. Prensner, T. Liefeld, Q. Gao, D. Yecies, S. Signoretti, E. Maher, F. J. Kaye, H. Sasaki, J. E. Tepper, J.

- A. Fletcher, J. Taberero, J. Baselga, M. S. Tsao, F. Demichelis, M. A. Rubin, P. A. Janne, M. J. Daly, C. Nucera, R. L. Levine, B. L. Ebert, S. Gabriele, A. K. Rustgi, C. R. Antonescu, M. Ladanyi, A. Letai, L. A. Garraway, M. Loda, D. G. Beer, L. D. True, A. Okamoto, S. L. Pomeroy, S. Singer, T. R. Golub, E. S. Lander, G. Getz, W. R. Sellers, M. Meyerson, The landscape of somatic copy-number alteration across human cancers. *Nature*. **463**, 899–905 (2010).
36. M. Kalkat, J. De Melo, K. A. Hickman, C. Lourenco, C. Redel, D. Resetca, A. Tamachi, W. B. Tu, L. Z. Penn, MYC deregulation in primary human cancers. *Genes (Basel)*. **8**, 2–30 (2017).
37. D. Hawksworth, L. Ravindranath, Y. Chen, B. Furusato, I. A. Sesterhenn, D. G. Mcleod, S. Srivastava, G. Petrovics, Overexpression of C-MYC oncogene in prostate cancer predicts biochemical recurrence. *Prostate Cancer Prostatic Dis*. **13**, 311–315 (2010).
38. J. K. Lee, J. W. Phillips, B. A. Smith, J. W. Park, T. Stoyanova, E. F. McCaffrey, R. Baertsch, A. Sokolov, J. G. Meyerowitz, C. Mathis, D. Cheng, J. M. Stuart, K. M. Shokat, W. C. Gustafson, J. Huang, O. N. Witte, N-Myc Drives Neuroendocrine Prostate Cancer Initiated from Human Prostate Epithelial Cells. *Cancer Cell*. **29**, 536–547 (2016).
39. S. Bai, S. Cao, L. Jin, M. Kobelski, B. Schouest, X. Wang, N. Ungerleider, M. Baddoo, W. Zhang, E. Corey, R. L. Vessella, X. Dong, K. Zhang, X. Yu, E. K. Flemington, Y. Dong, A positive role of c-Myc in regulating androgen receptor and its splice variants in prostate cancer. *Oncogene*, 4977–4989 (2019).
40. E. Hörnberg, E. B. Ylitalo, S. Crnalic, H. Antti, P. Stattin, A. Widmark, A. Bergh, P. Wikström, Expression of androgen receptor splice variants in prostate cancer bone

- metastases is associated with castration-resistance and short survival. *PLoS One*. **6** (2011), doi:10.1371/journal.pone.0019059.
41. C. Lu, L. Brown, E. S. Antonarakis, A. J. Armstrong, J. Luo, Androgen Receptor Variant-Driven Prostate Cancer II: Advances in Laboratory Investigations. *Prostate Cancer Prostatic Dis.* **23**, 381–397 (2020).
 42. L. Cato, J. de Tribolet-Hardy, I. Lee, J. T. Rottenberg, I. Coleman, D. Melchers, R. Houtman, T. Xiao, W. Li, T. Uo, S. Sun, N. C. Kuznik, B. Göppert, F. Ozgun, M. E. van Royen, A. B. Houtsmuller, R. Vadhi, P. K. Rao, L. Li, S. P. Balk, R. B. Den, B. J. Trock, R. J. Karnes, R. B. Jenkins, E. A. Klein, E. Davicioni, F. J. Gruhl, H. W. Long, X. S. Liu, A. C. B. Cato, N. A. Lack, P. S. Nelson, S. R. Plymate, A. C. Groner, M. Brown, ARv7 Represses Tumor-Suppressor Genes in Castration-Resistant Prostate Cancer. *Cancer Cell* (2019), doi:10.1016/j.ccell.2019.01.008.
 43. M. Savino, D. Annibali, N. Carucci, E. Favuzzi, M. D. Cole, I. Gerard, L. Soucek, S. Nasi, The Action Mechanism of the Myc Inhibitor Termed Omomyc May Give Clues on How to Target Myc for Cancer Therapy. **6** (2011), doi:10.1371/journal.pone.0022284.
 44. L. Soucek, R. Jucker, L. Panacchia, R. Ricordy, F. Tatò, S. Nasi, Omomyc, a potential Myc dominant negative, enhances Myc-induced apoptosis. *Cancer Res.* **62**, 3507–3510 (2002).
 45. C. M. Eischen, J. D. Weber, M. F. Roussel, C. J. Sherr, J. L. Cleveland, Disruption of the ARF-Mdm2-p53 tumor suppressor pathway in Myc-induced lymphomagenesis. *Genes Dev.* **13**, 2658–2669 (1999).
 46. L. A. Jung, A. Gebhardt, W. Koelmel, C. P. Ade, S. Walz, J. Kuper, B. Von Eyss, S.

- Letschert, C. Redel, L. D'Artista, A. Biankin, L. Zender, M. Sauer, E. Wolf, G. Evan, C. Kisker, M. Eilers, OmoMYC blunts promoter invasion by oncogenic MYC to inhibit gene expression characteristic of MYC-dependent tumors. *Oncogene*. **36**, 1911–1924 (2017).
47. J. R. Whitfield, M. E. Beaulieu, L. Soucek, Strategies to inhibit Myc and their clinical applicability. *Front. Cell Dev. Biol.* **5**, 1–13 (2017).
48. L. A. Carabet, P. S. Rennie, A. Cherkasov, Therapeutic inhibition of myc in cancer. Structural bases and computer-aided drug discovery approaches. *Int. J. Mol. Sci.* **20** (2019), doi:10.3390/ijms20010120.
49. M. R. McKeown, J. E. Bradner, Therapeutic strategies to inhibit MYC. *Cold Spring Harb. Perspect. Med.* **4** (2014), doi:10.1101/cshperspect.a014266.
50. E. V. Prochownik, P. K. Vogt, Therapeutic Targeting of Myc. *Genes Cancer*. **1**, 650–659 (2010).
51. L. Boike, A. G. Cioffi, F. C. Majewski, J. Co, N. J. Henning, M. D. Jones, G. Liu, J. M. McKenna, J. A. Tallarico, M. Schirle, D. K. Nomura, Discovery of a Functional Covalent Ligand Targeting an Intrinsically Disordered Cysteine within MYC. *Cell Chem. Biol.* **28**, 4-13.e17 (2021).
52. J. E. Delmore, G. C. Issa, M. E. Lemieux, P. B. Rahl, J. Shi, H. M. Jacobs, E. Kastiris, T. Gilpatrick, R. M. Paranal, J. Qi, M. Chesi, A. C. Schinzel, M. R. McKeown, T. P. Heffernan, C. R. Vakoc, P. L. Bergsagel, I. M. Ghobrial, P. G. Richardson, R. A. Young, W. C. Hahn, K. C. Anderson, A. L. Kung, J. E. Bradner, C. S. Mitsiades, BET bromodomain inhibition as a therapeutic strategy to target c-Myc. *Cell*. **146**, 904–917 (2011).

53. N. B. Struntz, A. Chen, A. Deutzmann, R. M. Wilson, E. Stefan, H. L. Evans, M. A. Ramirez, T. Liang, F. Caballero, M. H. E. Wildschut, D. V. Neel, D. B. Freeman, M. S. Pop, M. McConkey, S. Muller, B. H. Curtin, H. Tseng, K. R. Frombach, V. L. Butty, S. S. Levine, C. Feau, S. Elmiligy, J. A. Hong, T. A. Lewis, A. Vetere, P. A. Clemons, S. E. Malstrom, B. L. Ebert, C. Y. Lin, D. W. Felsher, A. N. Koehler, Stabilization of the Max Homodimer with a Small Molecule Attenuates Myc-Driven Transcription. *Cell Chem. Biol.* **26**, 711-723.e14 (2019).
54. A. A. Antolin, M. Ameratunga, U. Banerji, P. A. Clarke, P. Workman, B. Al-Lazikani, The kinase polypharmacology landscape of clinical PARP inhibitors. *Sci. Rep.* **10**, 1–14 (2020).
55. J. Günther, J. Däbritz, E. Wirthgen, Limitations and Off-Target Effects of Tryptophan-Related IDO Inhibitors in Cancer Treatment. *Front. Immunol.* **10**, 1801 (2019).
56. M. S. Rao, R. Gupta, M. J. Liguori, M. Hu, X. Huang, S. R. Mantena, S. W. Mittelstadt, E. A. G. Blomme, T. R. Van Vleet, Novel Computational Approach to Predict Off-Target Interactions for Small Molecules. *Front. Big Data.* **2**, 1–17 (2019).
57. A. Lin, C. J. Giuliano, A. Palladino, K. M. John, C. Abramowicz, M. Lou Yuan, E. L. Sausville, D. A. Lukow, L. Liu, A. R. Chait, Z. C. Galluzzo, C. Tucker, J. M. Sheltzer, Off-target toxicity is a common mechanism of action of cancer drugs undergoing clinical trials. *Sci. Transl. Med.* **11** (2019), doi:10.1126/scitranslmed.aaw8412.
58. S. R. Frank, T. Parisi, S. Taubert, P. Fernandez, M. Fuchs, H. M. Chan, D. M. Livingston, B. Amati, MYC recruits the TIP60 histone acetyltransferase complex to chromatin. *EMBO Rep.* **4**, 575–580 (2003).

59. F. Martinato, M. Cesaroni, B. Amati, E. Guccione, Analysis of myc-induced histone modifications on target chromatin. *PLoS One*. **3** (2008), doi:10.1371/journal.pone.0003650.
60. H. Han, A. D. Jain, M. I. Truica, J. Izquierdo-Ferrer, J. F. Anker, B. Lysy, V. Sagar, Y. Luan, Z. R. Chalmers, K. Unno, H. Mok, R. Vatapalli, Y. A. Yoo, Y. Rodriguez, I. Kandela, J. B. Parker, D. Chakravarti, R. K. Mishra, G. E. Schiltz, S. A. Abdulkadir, Small-Molecule MYC Inhibitors Suppress Tumor Growth and Enhance Immunotherapy. *Cancer Cell*. **36**, 483-497.e15 (2019).
61. M. I. Truica, M. C. Burns, H. Han, S. A. Abdulkadir, Turning Up the Heat on MYC: Progress in Small-Molecule Inhibitors. *Cancer Res*. **81**, 248–253 (2021).
62. S. Venkatachalam, T. R. McFarland, N. Agarwal, U. Swami, Immune checkpoint inhibitors in prostate cancer. *Cancers (Basel)*. **13** (2021), doi:10.3390/cancers13092187.
63. A. G. Holmes, J. B. Parker, V. Sagar, M. I. Truica, P. N. Soni, H. Han, G. E. Schiltz, S. A. Abdulkadir, D. Chakravarti, A MYC inhibitor selectively alters the MYC and MAX cistromes and modulates the epigenomic landscape to regulate target gene expression. *Sci. Adv.* **8**, eabh3635 (2022).
64. C. A. Schneider, W. S. Rasband, K. W. Eliceiri, NIH Image to ImageJ: 25 years of image analysis. *Nat. Methods*. **9**, 671–675 (2012).
65. A. Subramanian, P. Tamayo, V. K. Mootha, S. Mukherjee, B. L. Ebert, M. A. Gillette, A. Paulovich, S. L. Pomeroy, T. R. Golub, E. S. Lander, J. P. Mesirov, Gene set enrichment analysis: A knowledge-based approach for interpreting genome-wide expression profiles. *Proc. Natl. Acad. Sci. U. S. A.* **102**, 15545–15550 (2005).

66. L. R. Thomas, Q. Wang, S. W. Fesik, W. P. Tansey, L. R. Thomas, Q. Wang, B. C. Grieb, J. Phan, A. M. Foshage, Q. Sun, E. T. Olejniczak, T. Clark, S. Dey, S. Lorey, B. Alicie, G. C. Howard, B. Cawthon, K. C. Ess, C. M. Eischen, Z. Zhao, S. W. Fesik, W. P. Tansey, Interaction with WDR5 Promotes Target Gene Recognition and Tumorigenesis by MYC Article Interaction with WDR5 Promotes Target Gene Recognition and Tumorigenesis by MYC. *Mol. Cell.* **58**, 440–452 (2015).
67. M. I. Love, W. Huber, S. Anders, Moderated estimation of fold change and dispersion for RNA-seq data with DESeq2. *Genome Biol.* **15**, 1–21 (2014).
68. M. J. Daly, N. Patterson, J. P. Mesirov, T. R. Golub, P. Tamayo, B. Spiegelman, PGC-1 α -responsive genes involved in oxidative phosphorylation are coordinately downregulated in human diabetes. *Nat. Genet.* **34**, 267–273 (2003).
69. J. Du, R. Xu, ROR α , a potential tumor suppressor and therapeutic target of breast cancer. *Int. J. Mol. Sci.* **13**, 15755–15766 (2012).
70. H. Kim, J. M. Lee, G. Lee, J. Bhin, S. K. Oh, K. Kim, K. E. Pyo, J. S. Lee, H. Y. Yim, K. Il Kim, D. Hwang, J. Chung, S. H. Baek, DNA damage-induced ROR α Is crucial for p53 stabilization and increased apoptosis. *Mol. Cell.* **44**, 797–810 (2011).
71. C. Y. McLean, D. Bristor, M. Hiller, S. L. Clarke, B. T. Schaar, C. B. Lowe, A. M. Wenger, G. Bejerano, GREAT improves functional interpretation of cis-regulatory regions. *Nat. Biotechnol.* **28**, 495–501 (2010).
72. C. A. Davis, B. C. Hitz, C. A. Sloan, E. T. Chan, J. M. Davidson, I. Gabdank, J. A. Hilton, K. Jain, U. K. Baymuradov, A. K. Narayanan, K. C. Onate, K. Graham, S. R. Miyasato, T. R. Dreszer, J. S. Strattan, O. Jolanki, F. Y. Tanaka, J. M. Cherry, The Encyclopedia of

- DNA elements (ENCODE): Data portal update. *Nucleic Acids Res.* **46**, D794–D801 (2018).
73. R. Zheng, C. Wan, S. Mei, Q. Qin, Q. Wu, H. Sun, C. H. Chen, M. Brown, X. Zhang, C. A. Meyer, X. S. Liu, Cistrome Data Browser: Expanded datasets and new tools for gene regulatory analysis. *Nucleic Acids Res.* **47**, D729–D735 (2019).
74. S. Mei, Q. Qin, Q. Wu, H. Sun, R. Zheng, C. Zang, M. Zhu, J. Wu, X. Shi, L. Taing, T. Liu, M. Brown, C. A. Meyer, X. S. Liu, Cistrome Data Browser: A data portal for ChIP-Seq and chromatin accessibility data in human and mouse. *Nucleic Acids Res.* **45**, D658–D662 (2017).
75. K. S. Zaret, J. S. Carroll, Pioneer transcription factors: Establishing competence for gene expression. *Genes Dev.* **25**, 2227–2241 (2011).
76. A. Mayran, J. Drouin, Pioneer transcription factors shape the epigenetic landscape. *J. Biol. Chem.* **293**, 13795–13804 (2018).
77. M. Conacci-Sorrell, L. McFerrin, R. N. Eisenman, An overview of MYC and its interactome. *Cold Spring Harb. Perspect. Med.* **4**, 1–24 (2014).
78. J. R. Conway, A. Lex, N. Gehlenborg, UpSetR: An R package for the visualization of intersecting sets and their properties. *Bioinformatics.* **33**, 2938–2940 (2017).
79. J. Vervoorts, J. M. Lüscher-Firzlauff, S. Rottmann, R. Lilischkis, G. Walsemann, K. Dohmann, M. Austen, B. Lüscher, Stimulation of c-MYC transcriptional activity and acetylation by recruitment of the cofactor CBP. *EMBO Rep.* **4**, 484–490 (2003).
80. E. E. Swinstead, T. B. Miranda, V. Paakinaho, S. Baek, I. Goldstein, M. Hawkins, T. S. Karpova, D. Ball, D. Mazza, L. D. Lavis, J. B. Grimm, T. Morisaki, L. Grøntved, D. M.

- Presman, G. L. Hager, Steroid Receptors Reprogram FoxA1 Occupancy through Dynamic Chromatin Transitions. *Cell*. **165**, 593–605 (2016).
81. S. Zheng, W. Wang, J. Aldahdooh, A. Malyutina, T. Shadbahr, Z. Tanoli, A. Pessia, J. Tang, SynergyFinder Plus: Toward Better Interpretation and Annotation of Drug Combination Screening Datasets. *Genomics. Proteomics Bioinformatics* (2022), doi:10.1016/j.gpb.2022.01.004.
82. C. Lourenco, D. Resetca, C. Redel, P. Lin, A. S. MacDonald, R. Ciaccio, T. M. G. Kenney, Y. Wei, D. W. Andrews, M. Sunnerhagen, C. H. Arrowsmith, B. Raught, L. Z. Penn, MYC protein interactors in gene transcription and cancer. *Nat. Rev. Cancer*. **21**, 579–591 (2021).
83. M. Kalkat, D. Resetca, C. Lourenco, P. K. Chan, Y. Wei, Y. J. Shiah, N. Vitkin, Y. Tong, M. Sunnerhagen, S. J. Done, P. C. Boutros, B. Raught, L. Z. Penn, MYC Protein Interactome Profiling Reveals Functionally Distinct Regions that Cooperate to Drive Tumorigenesis. *Mol. Cell*. **72**, 836-848.e7 (2018).
84. D. Leclerc, D. N. T. Pham, N. Lévesque, M. Truongcao, W. D. Foulkes, C. Sapienza, R. Rozen, Oncogenic role of PDK4 in human colon cancer cells. *Br. J. Cancer*. **116**, 930–936 (2017).
85. E. Atas, M. Oberhuber, L. Kenner, The Implications of PDK1–4 on Tumor Energy Metabolism, Aggressiveness and Therapy Resistance. *Front. Oncol.* **10**, 1–9 (2020).
86. B. L. Woolbright, D. Choudhary, A. Mikhalyuk, C. Trammel, S. Shanmugam, E. Abbott, C. C. Pilbeam, J. A. Taylor, The role of pyruvate dehydrogenase kinase-4 (PDK4) in bladder cancer and chemoresistance. *Mol. Cancer Ther.* **17**, 2004–2012 (2018).

87. I. Aversa, F. Zolea, C. Ieranò, S. Bulotta, A. M. Trotta, M. C. Faniello, C. De Marco, D. Malanga, F. Biamonte, G. Viglietto, G. Cuda, S. Scala, F. Costanzo, Epithelial-to-mesenchymal transition in FHC-silenced cells: The role of CXCR4/CXCL12 axis. *J. Exp. Clin. Cancer Res.* **36**, 1–15 (2017).
88. N. Lobello, F. Biamonte, M. E. Pisanu, M. C. Faniello, Ž. Jakopin, E. Chiarella, E. D. Giovannone, R. Mancini, G. Ciliberto, G. Cuda, F. Costanzo, Ferritin heavy chain is a negative regulator of ovarian cancer stem cell expansion and epithelial to mesenchymal transition. *Oncotarget.* **7**, 62019–62033 (2016).
89. R. Siersbæk, J. G. S. Madsen, B. M. Javierre, R. Nielsen, E. K. Bagge, J. Cairns, S. W. Wingett, S. Traynor, M. Spivakov, P. Fraser, S. Mandrup, Dynamic Rewiring of Promoter-Anchored Chromatin Loops during Adipocyte Differentiation. *Mol. Cell.* **66**, 420-435.e5 (2017).
90. A. J. Rubin, B. C. Barajas, M. Furlan-Magaril, V. Lopez-Pajares, M. R. Mumbach, I. Howard, D. S. Kim, L. D. Boxer, J. Cairns, M. Spivakov, S. W. Wingett, M. Shi, Z. Zhao, W. J. Greenleaf, A. Kundaje, M. Snyder, H. Y. Chang, P. Fraser, P. A. Khavari, Lineage-specific dynamic and pre-established enhancer-promoter contacts cooperate in terminal differentiation. *Nat. Genet.* **49**, 1522–1528 (2017).
91. M. Ni, Y. Chen, T. Fei, D. Li, E. Lim, X. S. Liu, M. Brown, Amplitude modulation of androgen signaling by c-MYC. *Genes Dev.* **27**, 734–748 (2013).
92. S. C. Chan, Y. Li, S. M. Dehm, Androgen receptor splice variants activate androgen receptor target genes and support aberrant prostate cancer cell growth independent of canonical androgen receptor nuclear localization signal. *J. Biol. Chem.* (2012),

doi:10.1074/jbc.M112.352930.

93. J. L. L. Robinson, J. S. Carroll, FoxA1 is a key mediator of hormonal response in breast and prostate cancer. *Front. Endocrinol. (Lausanne)*. **3**, 1–6 (2012).
94. A. Hurtado, K. A. Holmes, C. S. Ross-Innes, D. Schmidt, J. S. Carroll, FOXA1 is a key determinant of estrogen receptor function and endocrine response. *Nat. Genet.* **43**, 27–33 (2011).
95. P. A. Carroll, B. W. Freie, H. Mathsyaraja, R. N. Eisenman, The MYC transcription factor network: balancing metabolism, proliferation and oncogenesis. *Front. Med.* **12**, 412–425 (2018).
96. B. Mukherjee, S. D. Morgenbesser, R. A. DePinho, Myc family oncoproteins function through a common pathway to transform normal cells in culture : cross -interference by Max and trans-acting dominant mutants. *Genes Dev.* **6**, 1480–1492 (1992).
97. A. Augert, H. Mathsyaraja, A. H. Ibrahim, B. Freie, M. J. Geuenich, P.-F. Cheng, S. P. Alibeckoff, N. Wu, J. B. Hiatt, R. Basom, A. Gazdar, L. B. Sullivan, R. N. Eisenman, D. MacPherson, MAX Functions as a Tumor Suppressor and Rewires Metabolism in Small Cell Lung Cancer. *Cancer Cell.* **0** (2020), doi:10.1016/J.CCELL.2020.04.016.
98. N. B. Struntz, A. Chen, A. Deutzmann, C. Y. Lin, D. W. Felsher, A. N. Koehler, N. B. Struntz, A. Chen, A. Deutzmann, R. M. Wilson, E. Stefan, H. L. Evans, Stabilization of the Max Homodimer with a Small Molecule Attenuates Myc-Driven Transcription Article Stabilization of the Max Homodimer with a Small Molecule Attenuates Myc-Driven Transcription. *Cell Chem. Biol.* **26**, 711-723.e14 (2019).
99. I. M. N. Wortel, L. T. van der Meer, M. S. Kilberg, F. N. van Leeuwen, Surviving Stress:

- Modulation of ATF4-Mediated Stress Responses in Normal and Malignant Cells. *Trends Endocrinol. Metab.* **28**, 794–806 (2017).
100. I. M. N. Wortel, L. T. van der Meer, M. S. Kilberg, F. N. van Leeuwen, Surviving Stress: Modulation of ATF4-Mediated Stress Responses in Normal and Malignant Cells. *Trends Endocrinol. Metab.* **28**, 794–806 (2017).
101. K. Pakos-Zebrucka, I. Koryga, K. Mnich, M. Ljujic, A. Samali, A. M. Gorman, The integrated stress response. *EMBO Rep.* **17**, 1374–1395 (2016).
102. D. Denton, S. Nicolson, S. Kumar, Cell death by autophagy: Facts and apparent artefacts. *Cell Death Differ.* **19**, 87–95 (2012).
103. K. Ameri, A. L. Harris, Activating transcription factor 4. *Int. J. Biochem. Cell Biol.* **40**, 14–21 (2008).
104. C. J. Huggins, M. K. Mayekar, N. Martin, K. L. Saylor, M. Gonit, P. Jailwala, M. Kasoji, D. C. Haines, O. A. Quiñones, P. F. Johnson, C/EBP γ Is a Critical Regulator of Cellular Stress Response Networks through Heterodimerization with ATF4. *Mol. Cell. Biol.* **36**, 693–713 (2016).
105. F. Tameire, I. I. Verginadis, N. M. Leli, C. Polte, C. S. Conn, R. Ojha, C. Salas Salinas, F. Chinga, A. M. Monroy, W. Fu, P. Wang, A. Kossenkov, J. Ye, R. K. Amaravadi, Z. Ignatova, S. Y. Fuchs, J. A. Diehl, D. Ruggero, C. Koumenis, ATF4 couples MYC-dependent translational activity to bioenergetic demands during tumour progression. *Nat. Cell Biol.* **21**, 889–899 (2019).
106. I. J. Tripodi, M. A. Allen, R. D. Dowell, Detecting differential transcription factor activity from ATAC-Seq data. *Molecules* (2018), doi:10.3390/molecules23051136.

107. G. Qing, B. Li, A. Vu, N. Skuli, Z. E. Walton, X. Liu, P. A. Mayes, D. R. Wise, C. B. Thompson, J. M. Maris, M. D. Hogarty, M. C. Simon, ATF4 Regulates MYC-Mediated Neuroblastoma Cell Death upon Glutamine Deprivation. *Cancer Cell*. **22**, 631–644 (2012).
108. G. Qing, B. Li, A. Vu, N. Skuli, Z. E. Walton, X. Liu, P. A. Mayes, D. R. Wise, C. B. Thompson, J. M. Maris, M. D. Hogarty, M. C. Simon, ATF4 Regulates MYC-Mediated Neuroblastoma Cell Death upon Glutamine Deprivation. *Cancer Cell*. **22**, 631–644 (2012).
109. Y. Park, A. Reyna-Neyra, L. Philippe, C. C. Thoreen, mTORC1 Balances Cellular Amino Acid Supply with Demand for Protein Synthesis through Post-transcriptional Control of ATF4. *Cell Rep*. **19**, 1083–1090 (2017).
110. K. Tamura, B. Hua, S. Adachi, I. Guney, J. Kawauchi, M. Morioka, M. Tamamori-Adachi, Y. Tanaka, Y. Nakabeppu, M. Sunamori, J. M. Sedivy, S. Kitajima, Stress response gene ATF3 is a target of c-myc in serum-induced cell proliferation. *EMBO J*. **24**, 2590–2601 (2005).
111. Y. Huang, M. Furuno, T. Arakawa, S. Takizawa, M. de Hoon, H. Suzuki, E. Arner, A framework for identification of on- and off-target transcriptional responses to drug treatment. *Sci. Rep*. **9**, 1–9 (2019).
112. R. Kunder, M. Velyunskiy, S. F. Dunne, B.-K. Cho, D. Kanojia, L. Begg, A. M. Orriols, E. Fleming-Trujillo, P. Vadlamani, A. Vialichka, R. Bolin, J. N. Perrino, D. Roth, M. R. Clutter, N. A. Zielinski-Mozny, Y. A. Goo, M. Cristofanilli, M. L. Mendillo, A. Vassilopoulos, D. Horiuchi, Synergistic PIM kinase and proteasome inhibition as a

- therapeutic strategy for MYC-overexpressing triple-negative breast cancer. *Cell Chem. Biol.*, 1–15 (2021).
113. J. B. Parker, S. Palchaudhuri, H. Yin, J. Wei, D. Chakravarti, A Transcriptional Regulatory Role of the THAP11-HCF-1 Complex in Colon Cancer Cell Function. *Mol. Cell. Biol.* **32**, 1654–1670 (2012).
114. J. D. Buenrostro, B. Wu, H. Y. Chang, W. J. Greenleaf, ATAC-seq: A method for assaying chromatin accessibility genome-wide. *Curr. Protoc. Mol. Biol.* (2015), doi:10.1002/0471142727.mb2129s109.
115. M. R. Corces, A. E. Trevino, E. G. Hamilton, P. G. Greenside, N. A. Sinnott-Armstrong, S. Vesuna, A. T. Satpathy, A. J. Rubin, K. S. Montine, B. Wu, A. Kathiria, S. W. Cho, M. R. Mumbach, A. C. Carter, M. Kasowski, L. A. Orloff, V. I. Risca, A. Kundaje, P. A. Khavari, T. J. Montine, W. J. Greenleaf, H. Y. Chang, An improved ATAC-seq protocol reduces background and enables interrogation of frozen tissues. *Nat. Methods.* **14**, 959–962 (2017).
116. A. Dobin, C. A. Davis, F. Schlesinger, J. Drenkow, C. Zaleski, S. Jha, P. Batut, M. Chaisson, T. R. Gingeras, STAR: Ultrafast universal RNA-seq aligner. *Bioinformatics.* **29**, 15–21 (2013).
117. D. Risso, J. Ngai, T. P. Speed, S. Dudoit, Normalization of RNA-seq data using factor analysis of control genes or samples. *Nat. Biotechnol.* **32**, 896–902 (2014).
118. S. Heinz, C. Benner, N. Spann, E. Bertolino, Y. C. Lin, P. Laslo, J. X. Cheng, C. Murre, H. Singh, C. K. Glass, Simple Combinations of Lineage-Determining Transcription Factors Prime cis-Regulatory Elements Required for Macrophage and B Cell Identities.

- Mol. Cell.* **38**, 576–589 (2010).
119. Y. Zhang, T. Liu, C. A. Meyer, J. Eeckhoute, D. S. Johnson, B. E. Bernstein, C. Nussbaum, R. M. Myers, M. Brown, W. Li, X. S. Shirley, Model-based analysis of ChIP-Seq (MACS). *Genome Biol.* **9** (2008), doi:10.1186/gb-2008-9-9-r137.
 120. G. Stark, R and Brown, DiffBind: differential binding analysis of ChIP-Seq peak datatle, 1–29 (2016).
 121. F. Ramírez, D. P. Ryan, B. Grüning, V. Bhardwaj, F. Kilpert, A. S. Richter, S. Heyne, F. Dündar, T. Manke, deepTools2: a next generation web server for deep-sequencing data analysis. *Nucleic Acids Res.* **44**, W160–W165 (2016).
 122. Y. Liao, G. K. Smyth, W. Shi, FeatureCounts: An efficient general purpose program for assigning sequence reads to genomic features. *Bioinformatics.* **30**, 923–930 (2014).
 123. L. Lopez-Delisle, L. Rabbani, J. Wolff, V. Bhardwaj, R. Backofen, B. Grüning, F. Ramírez, T. Manke, pyGenomeTracks: reproducible plots for multivariate genomic datasets. *Bioinformatics*, 1–2 (2020).
 124. F. Ramírez, V. Bhardwaj, L. Arrigoni, K. C. Lam, B. A. Grüning, J. Villaveces, B. Habermann, A. Akhtar, T. Manke, High-resolution TADs reveal DNA sequences underlying genome organization in flies. *Nat. Commun.* **9** (2018), doi:10.1038/s41467-017-02525-w.
 125. J. M. Gaspar, NGmerge: Merging paired-end reads via novel empirically-derived models of sequencing errors. *BMC Bioinformatics.* **19**, 1–9 (2018).
 126. H. Zhao, Z. Sun, J. Wang, H. Huang, J. P. Kocher, L. Wang, CrossMap: A versatile tool for coordinate conversion between genome assemblies. *Bioinformatics.* **30**, 1006–1007

(2014).

Appendices

Table 1.

GSEA negative enrichment results for MYC-bound promoters comparing DMSO vs. 24-hr MYCi975 treatment and DMSO vs. 48-hr MYCi975 treatment. The table also contains the differential gene expression data from RNA-seq experiments on 22Rv1 cells treated with MYCi975 for 24 and 48 hrs.

“supplementalTable_1.xls”

Table 2.

Differential gene expression and differential binding data of all MYCi975 types, as well as GO enrichment results for each MYCi975 type (<http://geneontology.org>).

“supplementalTable_2.xls”

Vita

Education

- PhD** Northwestern University, Life Sciences Jun 2022
Dissertation: “A MYC inhibitor selectively alters the MYC and MAX cistromes and modulates the epigenomic landscape to regulate target gene expression”
 Committee: Drs. Debabrata Chakravarti, Sarki A. Abdulkadir (chair), Daniel R. Foltz, Grant D. Barish
- MS** Loyola University Chicago, Biochemistry and Molecular Biology May 2017
Thesis: “Potential Efficacy of Targeting MLL1 in breast cancer”
 Advisors: Drs. Nancy Zeleznik-Le, Andrew Dingwall, Clodia Osipo
- BA** Wittenberg University, Biochemistry and Molecular Biology May 2015
 Graduated Summa Cum Laude
 Advisor: Dr. Amil Anderson

Research Experience

PhD Dissertation, Northwestern University, Chicago, IL 2022

Advisor/Principal Investigator: Dr. Debabrata Chakravarti

- Project: Molecular mechanisms of cancer therapeutics
 - Led research efforts characterizing the mechanism of a small molecule inhibitor of the MYC oncogene
 - Teamwork and collaboration across multiple laboratories and disciplines
 - Primary investigations led to first-author publication in a high impact journal article and continued research
- Technical skills and training

- Utilized genomic sequencing, pharmacological and genetic ablation-based studies both *in vivo* and *in vitro* to determine the mechanism of a MYC inhibitor and build rational combination therapy models
- Highly proficient in multiple next-generation sequencing technologies including bulk-tissue, cell line and single-cell
- Extensive knowledge base of computer programming languages utilized to analyze, integrate and visualize genomic data
- Mastered *in vitro* cell culture of both normal and transformed (cancer) cell lines from multiple species including human, rat and mouse
- Molecular cloning and development of CRISPRa/CRISPRi, lentiviral and shRNA-based vectors
- Expert quality control, organization and troubleshooting skills
- Expert skills for nuclei isolation from cell culture and *in vivo* tumors

Master's Thesis, Loyola University Chicago, Maywood, IL

2017

Advisor: Dr. Nancy Zeleznik-Le

- Project: Investigating the efficacy of targeting MLL1 in breast cancer cell lines
 - RNA isolation along with qRT-PCR based gene expression analysis including primer design
 - Pharmacological and genetic ablation-based studies
 - Extensive cancer cell culturing techniques

Undergraduate Research, Wittenberg University, Springfield, OH

2014

Advisor: Dr. Amil Anderson

- Computational research on ligand binding affinities of bacterial proteins
- Utilized Gromacs 4.6.5 to run investigations on the Glucose/Galactose Binding Protein X-ray crystallography coordinates with simulation-based dynamics.
- Analyzed the affinity of Glucose and Galactose by free energy difference when implementing site-directed mutational iterations

Honors and Awards

Cell and Molecular Basis of Disease (CMBD) T32 Training Grant

2018

NIH: T32 GM008061

Computer Skills

Programming languages: R, bash, Unix/Linux

Genome Sequencing Applications: RNA, chromatin immunoprecipitation (ChIP), Ribosome profiling, DNA methylation, DNase I hypersensitivity, MNase, assay for transposable elements (ATAC), Hi-C, Hi-ChIP, genome wide association studies (GWAS), proteomics and cancer genome analysis

Peer reviewed Publications

Journal Papers in Press

A. G. Holmes, J. B. Parker, V. Sagar, M. I. Truica, P. N. Soni, H. Han, G. E. Schiltz, S. A. Abdulkadir, D. Chakravarti, A MYC inhibitor selectively alters the MYC and MAX cistromes and modulates the epigenomic landscape to regulate target gene expression. *Sci. Adv.* 8, 17 (2022)

Teaching/Training Experience

Northwestern University, Chicago, IL

July 2021 to Feb 2022

Undergraduate Student Research Training

- Developed training packets and designed lesson plans to teach the basics of human genome sequencing and differential gene expression analysis
- Hands-on training of standard molecular biological techniques
- Hands-on and remote learning of basic programming skills for biological sciences
- Directed training on independent research and critical thinking

Northwestern University, Chicago, IL

Dec 2021 to April 2021

CLIMB Group Mentor and Facilitator, Molecular Biology

- Hosted multiple meetings weekly to facilitate group learning and discussion
- Prepared review questions that particularly helped with student exams

Northwestern University, Chicago, IL

Dec 2020 to April 2020

Teaching Assistant, Molecular Mechanisms of Carcinogenesis

- Developed and maintained course data repository
- Fostered constructive group discussions
- Provided time and resources for one-on-one discussions and aid

Loyola University Chicago, Maywood, IL

Jan 2017 to May 2017

Teaching Assistant, Molecular Mechanisms of Oncogenesis

- Lead group discussion-based learning on primary cancer biology literature
- Maintained office hours and communication for students outside of the classroom

Presentations

Holmes AG. Small molecule targeting of MYC and the chromatin landscape in prostate cancer cells. August 19th, 2020. Center for Reproductive Science Seminar, Robert H. Lurie Comprehensive Cancer Center of Northwestern University.

Holmes AG, Achille N, Zeleznik-Le N. Potential efficacy of targeting MLL1 in breast cancer. St Albert's Day Poster Presentation. November 2nd, 2016. Maywood, IL

Holmes AG, Achille N, Zeleznik-Le N. Potential efficacy of targeting MLL1 in breast cancer. Biochemistry and Molecular Biology Retreat Poster Presentation. September 3rd, 2016. Maywood, IL

Holmes AG. Proteasome Inhibitors as cancer therapeutics. February 28th, 2015. Wittenberg University Senior Independent Research Thesis.

Non-profit/volunteer work*Invisible Children, Inc*

NGO representative, San Diego, CA, Jan 2009-Jan 2010

Liberty in North Korea

NGO Representative, Torrance, CA, Jan 2010-Sep 2010

Other

Interests/Hobbies: Botany, Mycology, turntablism, veganism and food security